Single molecular transistors and electron-vibron coupling

Gregers Alexander Kaat

1st December 2004

Abstract

We study single electron transport in a single-molecular dimer device with one vibrational mode. The vibron couples to the difference in charge on the two parts of the dimer, leading to correlation between the electronic and bosonic degrees of freedom. A correlated state is called a small polaron. We find that the correlation increases sharply as a function of a parameter α. This increase is reflected in the transport properties of the system in two ways: the small bias current becomes strongly inhibited in the polaronic regime; and a characteristic energy in the problem, the on-dimer effective electron hopping, becomes exponentially small, such that transport in the device may no longer be sequential. In this case, the dimer may become an effectively uncoupled double dot. We relate our findings to recent experiments on C_{70} dimers.

Contents

Chapter 1

Molecular electronics

1.1 The field

An aim of molecular electronics is to use single-molecular transistor devices for functions that today are performed by silicon chips. Basic conduction properties of interest include amplification, and current asymmetry effects such as rectification and negative differential restistance (NDR).

The generic single-molecular transistor device consists of one molecule (an 'island', or a 'quantum dot') connected to three electrodes, two for bias voltage (Fermi 'seas', denoted 'source' and 'drain') and one for gate voltage. The electrodes ('leads') are usually gold, pure or not, and 'good' or 'bad' depending on the treatment, leading to strong or weak coupling between the lead electronic states and the electronic states of the molecule. Weak coupling is characterized by long dwell times for electrons on the molecule, hence an integer number of charges on the molecule, and by 'Coulomb blockade'. Strong coupling is characterized by fractional charge number, by tunneling broadening of the peaks in the differential conductance, and by the molecule effecting the limit on electrical transport.

Molecules of interest are usually organic, such as fullerenes, DNA, carbon nanotubes (CNT), or strings of connected benzene rings such as OPV5. Long molecules with each end attached to electrodes are called molecular wires. Molecular properties of interest include of course the electronic states, but also vibrational states and even conformational states, as molecules may change their shape in response to a change in electrical charge on the molecule. Molecular switches is the term for molecules that can be turned 'on' or 'off' with respect to electric conduction due perhaps to a conformational change. The construction of logic gates using molecular switches was proposed early on [3] [4], using molecules of the 'DBA' form (below).

Nanoelectromechanical (NEM) coupling between quantized mechanical and electrical degrees of freedom is a subject of much interest. The mechanical motion may be a quantized oscillatory motion of a molecule; such a motion may couple

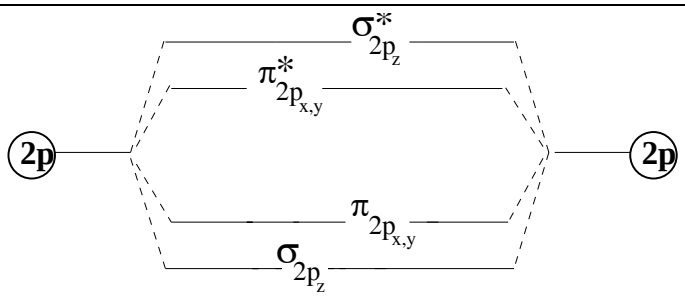

Figure 1.1: Hybridized levels of the 2p orbitals of two neighbouring atoms. The hybrid orbitals are the bonding and antibonding combinations of the corresponding atomic orbitals. The hybridizing atomic orbitals correspond to the same spin.

Figure 1.2: The four sp^3 hybrid orbitals [1].

to an electronic degree of freedom (such as localization to a site, or spin) through a local electrical or magnetic field. The oscillatory motion could be a motion of the molecule as a whole, or an internal vibrational mode. It could even be a large amplitude oscillation of the molecule between the electrodes, where the tunneling rates couple to the position of the molecule, a so-called 'shuttling' effect (discussed below).

Measurements on molecular devices, apart from the measurement of IV curves, rely heavily on scanning tunneling microscopy (STM), allowing the experimenter to 'see' and manipulate single atoms on surfaces.

1.2 Some basic chemistry

Before we can proceed, we must introduce some concepts and terminology from chemistry.

The orbitals of a molecule may be constructed as linear combinations of the individual atomic orbitals. Two s orbitals of equal energy on different atoms are nonorthogonal and hybridize into bonding and antibonding combinations, denoted σ and σ^*, respectively. The hybridization of same-energy p orbitals depend on whether they meet head-on (say, p_z) or sideways (p_x and p_y). Two p_z orbitals hybridize into σ, σ^* orbitals with zero angular momentum about the bond axis. Two p_x or p_y orbitals hybridize into molecular π (bonding) and π^* (antibonding) orbitals with angular momentum 1 $\hbar$ about the bond axis. Usually, σ orbitals are stronger bonds than π orbitals, due to a larger overlap of the atomic orbitals. We indicate the hybridization energies in fig. (1.1).

The carbon atom in it's ground state is in the configuration $1s^2 2s^2 2p^2$. One 2s electron is easily excited to 2p, and C atoms in this state form bonds involving as much as one s electron and three p electrons from each atom. In a benzene ring,

one s and two p electrons form localized bonds, as the p electrons of neighbouring C atoms hybridize and the s electron hybridize head-on with a H atom. The remaining p orbitals are in the direction orthogonal to the plane of the ring and linearly combine into delocalized orbitals of the entire ring.

The localized orbitals are denoted sp^2. They are:

$$\frac{1}{\sqrt{3}}s + \frac{\sqrt{2}}{\sqrt{3}}p_x \tag{1.1}$$

$$\frac{1}{\sqrt{3}}s - \frac{1}{\sqrt{6}}p_x \pm \frac{1}{\sqrt{2}}p_y \tag{1.2}$$

The sp^2 orbitals lie in a plane, and leave one p electron (p_z, here) unhybridized. See fig. (1.3).

In fullerenes ('bucky ball' molecules, eg. C_{60}), the hybridization of the C atoms is approximately sp^2, the deviation a result of nonplanarity of the 'surface' of the 'ball'. The unhybridized p_z orbital is orthogonal to the approximate sp^2 plane, free to bond with, usually, a hydrogen atom.

A different hybridization of relevance here is sp^3, which is the structure of, eg., CH_4. The orbitals, depicted in fig. (1.2), are:

$$\frac{1}{2}\left(s + p_x + p_y + p_z\right) \tag{1.3}$$

$$\frac{1}{2}\left(s + p_x - p_y - p_z\right) \tag{1.4}$$

$$\frac{1}{2}\left(s - p_x + p_y - p_z\right) \tag{1.5}$$

$$\frac{1}{2}\left(s - p_x - p_y + p_z\right) \tag{1.6}$$

$$\tag{1.7}$$

Often, the levels relevant for chemical and transport properties are the 'HOMO' and 'LUMO' levels, the highest occupied/ lowest unoccupied molecular orbitals.

1.3 DBA transistors

Transport of electrons through a single molecule depends on the quantum mechanical electron states, which in general are delocalized combinations of atomic eigenstates. The molecular states are modified by coupling to the electrodes, however. In a situation where the lead coupling is strong compared to the hybridization of two localized orbitals, and the localized orbitals couple to different electrodes, the molecule becomes a system where charge may be transfered from one part to the other.

In their 1974 paper [2], which is sometimes seen as the beginning of theoretical molecular electronics, Aviram and Ratner consider a single organic molecule with

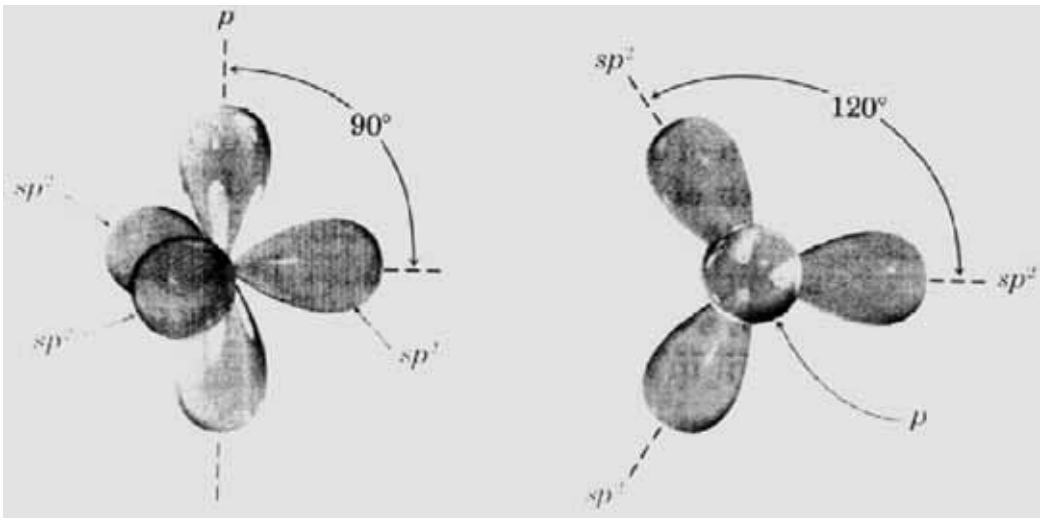

Figure 1.3: The three sp^2 hybrid orbitals, and the unhybridized p orbital orthogonal to the sp^2 plane, in side view and in top view [1].

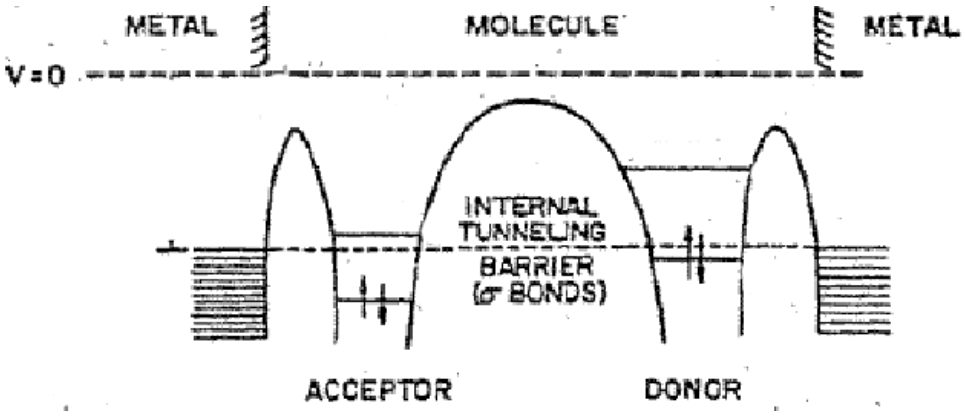

Figure 1.4: Aviram and Ratner's molecular rectifier at zero bias voltage, that is, with left and right Fermi levels aligned. The HOMO and LUMO levels of the acceptor and the donor are indicated.

donor and acceptor sites, inserted between metal electrodes strongly coupled to the respective site orbitals. The sites are assumed separated by a σ bridge, a part of the molecule that separates the sites in space by insulating σ electron bonds for the purpose of insuring that coupling between the donor and acceptor sites is weak. This creates a tunneling barrier between the isolated states on the two parts of the molecule. The σ bridge is also assumed to give the molecule sufficient rigidity that it does not interact mechanically with the electron transfer processes. The donor and acceptor sites are aromatic subunits (ie., modified benzene rings) of the molecule, which are heightened/ lowered, respectively, with respect to the density of π electrons in the ring. A specific example of a donor-bridge-acceptor (DBA) molecule, suggested in [2], is drawn in fig. (1.5). The donor part is tetrathiofulvalene (TTF), and the acceptor part is tetracyanoquinjonedimethane (TCNQ).

A rectifying device is depicted in fig. (1.4). At zero bias voltage, the electrode Fermi levels are equal. The charge-neutral acceptor LUMO is just above the left lead Fermi level, and the charge-neutral donor HOMO is just below the right lead Fermi level. Applying a small bias voltage, heightening the left lead chemical potential to the acceptor LUMO level, and lowering the right lead level to the donor HOMO, allows current to run through the device by a two-step process. Step one is the injection of a left Fermi sea electron to the acceptor LUMO, and the injection of a hole from the right Fermi sea to the donor HOMO. The molecular state thus created is called a 'zwitterion' [6]. In step two, the electron and hole recombine through a 'downhill' inelastic tunneling process, during which energy is transfered to unspecified vibrational degrees of freedom.

In the opposite direction of the bias voltage, current can run if the left electrode potential is lowered to the HOMO level of the neutral acceptor, and the right electrode potential raised to the donor LUMO. This requires a much larger voltage. The device, therefore, is rectifying at low bias voltages.

1.4 SETs in the sequential tunneling regime

A molecular, single-electron transistor (SET) device consists of a molecular 'island' coupled to 'source' and 'drain' electrodes (Fermi 'seas') and, capacatively, to a 'gate' electrode. Electron transport through the device happens one electron at a time, as electrons jump onto the molecule from one electrode into a molecular orbital, relaxes to some distribution of eigenstates with dissipation of energy to an environment, and then jumps off the molecule to (probably) the other electrode.

The condition that the number of electrons on the island is an integer at all times requires that coupling to the electrodes is weak, meaning that the time between tunneling processes is long compared to all relevant time scales in the problem; this enables us to treat the island as an isolated system between tunneling events [52]. This is the 'sequential transport' regime, in which the tunnelings are treated as incoherent processes and we may work with wave functions defined for the isolated molecule rather than for the system of the molecule plus the electrodes.

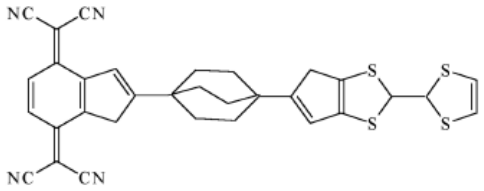

Figure 1.5: The DBA type molecule suggested by Aviram and Ratner as a molecular rectifier. The hexagon to the left connected to the CNs by double bonds is TCNQ, and the part consisting of two pentagons involving sulfurs to the right is TTF.

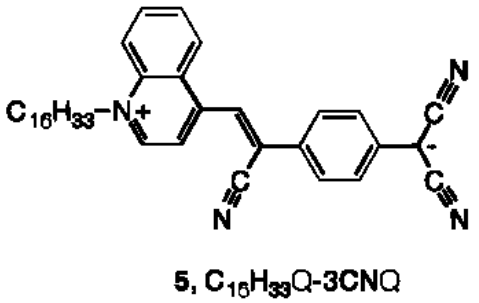

Figure 1.6: Hexadecylquinolinium Tricyanoquinodimethanide, the DBA type molecule used by Metzger et al.

Mathematically, this means that the density matrix of the full system is assumed separable in the molecular and the electrode degrees of freedom; separability is discussed in chapter 2.

Coulomb charging energies are usually large. For two charge states, this energy is inversely proportional to the capacitance of the gate electrode, hence to a characteristic length of the island. If the island is a small molecule, charging energies may be very large. If no gate voltage is applied, the molecule prefers to be electrically neutral. For current to run at small bias voltages, the ground states belonging to two neighbouring charge states must be energetically aligned through the gate voltage. If the gate voltage exactly compensates for the difference in energy between the ground states belonging to two neighbouring charge numbers, the molecule can 'flip' freely between the two ground states, and current can run at arbitrarily small bias voltages. When the bias voltage is turned up, current still runs only via the same two charge states, because all other charge states are further away in energy than the applied bias voltage and the appropriately low temperature can make up for. Current is therefore a result of transport of single electrons.

The conductance strongly depends on small changes in the gate voltage near the critical value that aligns the ground states. A small change in the gate voltage away from the critical value stabilizes one of the charge states, and then current can only run at bias voltages large enough to bridge the gap in energy thus created between the two ground states. This effect is called the 'Coulomb blockade'.

If the molecule has several eigenstates, then the excited states become energetically accessible and contribute to the current when the voltage is increased. This results in IV curves with steps. The differential conductance, defined as $\frac{\partial I}{\partial V}$, is a series of broadened δ-functions, with the broadening a result of finite temperature,

electron tunneling, and dissipation. The area under one peak is the height of the corresponding step on the IV curve.

1.5 Various experimental work, 1997-2003

Attaching three or more electrodes to a single molecule, a requirement for constructing a molecular electronics device, has not been possible until a few years ago. Stepping stones toward single-molecule devices have involved monolayers of single molecules. The Langmuir-Blodgett method is a way of producing ordered layers of molecules by selfassembly, so-called Langmuir-Blodgett films. Effective single-molecule devices have been constructed from selfassembled monolayers (SAM).

In 1997, Reed et al. [5] utilized a so-called 'break-junction' technique, when they self-assembled benzene-1,4-dithiol molecules on a gold wire, which was then stretched until it broke, resulting in two Au electrodes covered by a SAM. Bringing the electrodes together created a gold-sulfur-aryl-sulfur-gold system, through which room temperature IV characteristics could be measured. Still, only two electrodes could be connected to the conducting molecule in this way.

A DBA rectifier was constructed and IV characteristics measured in 1997 by Metzger et al.[6]. The molecule, Hexadecylquinolinium Tricyanoquinodimethanide, fig. (1.6), was actually part of a Langmuir-Blodgett film, monolayer and multilayer both used, which was 'sandwiched' between metallic electrodes. For the monolayer device, current ran through single molecules, and current asymmetry and rectification at low voltages was demonstrated. The rectification mechanism was a variant of the one proposed by Aviram and Ratner, with the bridge part of the molecule a π orbital rather than a σ one, inducing a permanent dipole moment in the bond. The molecule in it's ground state therefore was not of the form D-π-A, but D^+-π-A^-, in obvious notation.

An alternative use for STM was the idea of Joachim et al. [7], 1997, when an STM tip was used to apply electromechanical pressure on a C_{60} molecule on a surface. The resulting deformation of the molecular cage shifted the HOMO and LUMO levels, and the change in resonances drastically changed the electrical conductivity. Hence, a small change in STM tip voltage (and therefore tip position) led to a large change in conductance, making the setup the first single-molecule electromechanical amplifier (with a gain of approximately 4-5).

In 1999, NDR was observed by Chen et al. [8] for devices consisting of a SAM of 2'-amino-4-ethynylphenyl-4'-ethynylphenyl-5'-nitro-1-benzenethiol molecules coupled to gold electrodes, fig. (1.7). The NDR is explained as the result of a one-electron reduced state of the molecule being conducting, while a two-electron reduced state is isolating. Current runs for an interval of bias voltages corresponding to the conducting state, and NDR sets in when the isolating state is brought into resonance.

Also in 1999, Park et al. presented a method for fabrication of gold electrodes at nanometer separation [9]. They passed a large electrical current through a gold

nanowire, causing electromigration, ie. motion of the gold atoms due to the large electrical field. Eventually the wire broke, leaving a nm sized gap between the ends, ie. the electrodes.

In 2000, the method described above was utilized in the pioneering experiment of H. Park et al. described in detail below, where single-molecule C_{60} SET devices were constructed. Similar methods of fabrication to these were utilized in 2002 by J. Park et al. [16] with different molecules, containing an organic part of variable length, linking a Co ion to the gold electrodes. By varying the length of the organic part, they could control the strength of the coupling between the electrodes and the Co ion. At weak coupling, single-electron transport with a Coulomb blockade effect was measured, but at stronger electrode coupling Kondo tunneling was observed, with nonzero, small bias conductance in the previously Coulomb blockaded regime. Kondo tunneling in single-molecule transistors was also observed in [17] at that time.

Room temperature SETs with metallic, single-wall CNTs as the active element were fabricated in 2001 by Postma et al. [11]. This was done by attaching electrodes to the ends of single CNTs, into which had been build tunneling barriers in the form of sharp bends in the tube. The bends had been created by manipulation with an atomic force microscope. The SET 'island' was the short part of the CNT between the bends. The experimenters observed Coulomb blockade at room temperature, and addition energies of 120 meV $\sim$ 1300 K. At low T, energy levels of the island were resolved, with energy differences of 38 meV, and the Coulomb charging energy was deduced to be 41 meV. The conductance peak and width were both found to increase with temperature, in contrast to conventional SETs. From the dependence of the conductance on temperature (a power-law), they proposed that the transport mechanism was a Luttinger liquid-like, correlated sequential tunneling mechanism, with the 'island' acting as an impurity.

Also in 2001, CNT logic gates were constructed by several groups [12, 13, 14].

Finally, we mention the OPV5 SETs of Kubatkin et al. [18], 2003. The OPV5 molecule, fig. (1.9), consists of five benzene rings connected by four double bonds, and with one thiol group at each end. From the IV measurements on OPV5 devices, charge on the molecule was deduced to be highly localized, in contrast to expectations from experiments on OPV5 in a solution (ie., no electrode couplings). The interpretation was that a charge on the molecule was strongly attracted to it's mirror charge in the electrode, leading to strong localization of charges close to a lead. Even though the overlaps of the electron states of the electrodes and of the molecule were small, hence tunneling coupling weak and the device a SET, the electrostatic interactions were strong, leading to 'polaron effects', ie. localized electron states.

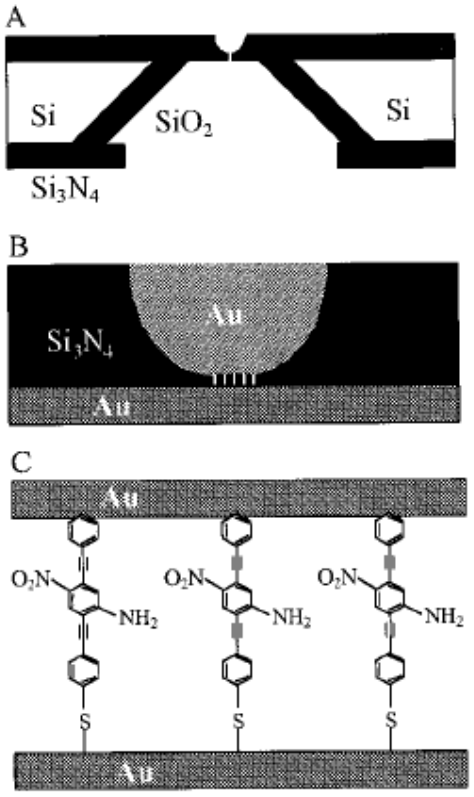

Figure 1.7: Molecular electronic device of Chen et al. [8]. (A) shows a silicon wafer with a nanopore etched through a silicon nitride membrane. (B) shows the Au-SAM-AU junction in the pore area. (C) shows the conducting molecules sandwitched between the Au electrodes.

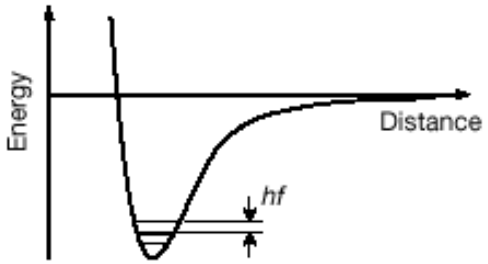

Figure 1.8: The electrostatic potential in which Park et al.'s C_{60}s perform small oscillations [10].

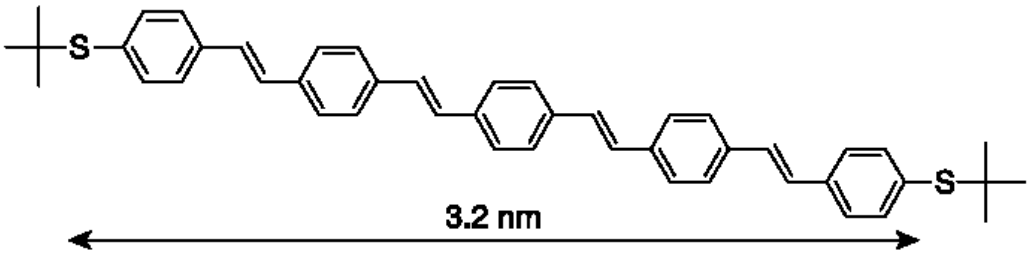

Figure 1.9: The OPV5 molecule, from [18].

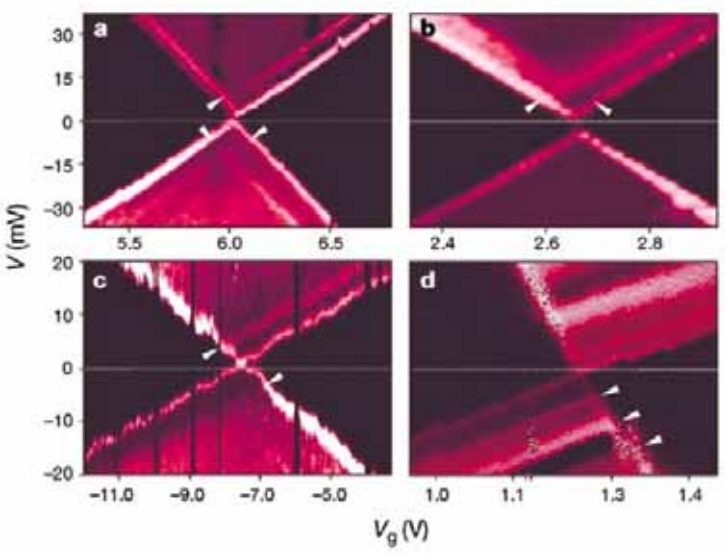

Figure 1.10: Measured diamond plots for Park et al.'s C_{60} transistors, displaying sidebands corresponding to 5 meV vibronic excitations, marked with arrows on the plots.

1.6 Experiment: Nanomechanical oscillations in a single-C_{60} transistor

One experiment that generated much interest was the fabrication of and measurements on single C_{60} transistor devices in 2000 by Park et al. [10]. Each device was defined on an isolating layer of SiO_2 on top of a doped silicon wafer, serving as gate electrode. A toulene solution of C_{60} was deposited on a pair of connected gold electrodes, which had been fabricated by electron-beam lithography. Then the electromigration technique of [9] was utilized to create a nm-sized gap between the electrodes. When the procedure was succesful, the result was a single C_{60} molecule weakly coupled to gold leads and a gate electrode. Van der Waals interactions between the molecule and the electrodes held the molecule in an equilibrium position in an electrostatic potential, fig. (1.8). Bias (V) and gate (V_g) voltages were controlled in the experiments.

IV-curves were measured at different gate voltages, as V_g was varied in an interval much smaller than the Coulomb charging energy of approximately 100 meV, around the value V_c where two charge states (which exact ones was unknown) had the same energy. The resulting 'diamond plots' - density plots of the differential conductance $\frac{\partial I}{\partial V}$ as a function of V and V_g - are presented in fig. (1.10). They show a 'conductance gap', as the differential conductance for a given V_g is 0 for $|V|$ smaller than some value; inside the conductance gap is the Coulomb block-

ade regime. Outside the gap, at increasing $|V|$, new excitations of the molecule become energetically accessible, revealing themselves as peaks in the differential conductance as they provide new states by which the electron tunnel through the molecule. Such peaks are called sidebands.

The main sidebands are equally spaced lines with a spacing of approximately 5 meV. The experimenters attributed them to electromechanical coupling between the charge state of the C_{60} and the quantized, oscillatory center of mass motion of the molecule. From this they concluded that the electron tunneling processes involved excitations of vibrational levels, with a strong coupling to a single vibrational mode, probably the cm motion of the C_{60}.

In the analysis, the tunneling probabilities were taken to follow Franck-Condon theory [43], in which an electron tunneling process is considered 'instantaneous' on the time scale of the vibrations because the atomic nuclei are much heavier than the electrons. Thus, the nuclei can only respond to electronic movement after the jump has taken place. With this simplification, tunneling probabilities are proportional to overlaps between the electronic wave functions of different, nonorthogonal electron states. These overlaps are called Franck-Condon factors.

1.7 Electron-vibron coupling: quantum shuttling

We move on to some recent and current theory for molecular electronics devices.

In the original paper of Gorelik et al. [19], a system is considered where single electrons are 'shuttled' between lead electrodes by jumping onto a single molecule that moves in response to the charge state. The electrical current is a result of two processes: tunneling between the molecule and the leads, and the molecule moving backwards and forwards between the leads. The mechanical motion of the molecule can be treated classically if the characteristic decay length of the lead electrode coupling is large compared to the amplitude of the quantum fluctuations in the molecule position.

The theoretical assumption is that the molecule performs center of mass oscillations in the potential of the electrodes. Then, shuttling requires that the time-dependent charge of the molecule $q(t)$ is correlated with the molecule's velocity $\dot{x}(t)$ such that the time average $\langle q(t)\dot{x}(t)\rangle$ is nonzero [20]. To get to the shuttling regime, bias voltage must exceed some threshold value, because energy dissipates to environmental degrees of freedom (ie., via coupling of x to a bath of oscillators in the electrodes), and the oscillations can only be sustained if more energy is pumped into the system than is dissipated. Exceeding the threshold voltage, the amplitude of the mechanical oscillation grows exponentially until it settles at some value, a stable limit cycle, where equal amounts of energy are absorbed and dissipated.

In [21, 22, 23], the classical picture of the mechanical motion is extended to the quantum regime, and quantum shuttling is studied. It is found that the quantum

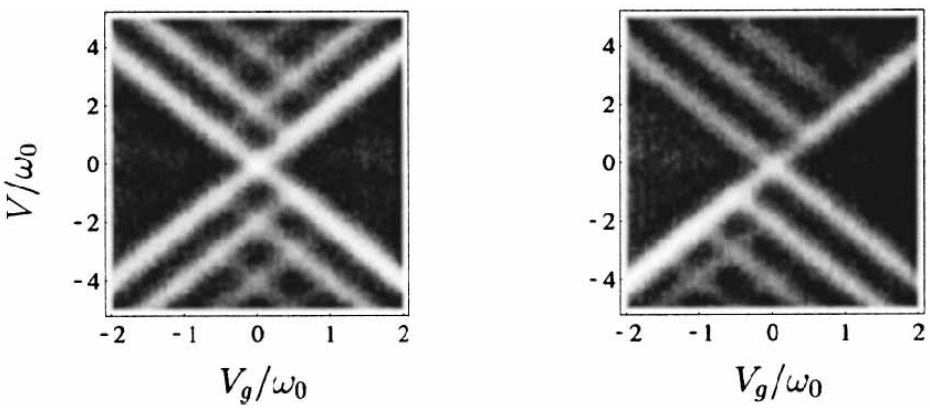

Figure 1.11: Diamond plots by Braig and Flensberg, describing sequential transport in devices like the C_{60} devices of Park et al. The plot to the left is for symmetrical coupling to the electrodes, the plot to the right is for highly asymmetrical electrode coupling.

vibrational ground state is unstable when dissipation is sufficiently weak, leading to a quantum shuttling regime, the details of which depend on the strength of the applied electrical field.

The C_{60} devices of Park et al. described above have been suggested to be quantum shuttling devices [24]. From the value of the current, they probably are not [25]. We know of no experiment that conclusively demonstrates quantum shuttling.

1.8 Vibrational sidebands and dissipative tunneling in molecular transistors

One theory paper of particular relevance to us is [28], in which single-electron transport is calculated for a device with coupling of the charge number to a single vibrational mode. The mode is assumed to be a molecular cm oscillation, the coordinate is denoted x_0, and the corresponding frequency is ω_0. Explicitly included in the model is coupling of x_0 to an environment consisting of a 'bath' of harmonic oscillators, ie. a substrate to which the molecule is attached. The coupling term in the Hamiltonian is of the Caldera-Legget type [44],

$$\sum_j \beta_j \; x_0 \; x_j \tag{1.8}$$

where the x_j are coordinates for the bath oscillator modes and the β_j are coupling constants.

The theoretical treatment is concerned with the effect on the IV characteristics of energy dissipation to the bath. This effect is to frictionally damp the oscillation, to shift the oscillation frequency, and to broaden the conductance peaks. In general, damping depends on frequency; disregarding frequency-dependence, dissipation is described by the frequency $\boldsymbol{\gamma}$, or the Q-factor, $Q = \frac{\omega_0}{\boldsymbol{\gamma}}$. Relaxation to a thermal equilibrium distribution between tunnelings requires that $\boldsymbol{\gamma} \gg \Gamma$, where Γ is the largest of the 'left' and 'right' tunneling rates.

In the limit of 'vanishing' coupling to the environment (large Q/ small $\boldsymbol{\gamma}$), where there is no dissipative broadening of the steps, but it nevertheless is assumed that $\boldsymbol{\gamma} \gg \Gamma$, the model simplifies. Now, the only consequence of the coupling is that the molecule equilibrates to it's thermal ground state between each tunneling event due to 'infinite' time intervals between tunnelings. In this limit, the Hamiltonian of the molecule reduces to an independent boson model [53]:

$$H_{IB} = \epsilon\ c^\dagger c + \lambda(a + a^\dagger)c^\dagger c + \omega_0 a^\dagger a \tag{1.9}$$

Here, the c operators are for the electron, the a operators are for the molecular vibrational mode, ϵ is the onsite energy, and λ is the electron-vibron coupling. This is basically sufficient to describe transport in the devices in the C_{60} experiments of Park et al. Solving the model, the spectral function for phonon emission into the dissipative environment, in the zero temperature case, becomes a series of delta functions at energies $n\omega_0$, $n \geq 0$, with corresponding weights given by a Poisson distribution as $e^{-g}g^n/n!$. Here, $g = l^2/2l_0^2$, where l is the classical oscillator displacement length, and l_0 is the quantum oscillator lenght. From this, transport in the limit considered is described by a series of peaks in the differential conductance, corresponding to steps on the IV curve of heights $\frac{g^n}{n!}\times$ the ground state current step height.

The diamond plots, fig. (1.11), are for symmetric and asymmetric tunneling contacts, respectively. The bias is applied symmetrically, and the zero point of the gate voltage is the electron on-site energy. Sidebands corresponding to vibrational excitations of the molecule are clearly visible. For the purposes of our own work, we consider these diamond plots in detail:

When the contacts are symmetrical, the diamond plot is obviously symmetrical around $V = 0$ reflecting of the symmetry of the device. Less obvious is the symmetry around $V_g = 0$, since the sign of V_g determines the number of electrons on the molecule. For two charge states, 'filled' and 'empty', for one sign of the gate voltage (say, $V_g > 0$) the molecule is most likely to be 'filled' and for the opposite sign, the molecule is most likely to be 'empty'. Therefore, for positive gate voltages, the conductance peaks are strong for transitions from 'filled' to 'empty' states, and determined by Franck-Condon factors corresponding to these overlaps. For negative V_g, the peaks are strong for transitions from 'empty' to 'filled' states, which in general could be different overlaps. However, for the molecule at hand, for both charge states the eigenstates are just bosonic, harmonic oscillator states, and so the two sets of overlaps are identical. This explains the symmetry around

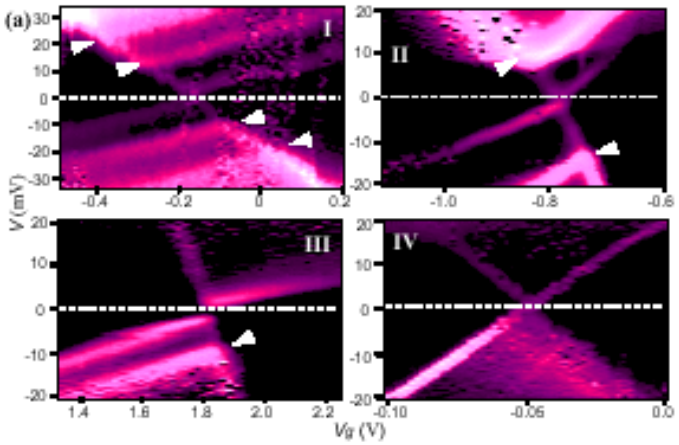

Figure 1.12: Diamond plots for the dimerized C_{70} devices of Pasupathy et al.

$V_g = 0$.

When contacts are asymmetrical, both of these symmetries are broken; however, inversion symmetry about (0,0) remains. With the 'left' tunneling rate much larger than the 'right' tunneling rate, for electrons travelling from 'left' to 'right' ($V > 0$), the molecule is 'filled' most of the time. The molecule relaxes to it's ground state between tunnelings, so out-tunnelings are mainly from the 'filled' ground state, and the current is due mainly to Franck-Condon factors involving just the ground state of the 'filled' molecule. This corresponds to the single line from $(V = 0, V_g = 0)$ to the upper right corner on the plot; lines parallel to this line are suppressed. In the opposite direction of the current, $V < 0$, the molecule is 'empty' most of the time, and therefore out-tunnelings are suppressed for the excited states of the 'empty' molecule, resulting in one line from (0,0) to the bottom left corner on the plot, but no strong lines parallel to this. The result for the 'full' diamond plot is suppression of the sidebands in one direction on the plot.

1.9 Experiment: Vibration-assisted electron tunneling in C_{140} single-molecule transistors

We now describe the single experiment that motivates our work in the following. In [30], Pasupathy et al. describe fabrication of and low temperature (1.5 K or less) measurements on C_{140} single-molecule devices. The C_{140} is dimerized C_{70}, a rugby-ball-like structure, see fig.s (1.13), (1.14). The dimer is inserted between two gold electrodes about 1 nm apart, and is capacitatively coupled to a gate electrode. The insertion is carried out at cryogenic temperature, using an electromigration technique. The dimer orientation in the constriction between the electrodes is

unknown. Note that the length of the C_{140} is comparable to the distance between the electrodes.

The measured diamond plots, fig. (1.12), show Coulomb blockade and sidebands corresponding to excitations of two charge states of the dimer. An excitation of 11 meV ($\sim$ 130 K, clearly resolvable at the experimental temperatures) is observed, and interpreted as a vibrational excitation, because it appears for both charge states, and because in one device, an excitation of the double frequency, 22 meV, is observed for both charge states. These features indicate that the excitation is vibrational rather than electronic. The 11 meV mode is not observed for single C_{70} molecules, and is therefore concluded to be an intercage mode of C_{140}, nonexistent for the monomers. The energy suggests that the mode is the intercage stretching mode. All this agrees with Franck-Condon physics; however, comparing the steps on the IV curves, assuming (naively) a Poissonian distribution for the step heights in analogy with the C_{60} experiments, reveals anomalously large electron-vibron coupling, with g-factors of as much as 5. Making matters worse, some of the devices show unexpected asymmetry in the IV-characteristics [31] (not shown). These devices act as recitifiers, with the current close to 0 in one direction of the bias voltage. Actually, some current does run in the blocked direction for small bias voltage, corresponding to current running through through the device via the ground states; however, as the bias voltage is turned just slighty up, negative differential conductance (NDC) sets in, negating the current. This is not explainable by Franck-Condon theory.

It seems clear that the current in the dimer devices cannot be understood by simple analogy with the C_{60} devices. In following sections, we shall try to understand the current starting from a pseudo-realistic model for the dimer.

1.10 The structure and some chemistry of C_{70}

At this point it is instructive to review some experimental and theoretical work on C_{70} dimers. The C_{70} fullerene, fig. (1.13), consists structurally of pentagons and hexagons. Experimentally, the structure has been deduced from electron diffraction data [33]. Theoretically, ab initio methods have been employed, on the Hartree-Fock level in [32], as well as molecular dynamics calculations for the outer shell electrons [34]. The equilibrium geometry of the molecule is D_{5h} [37], corresponding to two plane symmetries. Bonding lengths range from 1.37 to 1.46 Å, corresponding to the lengths of C-C single bonds (1.46 Å) and double bonds (1.37 Å), and 8 different lengths are present. From the bonding lengths, bonds that are part of two hexagons have double bond character, while bonds that are part of one hexagon and one pentagon have single bond character.

The molecule contains 8×70 outer shell orbitals, half of which are occupied. In a molecular orbital approximation, $\frac{3}{4}$ of the orbitals, the approximate sp^2 hybridized electrons, form strong bonds, while $\frac{1}{4}$ of the orbitals, the plane-orthogonal p orbitals, form less strong π bonds. Nonplanarity of the 'ball' surface leads to de-

viation from the standard sp^2 state [38]. For both types of bonds, in the molecular ground state, the 'bonding' orbitals are occupied, and the 'antibonding' orbitals are unoccupied. The HOMO orbital is the highest bonding π orbital belonging to the p_z electrons, and the LUMO orbital is the lowest unoccupied π^* orbital of the p_z electrons. The electronic structure relevant for chemistry is the structure of these π and π^* orbitals.

The C_{70} spectrum contains degeneracies and a HOMO-LUMO gap of 1.23 eV [36]. The ionization potential is (7.6 $\pm$0.1) eV [32], and the electron affinity (2.7 $\pm$0.1) eV. We return to these values in chapter 6. The vibrational spectrum is complicated, see ref. [37] for some vibrational spectroscopy results.

1.10.1 Dimerization of C_{70}

Dimerization of charge neutral C_{70} molecules happens basically by the breaking of double bonds in the polar hexagons and formation of two parallel covalent bonds between the balls, from neighbouring sites on the ball. The hybridization of the four C atoms involved change from sp^2 to sp^3 [38]. The process of dimerization is believed to be a [2+2] cyclo-addition, where hybridization is between the LUMO orbitals of the C_{70}s, or rather, between one LUMO for a C_{70} in it's ground state and one HOMO of an excited C_{70}, with the C_{70} photoexcited so that an electron occupies the level above the gap. Then, when the C_{70}s are brought together, the 'new' level of lower energy is occupied, and the energy of the system is minimized in a bound configuration.

Several dimer geometries can be pictured in this manner, but experiments [35] [37] and theory [36] indicate that there exists one dominant isomer. In fig. (1.13), the sites connected by the uppermost vertical bond are the ones involved in dimerization. The C_{70}s can be thus connected in two ways, and it is unclear which one is most likely to occur. The most symmetrical one is depicted in fig. (1.14). The intercage bonding length is 1.51 Å. The HOMO-LUMO gap is smaller than for C_{70}, a value of 0.96 eV is given in [36], and the spectrum contains fewer degeneracies due to the lower symmetry of the dimer. The spectrum of two uncoupled C_{70}s is of course doubly degenerate, apart from the degeneracies of the individual C_{70}s. When the molecules dimerize, the degeneracies near the Fermi level are lifted, that is, the HOMO level and levels just below become nondegenerate in the dimer.

Intercage vibrational modes include bending, twisting, and stretching modes, at frequencies in the range 2-17 meV.

1.11 Small polarons

Historically, polaron effects in molecular electronics devices are not well studied. The possibility that such effects may dominate the current in the C_{140} devices motivate us to briefly describe the physics of small polarons in a 1D lattice.

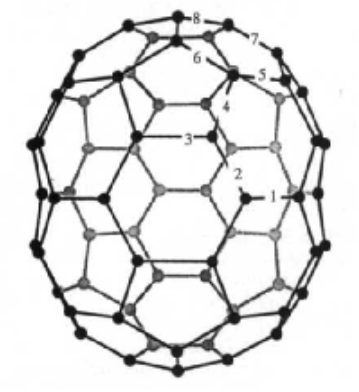

Figure 1.13: The structure of C_{70}, from [33]. Bonds 3,4,6,8 defining the pentagon are long, approximately 1.46 Å. The bonds 5,7 joining the apices of pentagons are short, 1.37 Å in average. Length of hexagon bonds of type 1 is 1.41 Å, similar to graphite. Type 2 bonds are of an intermediate length of 1.39 Å.

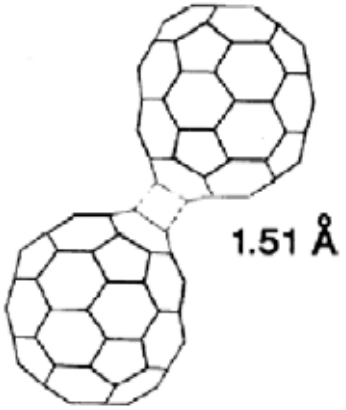

Figure 1.14: The dominant C_{140} isomer, from [36].

Consider an electron in a periodic lattice, where the electronic movement is discrete, as the electron hops between neighbouring sites due to the quantum mechanical overlap integrals of the identical electronic orbitals on the sites. The nuclei on the lattice points perform quantized oscillations around their equilibrium positions, and ionic positions couple linearly to the electronic occupation number operator at each site. If the electron is localized to one site, the corresponding oscillator position is displaced due to the interaction. The Hamiltonian (a 'Holstein Hamiltonian', after the original work of Holstein [46]) for a 1D lattice with N_s sites [53]:

$$H_H = \hbar\omega \sum_{i=1}^{N_s} a_i^\dagger a_i - t \sum_{\langle i,j \rangle} c_i^\dagger c_j + \lambda \sum_{i=1}^{N_s} c_i^\dagger c_i (a_i^\dagger + a_i) \tag{1.10}$$

The a_i operators are the boson operators for the vibrating sites, and the c_i operators are the fermion operators for the site-localized, identical electron orbitals. The parameters are ω for the vibrational frequency, which is the same for all sites, t for the nearest neighbour hopping energy, and λ for the electron-vibron interaction, which is local and has the same value for all sites. This model is relevant for the study of polarons. 'Polaron' is the term for a system consisting of electrons and an environment of bosons to which the electrons couple. An electron exerts forces on the ions, which move in response, exerting (quantized) forces on the

electron, with the result that the electron, no longer freely hopping around, is to some extend localized, while the lattice deforms around it. The quantized lattice deformation is the phonon cloud, and is a polarization of the medium. The polaron is a quasiparticle with an effective mass and selfenergy.

If the coupling is not very strong, the electron may be weakly localized to any number of sites; the system of the electron and the phonon cloud is called a 'large polaron'. For sufficiently strong coupling, the electron becomes 'selftrapped', meaning highly localized to one site and unwilling to hop, because in order to move, it must carry the heavy phonon cloud with it. A selftrapped, localized electron is called a 'small polaron', because the characteristic diameter of the electron + lattice deformation system is not very much larger than one lattice constant.

The Holstein Hamiltonian can accomodate multiple polarons if the number of electrons in the system is larger than 1. Polarons interact attractively, which may give rise to pair formation analogous to BCS theory, possibly even superconductivity; this is an open question [41]. A bound polaron pair is called a bipolaron.

1.12 Spin-boson model

The spin-boson model is a model of a two-state system (a 'qubit') coupled to a bath of harmonic oscillators:

$$H_{SB} = -t\hat{\sigma}_x + \Delta\hat{\sigma}_z - \hat{\sigma}_z \sum_\mu \lambda_\mu (b_\mu + b_\mu^\dagger) + \hat{1} \sum_\mu \hbar\omega_\mu b_\mu^\dagger b_\mu \tag{1.11}$$

The λ_μ are electron-phonon coupling constants, t is tunneling between the qubit states, and Δ is qubit level detuning. The operators $\hat{\sigma}_x$, $\hat{\sigma}_z$ are Pauli matrices (not necesarily corresponding to spin):

$$\hat{\sigma}_x = \begin{pmatrix} 0 & 1 \\ 1 & 0 \end{pmatrix} \quad \hat{\sigma}_y = \begin{pmatrix} 0 & -i \\ i & 0 \end{pmatrix} \quad \hat{\sigma}_z = \begin{pmatrix} 1 & 0 \\ 0 & -1 \end{pmatrix} \quad \hat{1} = \begin{pmatrix} 1 & 0 \\ 0 & 1 \end{pmatrix} \tag{1.12}$$

The model cannot be exactly solved. In literature, the model has been the subject of some investigation, see [45], [47], sometimes with quantum computation in mind, because this involves qubits permanently coupled to a measurement apparatus (the boson bath).

For our purposes, the qubit will be a spinless electron hopping between two molecular sites, and the oscillations will be just one mode of nuclear vibrations. Thus, a spin-boson-like model shall describe a dimer in a model for transport in devices like the C_{140} SETs of Pasupathy et al.

1.12.1 Born-Oppenheimer approximation to the spin-boson model

In a Born-Oppenheimer approximation the dynamics of a problem involving electrons in a potential determined by nuclear coordinates is solved in two stages: 1)

The electronic problem is solved for nuclei fixed at equilibrium positions, and 2) the nuclear dynamics on each electronic energy surface is treated [49]. The approximation consists of defining the electronic states with respect to static equilibrium potentials. Since the force on the electron really originates from instantaneous positions of nuclei and not nuclear equilibrium positions, a correction should in general be added [50].

Returning to the spin-boson Hamiltonian, a 'typical' oscillator frequency ω_c can be defined in such a way that no oscillator with a frequency much larger than ω_c is present [45]. Ín the limit $\omega_c \ll t, k_B T$ the model can be solved, as each electronic eigenstate becomes associated with a Born-Oppenheimer surface.

1.12.2 Entanglement of a qubit with a single oscillator mode

We introduce the entanglement concept in chapter 2. Loosely speaking, entanglement is correlation between different degrees of freedom in a system. In ref. [51], Levine and Muthukumar analyze a simple spin-boson model with just one oscillator mode ω and one corresponding λ and no asymmetry between the qubit levels ($\Delta = 0$) using a many-body approach. They show that the bosonic and electronic degrees of freedom become entangled in the ground state for sufficiently strong coupling λ. They introduce a parameter α as the ratio between the classical displacement energy and the hopping t, $\alpha = \lambda^2/m\omega^2 t$, where m is the mass of the boson oscillator. A numerical calculation indicates that when ω/t becomes small, the transition to an entangled regime becomes increasingly sharp around $\alpha = 1$. Entanglement is measured as entanglement entropy S_N, which we define in chapter 2. In the limit $\omega/t \to 0$, the first derivative of S_N with respect to α seems to become discontinuous. The authors conclude that in the limit considered, entanglement entropy behaves in a manner analogous to thermodynamical entropy in a second order phase transition.

It should be pointed out that the transition into an entangled regime is continuous for all nonzero, finite parameter values. Only in the limit $\omega/t \to 0$ does the first derivate of the entanglement entropy become discontinuous. No actual phase transition takes place in the ground state, which is in accordance with a general theorem [57].

Chapter 2

Entanglement

2.1 Some information theory

The Shannon entropy for a set of N states $\{a_i\}$ with corresponding probabilities $\{p(a_i)\}$ is defined as

$$S_S(p(a_i)) = -\sum_{i=1}^{N} p(a_i)\ \ln\ p(a_i) \tag{2.1}$$

The quantum mechanical generalization of the Shannon entropy is the von Neumann entropy, which is a measure of the degree of mixing of the 'state' described by the density matrix ρ:

$$S_N(\rho) = -\mathrm{Tr}[\rho\ \log_d\ \rho] \tag{2.2}$$

where the base d of the logarithm is the dimension of the Hilbert space, and ρ has trace 1. The von Neumann entropy is independent of the choice of basis for ρ. Let $\{\gamma\}$ denote a basis in which ρ is diagonal, and denote the diagonal matrix elements by c_γ:

$$\rho = \sum_{\gamma} c_\gamma |\gamma\rangle\langle\gamma| \tag{2.3}$$

A 'pure state' is defined as a density operator ρ for which $\rho^2 = \rho$. If ρ is on the form (2.3), the condition means that one c_γ is equal to 1 and the rest are 0. Such a density matrix is just some superposition of eigenstates with no (environmentally induced) mixing. The von Neumann entropy in a pure state is 0:

$$-\sum_{\gamma} c_\gamma \log_d c_\gamma = (d-1)\ 0\ \log_d 0 + 1\ \log_d 1 = 0 \tag{2.4}$$

The other extreme is the mixed state that maximizes the entropy. In the representation (2.3), this is the mixed state where $c_\gamma = d^{-1}$ for all γ. The von Neumann entropy is 1:

$$-\sum_{\gamma} c_\gamma \log_d c_\gamma = d\ (d^{-1}\ \log_d d^{-1}) = d\ (d^{-1} \cdot 1) = 1 \tag{2.5}$$

using $\log_d x = \ln x / \ln d$. The choice of logarithm normalizes S_N.

Let S_1 denote the von Neumann entropy without the normalization, ie. the logarithm is just the natural logarithm. Given a thermal distribution of eigenstates $|j\rangle$, meaning $\rho = Z^{-1} \sum_j e^{-\beta E_j} |j\rangle\langle j|$, with the Boltzmann weights $e^{-\beta E_j}$ and the partition function $Z = \sum e^{-\beta E_j}$, and defining the free energy functional $F = -\beta^{-1} \log Z$, it is straightforward to derive $F = \langle U \rangle - \beta^{-1} S_1$:

$$\begin{aligned} S_1 &= -\mathrm{Tr}[\rho \log \rho] = -\sum_j \frac{e^{-\beta E_j}}{Z} \log \frac{e^{-\beta E_j}}{Z} = -\sum_j \frac{e^{-\beta E_j}}{Z} (-\beta E_j - \log Z) \\ &= \sum_j \frac{e^{-\beta E_j}}{Z} (\beta E_j - \beta F) = (\sum_j \frac{e^{-\beta E_j}}{Z} \beta E_j) - \beta F = \beta \langle U \rangle - \beta F \end{aligned} \tag{2.6}$$

This shows that the unnormalized von Neumann entropy reduces to thermodynamical entropy in this case.

If all states are equally probable, and N denotes the number of states, $S_1 = \ln N$, as it should be.

Now, consider a system composed of two subsystems A and B, each subsystem corresponding to a set of degrees of freedom; let $|\alpha\rangle$ and $|\beta\rangle$ denote the respective basis states, with α (β) the variable, or the set of variables, that describe the subsystem A (B). A basis for the 'full' system is the product basis $|\alpha\rangle \otimes |\beta\rangle$. The state of the system is described by a density matrix

$$\rho = \sum_{\alpha' \beta' \alpha'' \beta''} \rho_{\alpha' \beta', \alpha'' \beta''} |\alpha' \beta'\rangle \langle \alpha'' \beta''| \tag{2.7}$$

We define the reduced density matrices of the subsystems as

$$\rho_A = \mathrm{Tr}_B \rho \equiv \sum_{\alpha' \alpha''} \sum_{\beta} \rho_{\alpha' \beta, \alpha'' \beta} |\alpha'\rangle \langle \alpha''| \tag{2.8}$$

and similarly for ρ_B. The reduction throws out the non-diagonal-terms in the degree of freedom which is 'traced out'.

If A and B interact, the subsystem variables become interdependent and possibly correlated [68].

For the von Neumann entropy, the following properties hold [58]:

$$S_N(\rho_A) + S_N(\rho_B) \geq S_N(\rho) \geq |S_N(\rho_A) - S_N(\rho_B)| \tag{2.9}$$

hence, if ρ is a pure state, such that $S_N(\rho) = 0$,

$$S_N(\rho_A) = S_N(\rho_B) \tag{2.10}$$

Additivity:

$$S_N(\rho_A) + S_N(\rho_B) = S_N(\rho_A \otimes \rho_B) \tag{2.11}$$

Concavity:

$$S_N(\sum_i p_i \rho_i) \geq \sum_i p_i S_N(\rho_i) \tag{2.12}$$

which means that the mixing of states maintains or increases their 'uncertainty' S_N.

It can be shown that correlation between two subsystems, measured as

$$S_N(\rho_A) + S_N(\rho_B) - S_N(\rho) \tag{2.13}$$

cannot increase unless the subsystems interact [58].

Assume now that the 'full' system is in a pure state. Then, the subsystems A and B are in pure states if α and β are independent variables. Correlations between A and B imply that the reduced density matrices are mixed states; interactions between A and B tend to create mixing in the subsystems. If the full system density matrix is the product of the reduced density matrices, the state of the system is a product state, and the subsystems are uncorrelated. Such a state is called 'separable'. The density matrix ρ_{AB} is separable if and only if it can be written as a linear combination of pure product states:

$$\rho_{AB} = \sum_j p(j)\ |\alpha_j\rangle\langle\alpha_j| \ \otimes\ |\beta_j\rangle\langle\beta_j| \tag{2.14}$$

where $|\alpha_j\rangle$ ($|\beta_j\rangle$) are states in A (B), and $p(j)$ is some probability distribution.

All this lead us to the idea of entanglement. An entanglement measure is a function S_E of the full system density matrix ρ, such that $S_E(\rho) \in [0,1]$, $S_E(\rho) = 0$ if ρ is separable, and some technical requirements are fulfilled [58, 59]. The point is that S_E measures the extend to which ρ is not separable. A standard measure is the von Neumann entropy of a subsystem, ie. $S_N(\rho_A)$, also known as the entanglement entropy. Another measure is the linear entropy of the subsystem,

$$S_L(\rho_A) = \frac{d}{d-1}(1 - \mathrm{Tr}[\rho_A^2]) \tag{2.15}$$

with d the dimension of the reduced Hilbert space. Linear entropy distinguishes itself from the von Neumann entropy by being a much simpler function of the density matrix elements: $S_L(\rho_A)$ is a sum of products of two matrix elements of ρ_A, rather than arbitrarily many, as $S_N(\rho_A)$ is. However, the von Neuman entropy is especially nice, because it reduces to thermodynamical entropy in the case of a thermal distribution of eigenstates.

A more complicated entanglement measure is the relative entropy of entanglement, defined as

$$S_R(\rho) = \min_{\sigma \in D}\ \mathrm{Tr}[\rho\ \log\rho - \rho\ \log\sigma] \tag{2.16}$$

where D is the set of all separable density matrices in the Hilbert space, and minimization is performed over D. Numerically, implementation of this measure is nontrivial, and we are not going to do it. However, the measure nicely illustrates what entanglement is: a mathematical 'distance', measured as a difference in a generalized entropy function, between the density matrix of the state and the 'nearest'

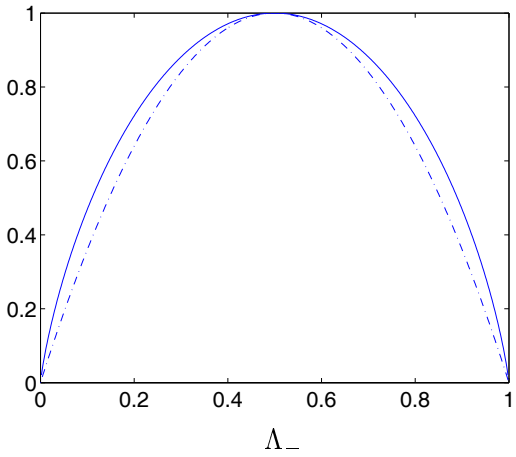

Figure 2.1: Entanglement entropy (-) and linear entropy (-·) as a functions of Λ_-.

separable matrix that exists in the Hilbert space. (The measure is not a legitimate metric, though.)

A legitimate measure of entanglement is related to the partially transposed density matrix, ρ^{T_B}, which is defined from ρ by applying

$$\rho_{\alpha'\beta',\alpha''\beta''} \rightarrow \rho_{\alpha'\beta'',\alpha''\beta'} \tag{2.17}$$

Nearly always, for an inseparable density matrix ρ, the partially transposed ρ^{T_B} will have at least one negative eigenvalue. Naturally, ρ and the 'traditionally' transposed, ρ^T, (properly normalized) always have only positive eigenvalues. The sum of the negative eigenvalues of ρ^{T_B} are a measure of entanglement [59] called 'negativity', which we denote $S_\div$:

$$S_\div(\rho) = 2\ \max(0, -\lambda_{neg}) \tag{2.18}$$

where λ_{neg} is the sum of the negative eigenvalues of ρ^{T_B}.

2.2 Entanglement of a qubit

As an example relevant to us, we consider a qubit described by a realvalued density matrix ρ_e, corresponding to a situation where the Hamiltonian of the 'full' system of the qubit + environment is real, and the system is in an eigenstate. In particular, the qubit-environment coupling contains no $\hat{\sigma}_y$ part. Denoting the qubit states a and b,

$$\rho_e = \begin{pmatrix} \rho_{aa} & \rho_{ab} \\ \rho_{ab} & 1-\rho_{aa} \end{pmatrix} \tag{2.19}$$

using that ρ_e is Hermitian and real, hence $\rho_{ba} = \rho_{ab}$, and that ρ_e has trace 1. Physically, the qubit may be a spinless electron with access to two localized site orbitals.

Let $\Lambda_\pm$ denote the eigenvalues of the matrix ρ_e. They are:

$$\Lambda_\pm = \frac{1}{2} \pm \sqrt{\frac{1}{4} - \rho_{aa} + \rho_{aa}^2 + \rho_{ab}^2} \tag{2.20}$$

and $\Lambda_+ + \Lambda_- = 1$ because diagonalization preserves the trace. In a basis where it is diagonal, ρ_e depends on just one independent variable:

$$\rho_e \to \begin{pmatrix} \Lambda_- & 0 \\ 0 & \Lambda_+ \end{pmatrix} = \begin{pmatrix} \Lambda_- & 0 \\ 0 & 1-\Lambda_- \end{pmatrix} \tag{2.21}$$

The mixing of the electronic eigenstates due to interaction with the environment is described by the entanglement entropy:

$$S_N(\rho_e) = -\mathrm{Tr}[\rho_e \log_2 \rho_e] \tag{2.22}$$

The trace is invariant under the unitary transformation that diagonalizes the matrix:

$$S_N(\rho_e) = -\Lambda_- \log_2 \Lambda_- - (1-\Lambda_-)\log_2(1-\Lambda_-) \tag{2.23}$$

When $\Lambda_- = \frac{1}{2}$ the electronic state is completely mixed and S_N is maximal. When $\Lambda_- = 0$ or 1, the qubit is in a pure state and $S_N = 0$.

Linear entropy is a much simpler function of the density matrix elements:

$$S_L = 2\Big(1 - \mathrm{Tr}[\rho_e^2]\Big) = 2\Big(1 - \Lambda_-^2 - \Lambda_+^2\Big) = 4\Big(\rho_{aa} - \rho_{aa}^2 - \rho_{ab}^2\Big) \tag{2.24}$$

where we diagonalized ρ_e in the trace. In terms of Λ_-,

$$S_L = 1 - (1-2\Lambda_-)^2 = -4\Lambda_-^2 + 4\Lambda_- \tag{2.25}$$

Comparing eq. (2.24) to eq.s (2.20) and (2.22), we see that $4\Big(\rho_{aa} - \rho_{aa}^2 - \rho_{ab}^2\Big)$ is the combination of matrix elements that determines entanglement entropy, as well. Both measures decrease with $|\rho_{aa} - \frac{1}{2}|$ and with $|\rho_{ab}|$.

In the absence of environment interaction, the electronic density matrix is a pure state. Write the electronic eigenstate as

$$v_a|a\rangle + v_b|b\rangle \tag{2.26}$$

where the coefficients are realvalued. Then, $1 - \rho_{bb} = \rho_{aa} = v_a^2$, $\rho_{ba} = \rho_{ab}$, and

$$\rho_{ab}^2 = (v_a v_b)^2 = \rho_{aa}\rho_{bb} = \rho_{aa}(1-\rho_{aa}) = \rho_{aa} - \rho_{aa}^2 \tag{2.27}$$

This leads to $\Lambda_\pm = 0, 1$ and to $S_L = S_N = 0$, as they should be. From eq. (2.27), we see how S_L (and S_N) is a numerical measure of how far a generalized qubit state is from being a state in the 2D Hilbert space.

In general, interaction with an environment causes dephasing of the qubit. A crude description [42] interprets environment interaction, through an operator $\hat{\sigma}_z$, as collisions that last a very short time and destroy the phase coherence in the qubit state. The ratio of the time between 'collisions' to the time between tunnelings between the states a and b determines the degree to which phase coherence is lost, and ρ_{ab} reduced from it's value (2.27).

Chapter 3

A model for transport in a dimer device

3.1 Motivation and a toy model

We want to understand the anomalous, observed diamond plots for the C_{70} dimers in ref. [30], section (1.9). As a starting point, we consider a 'toy model' without phonons that could account for the rectification and NDC:

Consider that each of the parts of the dimer can accomodate zero or one electron, call the dimer sites a, b, and that Coulomb repulsion between two electrons is much larger than all other energies, so only one electron can occupy the dimer at any time. The electron cannot tunnel between the dimer sites. Now, assume that the device is highly asymmetrical, in the sense that,

- 1): tunnelings between the dimer and the 'right' electrode are much smaller than tunnelings between the dimer and the 'left' electrode, and

- 2): 'right' tunneling at site a is practically 0 compared to 'right' tunneling at

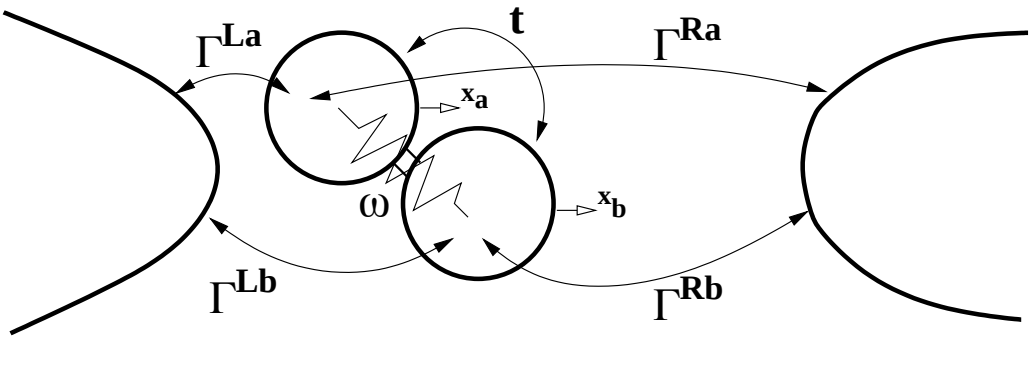

Figure 3.1: The dimer SET device considered in this work.

site b.

The geometry is the one depicted in fig. (3.1). The electron particle current from left to right is strongly inhibited, because whenever an electron tunnels onto site a, it gets stuck there for long periods of time, as the small rate Γ^{Ra} becomes a tight 'bottleneck' for the current. During these periods of time, no current can run via the b site due to 'infinite' Coulomb repulsion between electrons on the two sites. In the opposite direction of the bias voltage, there is no such blocking effect, because out-tunnelings from either site are much faster than the in-tunnelings. This accounts for the rectification. The model also gives rise to NDC at finite temperature: an electron on site a may tunnel out to the left against the bias voltage if $e|V| < k_B T$. This shortens the average time a blocking electron spends on the molecule, increasing the current when bias voltage is decreased. In the blocking direction, therefore, a larger current may run at small bias voltages than in the limit of large bias voltages. This means there must exist an interval of V where $\partial I/\partial V < 0$.

The problem with the rectification mechanism described above is that the model is not realistic: the dimer is not a double dot, because the localized electronic states are not orthogonal. A more realistic model might include two tunneling coupled, localized site orbitals, with the tunneling determined by the overlap of the orbitals. Also, we need our model to include electron-phonon coupling, because that is what we, and Pasupathy et al., are really concerned with. All this leads to a spin-boson-like model for the dimer.

Conceivably, if the electron-phonon interaction is strong, a polaron state could emerge, effectively confining the electron on the dimer to one site. In an asymmetrical device, this could lead to the observed asymmetries in the IV characteristics in the fashion described above.

3.2 The system

The system under consideration is a SET device consisting of a dimer attached to 'left' and 'right' leads and a gate voltage. The leads could be gold electrodes, and the gate voltage could be applied through a substrate. Each part of the dimer has one electron site, and the sites are assumed to be tunneling coupled, corresponding to two hybridized levels on opposite parts of the dimer. We neglect spin and possible degeneracies of the hybridizing orbitals. Coulomb repulsion between the sites is larger than all relevant energies. The coupling to the electrodes is weak compared to the other energies in the problem, hence we are in the incoherent, sequential transport regime, where the tunneling between the dimer and the electrode Fermi seas is described by Master equations ('classical' rate equations). The justification for this approach is that the 'dwell time', ie. the time an electron dwells on the island before tunneling out again, is large compared to the other timescales, given by h/E for any relevant energies E. This means that the dimer can be treated as a closed quantum system between tunneling events [52].

Due to van der Waals interactions between each part of the dimer and the electrodes, the two parts of the dimer perform small oscillations around their equilibrium positions in a potential [10]. We assume the existence of an intercage stretching mode of the dimer, and aknowledge that many other molecular modes may be present and affect the motion, such as 'bending' and 'twisting' intercage modes. When an electron hops onto a dimer site, the equilibrium position of the site is shifted due to a changing local electrical field, mainly a consequence of image charges in the leads [10].

The electron-vibron coupling turns out to be effectively a coupling between the difference in charge on the sites and the 'tilting' of the molecule. The frequency of the effective 'tilting' oscillation is a combination of the frequencies of the three (or more) modes. The effective 'tilting' mode is quantized.

3.2.1 Dissipation of energy

Energy dissipates from the system through an environment interaction, which we think of as a bath of boson oscillators to which the vibron linearly couple (as in [28]). We assume that the dissipation dampens the oscillations of the dimer much faster than the electronic dwell time, such that the molecule and electrodes are in thermal equilibrium just before tunneling takes place.

Formally, our assumption is $\boldsymbol{\gamma} \gg \Gamma$, where Γ is a characteristic tunneling rate (defined below), and the dissipational frequency $\boldsymbol{\gamma}$ (which we take independent of electron frequency) is the inverse oscillator life time divided by 2π. The Q-factor is defined as the mean energy stored in the oscillator divided by the energy dissipated during one period; it holds that $Q = \frac{\omega}{\boldsymbol{\gamma}}$. In the limit of small Γ, there is no tunneling broadening of the conductance peaks; this feature is implicit in our model.

We disregard dissipative broadening of the steps. In [28], this corresponds to the limit of 'vanishing' bath coupling, or infinite Q. For finite Q, the assumption is that thermal broadening dominates over dissipative broadening: $k_B T > \boldsymbol{\gamma}$, or $\frac{k_B T}{\omega} > \frac{1}{Q}$. Also, from [28], we must have $Q > \frac{2g}{\pi}$, or $\frac{\boldsymbol{\gamma}}{\omega} < \frac{\pi}{2g}$: for dissipation larger than this, the steps are smeared even at $T = 0$.

Putting it together, we require:

$$\frac{k_B T}{\omega}, \ \frac{\pi}{2g} > \frac{\boldsymbol{\gamma}}{\omega} \gg \frac{\Gamma}{\omega} \tag{3.1}$$

Thermal broadening of the conductance peaks is given by a distribution

$$P(\epsilon) \sim \frac{1}{T \cosh^2(\epsilon / k_B T)} \tag{3.2}$$

Our approach assumes that even though T is in a sense large, it is not large enough to interfere with the state of the dimer except through the Boltzmann probability distribution for the relaxed states. Temperature does not directly disturb the phase coherence of the electron.

We make one further, initial assumption that we shall eventually move beyond: we assume that the dissipation $\boldsymbol{\gamma}$ does not interfere with the system beyond causing relaxation. In particular, dissipation is not strong enough to cause localization of the electron. This could in general happen, because dissipation to a substrate is well-described by coupling of the form (1.8), and strong enough coupling will cause the system ground state to be an approximate eigenstate of x. In a model where x couples to $\hat{\sigma}_z$, such as the one we define below, this localizes the electron.

3.2.2 Device geometry

The two parts of the dimer are identical, each has mass m and vibrate in the local electrical field at frequencies ω_a, ω_b if no molecular modes interfere; such modes are considered below. We assume an equilibrium geometry for the dimer in which the four distances between the dimer sites and the electrodes may be unequal. The distances are inversely related to the tunneling rates. See fig. (3.1).

The vibrational modes are described by terms

$$\frac{p_a}{2m} + \frac{p_b}{2m} + \frac{1}{2}m\omega_a^2 x_a^2 + \frac{1}{2}m\omega_b^2 x_b^2 \tag{3.3}$$

in the Hamiltonian, with the coordinates x_a, x_b denoting the one dimensional, parallel displacements of the sites, see fig. (3.1). Phonons couple linearly to the displacements:

$$\lambda_1(n_a x_a + n_b x_b) \tag{3.4}$$

where n_a, n_b are the electron number operators for the respective sites, and λ_1 is the coupling constant, which is assumed equal for the two modes. We introduce transformed coordinates,

$$x = x_a - x_b \qquad y = x_a + x_b \tag{3.5}$$

For simplicity, we assume $\omega_a = \omega_b$. The oscillator terms become

$$\frac{p_x}{2m} + \frac{p_y}{2m} + \frac{1}{2}m\omega_a^2 x^2 + \frac{1}{2}m\omega_a^2 x_y^2 \tag{3.6}$$

The interaction terms become

$$\lambda N y + \lambda x(n_a - n_b) \qquad\qquad \lambda \equiv \frac{\lambda_1}{2} \tag{3.7}$$

where $N = n_a + n_b$ is the electron total number operator, which changes only on the slow time scale of the in- and out-tunneling rates. Coupling to N is effectively a constant contribution to the energy, and the y oscillator is effectively decoupled from the rest of the Hamiltonian. We therefore neglect the y mode, turning our attention to the coupling between the charge difference of the sites and the 'tilting' coordinate, x.

We now consider how the 'tilting' mode is affected by the modes of the molecule, in particular the intercage 'stretching' mode, which according to [30] in fact gives rise to the observed vibrational sidebands in the C_{70} dimer experiments. Let ω_I denote the frequency of the stretching mode. Clearly, this mode is geometry-dependent, because if the dimer is orientated along the direction of the displacements, the mode follows the x coordinate, and if the dimer is in a direction orthogonal to the 1D displacements, the mode is independent of the 'field' modes and does not couple to vibrations, anyway.

A rough treatment assumes the C_{70}s are points in space, not worrying about keeping them face to face during the motion. This corresponds to neglecting intercage bending and twisting modes of the dimer. In the appendix, we show that this approach leads to an angular dependence of the effective 'tilting' frequency,

$$\omega^2 = \omega_a^2 + \omega_I^2 \sin^2\theta_0 \tag{3.8}$$

where θ_0 is the angle between the dimer and the plane normal to the displacement x. Realistically, the angular dependence is more complicated; the point is that when we compare to experiment, we have to keep in mind that the mode we observe may not have a simple origin. In experiments, the placement of the molecule in the constriction is unknown.

In the following, we shall therefore consider ω an effective frequency of the 'tilting' mode, not judging whether it comes about as an intercage stretching mode, a mode determined by the electric potential, other molecular modes, or combinations thereof.

3.2.3 Model Hamiltonian

Let $\eta \in \{L, R\}$ denote the electrode Fermi seas and $\sigma \in \{a, b\}$ the dimer electron sites. The full Hamiltonian is

$$H + H_U + \sum_\eta (H_{T\eta} + H_\eta) \tag{3.9}$$

where H is the Hamiltonian for the dimer, $H_{T\eta}$ is the Hamiltonian for tunneling between the dimer and the lead η, and H_η is the Hamiltonian for the lead electrons.

The dimer Hamiltonian:

$$H = \frac{p_x^2}{2m} + \frac{p_y^2}{2m} + \frac{1}{2}m\omega^2 x^2 + \frac{1}{2}m\omega_a^2 y^2 + \lambda N y + \lambda x(n_a - n_b) - t(c_a^\dagger c_b + c_b^\dagger c_a) + \epsilon_a n_a + \epsilon_b n_b \tag{3.10}$$

The coordinates x, y were defined in the previous section, with ω an effective frequency for the 'tilting' motion. The annihilation operators for the spinless electron are c_σ with σ denoting the site. The electron number operators are $n_\sigma = c_\sigma^\dagger c_\sigma$. The energy for tunneling between the electron sites is t; we have defined $t > 0$. For the coupling, we assume $\lambda > 0$ without loss of generality. The dimer on-site energies are ϵ_σ.

The lead Hamiltonian:

$$H_\eta = \sum_k \xi_{k\eta} c^\dagger_{k\eta} c_{k\eta} \tag{3.11}$$

the electron energies $\xi_{k\eta}$ defined relative to the chemical potentials of the leads.

The tunneling Hamiltonian:

$$H_{T\eta} = \sum_{\sigma k} (T_{k\eta\sigma} c^\dagger_{k\eta} c_\sigma + T^*_{k\eta\sigma} c^\dagger_\sigma c_{k\eta}) \tag{3.12}$$

The tunneling amplitudes $T_{k\eta\sigma}$ depend on the position of the dimer between the electrodes. They change on a scale of nm [28], and the dimer is about a nm long; therefore, we distinguish between $T_{k\eta\sigma}$ for $\sigma = a, b$. The oscillator displacements l (defined below) are a few pm, and so we disregard the dependence of the $T_{k\eta\sigma}$ on oscillator position.

The Coulomb repulsion between two electrons on the dimer:

$$H_U = U n_a n_b \tag{3.13}$$

We assume that we are in a regime of 'infinite' Coulomb repulsion, $U \approx \infty$, prohibiting the doubly occupied state. This is realistic in small systems. We therefore need to consider only two charge states, which we denote by 'empty' and 'filled' for $N = 0, 1$. The approximation in the incoherent transport approach is that N is always an integer and the charge states may be treated separately.

The on-site energies depend on the gate voltage. We rewrite the onsite energy terms as

$$\Delta(n_a - n_b) + \frac{1}{2} N(\epsilon_a + \epsilon_b) \tag{3.14}$$

with $\Delta \equiv \frac{1}{2}(\epsilon_a - \epsilon_b)$, which can be assumed gate voltage independent at realistic energies; that is, a change in gate voltage translates ϵ_a and ϵ_b by the same energy. We can therefore assume $\epsilon_a \geq \epsilon_b$ without loss of generality. This means $\Delta \geq 0$.

At fixed gate voltage, the second term in eq. (3.14) is a constant energy difference between the 'empty' and 'filled' sets of dimer eigenstates. In reality, the gate voltage may not determine the onsite energies in a linear fashion, but for simplicity we assume that it does, or rather, we define the gate voltage V_g from it's effect on the onsite energies:

$$eV_g = \frac{1}{2}(\epsilon_a + \epsilon_b) \tag{3.15}$$

Previously, we argued that the y mode is not interesting, because the mode is decoupled from the rest of the problem, merely giving rise to harmonic oscillator levels superimposed on the x part of the problem. Now, we implement the decision to ignore y by assuming that the y oscillator remains in it's ground state. We shall even ignore the ground state energy of $\omega_a/2$. The great thing about this simplification is that it shall allow us to diagonalize H numerically.

The electron-vibron coupling term we are left with is the term $\lambda x(n_a - n_b)$. The coupling is to the charge difference between the two parts of the dimer, and x

is a cordinate for the tilting of the dimer with respect to its equilibrium position in the electric potential. This interaction may be nonzero for the filled dimer only; for the empty (or double-occupied, had we allowed it) dimer, the eigenstates are just the states of a quantized harmonic oscillator.

Introducing the boson operators a, $a^\dagger$ for the x oscillator, and the quantum oscillator length

$$l_0 = \sqrt{\frac{\hbar}{m\omega}} \tag{3.16}$$

and defining $\lambda' = \frac{l_0}{\sqrt{2}}\lambda$, we are left with a numerically diagonalizable Hamiltonian:

$$H = \hbar\omega(a^\dagger a + \frac{1}{2}) + \lambda'(a^\dagger + a)(n_a - n_b) - t(c_a^\dagger c_b + c_b^\dagger c_a) + \Delta(n_a - n_b) \tag{3.17}$$

This is a spin-boson like model,

$$H = \hbar\omega(a^\dagger a + \frac{1}{2}) + \lambda'(a^\dagger + a)\hat{\sigma}_z - t\hat{\sigma}_x + \Delta\hat{\sigma}_z \tag{3.18}$$

where $\hat{\sigma}_x$, $\hat{\sigma}_z$ are Pauli matrices (1.12) in the basis of the c operators. Of the energies $\hbar\omega$, t, λ', Δ, only three are independent energy variables in the Hamiltonian. The Hamiltonian in dimensionless form:

$$\frac{1}{\hbar\omega}H = a^\dagger a + \frac{1}{2} + \sqrt{g}\ \hat{\sigma}_z\ (a^\dagger + a) - \frac{2g}{\alpha}\ \hat{\sigma}_x + \delta\ \hat{\sigma}_z \tag{3.19}$$

Here, we have defined dimensionless parameters g, α, and δ,

$$g = \frac{l^2}{2{l_0}^2} = \frac{\lambda^2}{2m\hbar\omega^3} = \frac{l_0^2\lambda^2}{2\hbar^2\omega^2} \tag{3.20}$$

$$\alpha = \frac{\lambda^2}{m\omega^2 t} = \frac{l_0^2\lambda^2}{\hbar\omega t} \tag{3.21}$$

$$\delta = \frac{\Delta}{\hbar\omega} \tag{3.22}$$

where l is the classical oscillator displacement length,

$$l = \frac{\lambda}{k} \qquad k = m\omega^2 \tag{3.23}$$

Hence, $2g$, being the ratio of the oscillator displacement squared to the quantum oscillator length squared, is a measure of how far into the classical regime the quantized oscillator is. The classical oscillator displacement energy is $E_{disp} \equiv \lambda l$, and the ratio of λl to the tunneling energy t is the parameter α. When α is far from 1, one of the energies E_{disp}, t dominate over the other.

Note the relation $2g\hbar\omega = \alpha t$.

The Hamiltonian can be expressed in terms of bonding and antibonding electron states by defining operators

$$d_\pm = \frac{1}{\sqrt{2}}(c_a \pm c_b) \qquad d_\pm^\dagger = \frac{1}{\sqrt{2}}(c_a^\dagger \pm c_b^\dagger) \tag{3.24}$$

These are the creation and annihilation operators for the electron bonding and antibonding states. The corresponding number operators are

$$n_\tau = d_\tau^\dagger d_\tau \qquad (\tau \in \{+,-\}) \tag{3.25}$$

Easy calculation yields

$$n_\tau = \frac{1}{2}(N + \mathrm{sign}(\tau)(c_a^\dagger c_b + c_b^\dagger c_a)) \qquad (\mathrm{sign}(\tau) \sim \tau) \tag{3.26}$$

$$c_a^\dagger c_a - c_b^\dagger c_b = -(d_+^\dagger d_- + d_-^\dagger d_+) \qquad c_a^\dagger c_b + c_b^\dagger c_a = d_+^\dagger d_+ - d_-^\dagger d_- \tag{3.27}$$

For the Pauli matrices, the transformation to bonding and antibonding states corresponds to the replacement

$$\hat{\sigma}_z \to -\hat{\sigma}_x \qquad \hat{\sigma}_x \to \hat{\sigma}_z \tag{3.28}$$

From this point forward we will work in units where $\hbar = 1$. The mass enters the problem only through the l_0 parameter, which is a natural unit for length. Of the four energy parameters, H depends independently on only three; a convenient energy unit is ω.

3.3 Diagonalization

The matrix for the 'filled' dimer Hamiltonian ($N = 1$) at $V_g = 0$ is calculated:

$$H_{(N=1)} = \sum_{\sigma n, \sigma' n'} |\sigma n\rangle\langle\sigma' n'|\langle\sigma n|H|\sigma' n'\rangle \tag{3.29}$$

where we have chosen the basis $\{|\sigma, n\rangle\}$ where $\sigma \in \{a, b\}$ denotes the occupied electron site, and $\{n\}$ are the vibron levels.

The matrix representation of $H_{(N=1)}$ written out:

$$\begin{pmatrix}
(\frac{1}{2}+\delta)\omega & -t & \lambda' & 0 & 0 & 0 & 0 & 0 & \dots \\
-t & (\frac{1}{2}-\delta)\omega & 0 & -\lambda' & 0 & 0 & 0 & 0 & \dots \\
\lambda' & 0 & (\frac{3}{2}+\delta)\omega & -t & \sqrt{2}\lambda' & 0 & 0 & 0 & \dots \\
0 & -\lambda' & -t & (\frac{3}{2}-\delta) & 0 & -\sqrt{2}\lambda' & 0 & 0 & \dots \\
0 & 0 & \sqrt{2}\lambda' & 0 & (\frac{5}{2}+\delta)\omega & -t & \sqrt{3}\lambda' & 0 & \dots \\
0 & 0 & 0 & -\sqrt{2}\lambda' & -t & (\frac{5}{2}-\delta)\omega & 0 & -\sqrt{3}\lambda' & \dots \\
0 & 0 & 0 & 0 & \sqrt{3}\lambda' & 0 & (\frac{7}{2}+\delta)\omega & -t & \dots \\
0 & 0 & 0 & 0 & 0 & -\sqrt{3}\lambda' & -t & (\frac{7}{2}-\delta)\omega & \dots \\
\vdots & \vdots & \vdots & \vdots & \vdots & \vdots & \vdots & \vdots & \ddots
\end{pmatrix} \tag{3.30}$$

The matrix is of infinite dimension; we use a sufficiently large matrix and diagonalize numerically in a truncated Hilbert space of dimension D, using Matlab. In

the diagonalization, the number of bosonic states in the truncated basis should be larger than $2\sqrt{(\frac{2g}{\alpha})^2+\delta^2}$, a sufficiently large number of bosons to span the electronic band gap (section (3.5.1)), and larger than $\frac{E_{disp}}{\omega} = 2g$ to span the energy difference between the different dimer displacements. In practize, we always check that our truncated Hilbert space is large enough, by comparing the results of calculations for different D. Not all expectation values of physical observables converge equally fast as a functions of D. Usually, we can get away with H a 100×100 matrix, because $g > 10$ is physically not very relevant.

A matrix M is constructed from the normalized eigenvectors by sorting them by their eigenvalues and using them as columns; let $M_{\sigma n,j}$ denote the matrix elements. M is real because H is real. $M_{\sigma n,j}$ is the overlap between the basis state $\{|\sigma, n\rangle\}$ and the j'th eigenstate of $H_{(N=1)}$. Electron transport depends on these overlaps.

3.3.1 Exact calculations of 'filled' dimer expectation values

In the course of this work, we will calculate 'exact' expectation values for some relevant operators. Consider an exact eigenstate of the 'filled' dimer in our numerical diagonalization:

$$|\Psi\rangle = \sum_{\sigma n} \nu_{\sigma n} |\sigma n\rangle \tag{3.31}$$

If $|\Psi\rangle$ is the j'th eigenstate, then $\nu_{\sigma n} = M_{\sigma n,j}$. The coefficients $\nu_{\sigma n}$ are all real.

The eigenstate (3.31) corresponds to the density operator

$$\rho = \sum_{\sigma n} \sum_{\sigma' n'} \nu_{\sigma' n'} \nu_{\sigma n} |\sigma n\rangle\langle \sigma' n'| \tag{3.32}$$

The reduced density matrix ρ_e for the electron is found by 'tracing out' the bosons,

$$\rho_e = \sum_{\sigma\sigma'} \Big(\sum_n \rho_{\sigma n,\sigma' n} \Big) |\sigma\rangle\langle\sigma'| \cong \begin{pmatrix} \rho_{aa} & \rho_{ab} \\ \rho_{ab} & 1-\rho_{aa} \end{pmatrix} \tag{3.33}$$

where $\rho_{aa} \in [0,1]$, $\rho_{ab} \in [0, \frac{1}{2}]$. We have used that ρ_e is real, as in section 2.2.

For any physical observable $\hat{O}$, if the system is in a state like (3.31), the expectation value of $\hat{O}$ is $\langle\Psi|\hat{O}|\Psi\rangle$. In the appendix, we list how expectation values of various operators are given from the 'exact' eigenstate coefficients $\nu_{\sigma n}$.

We introduce the convention that whenever we perform 'exact', numerical calculations, we set $l_0 = 1$, $\omega = 1$.

3.4 The isolated electron

We pause to consider the isolated electron without coupling to the bosons; we shall need the notation. Defining

$$K \equiv -\frac{\delta\omega}{t} \qquad K_+ = K + \sqrt{1+K^2} \qquad K_- = K - \sqrt{1+K^2} \tag{3.34}$$

the electron Hamiltonian in basis of the c operators can be written

$$H_e = t \begin{pmatrix} -K & -1 \\ -1 & K \end{pmatrix} \tag{3.35}$$

The eigenenergies are

$$E_\pm = \pm t\sqrt{1+K^2} \tag{3.36}$$

and the corresponding eigenvectors can be written (derivation in the appendix),

$$v^{(+)} = \frac{1}{\sqrt{1+K_+^2}} \begin{pmatrix} K_+ \\ 1 \end{pmatrix} \qquad v^{(-)} = \frac{1}{\sqrt{1+K_-^2}} \begin{pmatrix} K_- \\ 1 \end{pmatrix} \tag{3.37}$$

When $K \to 0$, then $K_+ \to 1$, $K_- \to -1$, and $v^{(+)}$ becomes the bonding state $(1,1)/\sqrt{2}$, and $v^{(-)}$ becomes the antibonding state $(-1,1)/\sqrt{2}$. When $K \to \infty$ the states become localized, as $v^{(+)} \to (1,0)$ and $v^{(-)} \to (0,1)$.

Localization in the eigenstate is measured by $\langle\hat{\sigma}_z\rangle$ which becomes $+1$ when the state is localized to site a, -1 when the state is localized to site b, and 0 when the electron density is equally distributed over the sites. When $\delta\omega \gg t$ the state is approximately localized, with $|\langle\hat{\sigma}_z\rangle| \approx 1$.

Hybridization of the localized site orbitals is measured by $\langle\hat{\sigma}_x\rangle$ which is 1 in the bonding state, -1 in the antibonding state, and 0 in a localized state. When $t \gg \delta\omega$, $|\langle\hat{\sigma}_x\rangle| \approx 1$.

In either eigenstate,

$$|\langle\hat{\sigma}_z\rangle| = \frac{|K|}{\sqrt{1+K^2}} = \sin(\arctan(|K|)) \tag{3.38}$$

$$|\langle\hat{\sigma}_x\rangle| = \frac{1}{\sqrt{1+K^2}} = \cos(\arctan(|K|)) \tag{3.39}$$

derived in the appendix and plotted in fig. (3.2). The consequences of an electronic eigenstate asymmetry δ is to localize the electron toward the lower energy site, and to reduce the hybridization, as well as enlarge the electronic band width from $2t$ to $2t\sqrt{1+\delta^2\omega^2/t^2}$.

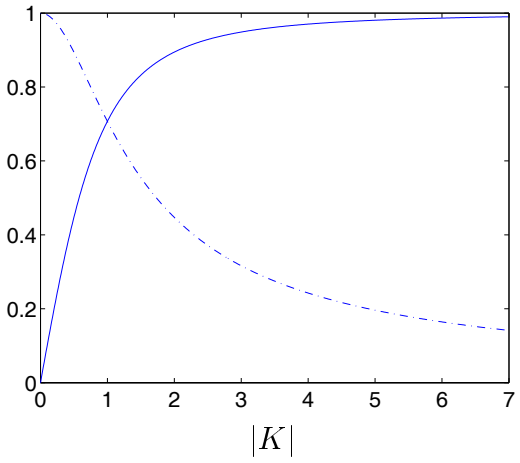

Figure 3.2: Plotted as functions of $|K|$: $\frac{1}{\sqrt{1+K^2}}$ (-·), $\frac{|K|}{\sqrt{1+K^2}}$ (-).

3.5 Sequential transport

Treating sequential transport in a quantum dot, the standard approach is to calculate tunneling rates from Fermi's Golden Rule and then express the current from rate equations, a so-called Master equation approach; eg., ref. [52]. In our double dot, we must show some care, because tunnelings to and from the 'island' can occur by two sites, and in general the relative phase between the site orbitals could be important. Therefore, we sketch the calculation here.

Consider the rate Γ^{η}_{10} for in-tunneling from the lead $\eta \in \{a, b\}$ when the system is in some definite initial state $|I\rangle$. By the Golden Rule, the rate is a sum over possible final states of the full system, consisting of the molecule and the leads, such that energy is conserved. With $|F\rangle$ denoting the final states,

$$\Gamma^{\eta}_{10} = \frac{2\pi}{\hbar} \sum_{F} |\langle F|H_{T\eta}|I\rangle|^2 \; \delta(E_I - E_F) \tag{3.40}$$

Following standard calculations [52], we insert product states, ie. $|I\rangle = |FS\rangle \otimes |i\rangle$ and $|F\rangle = c_{k\eta}|FS\rangle \otimes |f\rangle$, with $|FS\rangle$ denoting the Fermi sea thermal ground state, and $|f\rangle$, $|i\rangle$ denoting the final and initial states of the molecule. Inserting $H_{T\eta}$, the electrode part of the rate eventually becomes the Fermi function,

$$n_{\eta}(\epsilon_{k\eta}) = \frac{1}{e^{\beta(\epsilon_{k\eta} - \mu_{\eta})} + 1} \tag{3.41}$$

and the rate becomes ($\hbar \to 1$)

$$\Gamma^{\eta}_{10} = 2\pi \sum_{k,f} |\langle f|T^{*}_{k\eta a} c^{\dagger}_{a} + T^{*}_{k\eta b} c^{\dagger}_{b}|i\rangle|^2 \; n_{\eta}(\epsilon_{k\eta}) \; \delta(E_i - (E_f - \epsilon_{k\eta})) \tag{3.42}$$

where E_f depends on the gate voltage. Using $|a+b|^2 = |a|^2 + |b|^2 + 2\ \mathrm{Re}(a\ b^*)$,

$$|\langle f|T^*_{k\eta a}c^\dagger_a + T^*_{k\eta b}c^\dagger_b|i\rangle|^2 = \\ |\langle f|T^*_{k\eta a}c^\dagger_a|i\rangle|^2 + |\langle f|T^*_{k\eta b}c^\dagger_b|i\rangle|^2 + 2\ \mathrm{Re}\Big(\langle f|T^*_{k\eta a}c^\dagger_a|i\rangle\langle f|T^*_{k\eta b}c^\dagger_b|i\rangle^*\Big) \quad (3.43)$$

The rate can be split up:

$$\Gamma^\eta_{10} = \sum_\sigma \Gamma^{\eta\sigma}_{10} + \Gamma^{\eta c}_{10} \quad (3.44)$$

where $\Gamma^{\eta\sigma}_{10}$ are the terms proportional to $|T_{k\eta\sigma}|^2$, and $\Gamma^{\eta c}_{10}$ contains the crossterms $T^*_{k\eta a}T_{k\eta b}$.

First, we treat the 'diagonal' terms. The sum over k is replaced by an integral, $\sum_k \to \int d\epsilon\rho_\eta(\epsilon)$, where the density of states $\rho_\eta(\epsilon)$ is for the gold electrodes, and is considered continuous. The calculation is simplified by taking $\rho_\eta(\epsilon)$ as ϵ-independent, which is justified, because the density of states of gold is approximately constant near the Fermi level, and we will consider only bias voltages sufficiently small that the deviation is insignificant. Also, $|T_{\eta\sigma}(\epsilon)|^2$ can be taken as a constant on the energy scale. Introducing

$$\Gamma^{\eta\sigma} \equiv 2\pi\rho_\eta|T_{\eta\sigma}|^2 \quad (3.45)$$

the diagonal contributions become

$$\Gamma^{\eta\sigma}_{10} = \Gamma^{\eta\sigma}\sum_f \int \mathrm{d}\epsilon|\langle f|c^\dagger_\sigma|i\rangle|^2 n_\eta(\epsilon)\delta(E_i - (E_f - \epsilon)) = \Gamma^{\eta\sigma}\sum_f |\langle f|c^\dagger_\sigma|i\rangle|^2 n_\eta(E_f - E_i) \quad (3.46)$$

which are simple functions of the matrix elements we have calculated in our exact diagonalization of $H_{(N=1)}$.

The rate $\Gamma^{\eta c}_{10}$, on the other hand, seems entirely intractable, because it depends on the crossterms $T^*_{k\eta a}T_{k\eta b}$. While the absolute squares of $T_{k\eta\sigma}$ are important parameters in the problem, the relative phase between the opposite site tunneling amplitudes at some k could be anything. However, $T^*_{k\eta a}T_{k\eta b} \sim e^{ikd}$ where d is the distance between the site localized orbitals. The length d is large compared to the Fermi wave length, $k_F d \gg 1$, and therefore the phase is very fast rotating when k is varied near the Fermi level. Therefore, the average over k should be very close to 0, and we let $\Gamma^{\eta c}_{10} = 0$ in the following.

Having assumed that the initial state in the tunneling processes is a thermal distribution of eigenstates of the molecule, we insert a Boltzmann distribution of states for the initial state. The in-tunneling rates become

$$\Gamma^{\eta\sigma}_{10} = \Gamma^{\eta\sigma}\sum_{i_0}\sum_{f_1}|\langle f_1|c^\dagger_\sigma|i_0\rangle|^2\frac{e^{-\beta E_{i_0}}}{Z_0}n_\eta(E_{f_1}(V_g) - E_{i_0}) \quad (3.47)$$

where the added subscript 0 or 1 refers to the 'empty' or 'filled' charge state of the molecule, $\beta = 1/k_BT$, and $Z_0 = \sum_{n=0}^\infty e^{-\beta E_{i_0}}$. The 'empty' molecule eigenstates

are just harmonic oscillator states with energies $(n+\frac{1}{2})\omega$, and the 'empty' molecule ground state energy is $E_{0_0} = \frac{\omega}{2}$. The 'filled' molecule eigenenergies at $V_g = 0$ were found in the diagonalization of H. The 'filled' eigenenergies here are gate voltage dependent, $E_{f_1}(V_g) = E_{f_1}(V_g = 0) + eV_g$. The 'filled' molecule ground state energy is E_{0_1}.

By similar calculations and approximations, the out-tunneling rates become

$$\Gamma_{01}^{\eta\sigma} = \Gamma^{\eta\sigma} \sum_{i_1} \sum_{f_0} |\langle f_0|c_\sigma|i_1\rangle|^2 \frac{e^{-\beta E_{i_1}(V_g)}}{Z_1}(1 - n_\eta(E_{f_0} + E_{i_1}(V_g))) \tag{3.48}$$

where $Z_1 = \sum_j e^{-\beta E_{j_1}}$ and $E_{i_1}(V_g) = E_{i_1}(V_g = 0) + eV_g$.

In the expression for $\Gamma_{10}^{\eta\sigma}$, for each initial state, the sum over final states is a sum over the columns of M, as the matrix elements in eq. (3.47) are the $M_{\sigma n,j}$, with j corresponding to f_1 and σn corresponding to i_0. In the $\Gamma_{01}^{\eta\sigma}$ expression, the matrix elements $\langle f_0|c_\sigma|i_1\rangle$ may be replaced by $\langle i_1|c_\sigma^\dagger|f_0\rangle$. Here, the sum over final states is a sum over the rows of M.

We define $\Gamma_{10}^{\eta} = \sum_\sigma \Gamma_{10}^{\eta\sigma}$ and $\Gamma_{01}^{\eta} = \sum_\sigma \Gamma_{01}^{\eta\sigma}$.

Now, let P_i, $i = 0, 1$, denote the probabilities for the molecule to be occupied by 0 or 1 electron. The steady state rate equations, with $\dot{P}_0 = \dot{P}_1 = 0$, are:

$$1 = P_0 + P_1 \tag{3.49}$$

$$0 = -P_0(\Gamma_{10}^L + \Gamma_{10}^R) + P_1(\Gamma_{01}^L + \Gamma_{01}^R) \tag{3.50}$$

From this follows

$$P_1 = 1 - P_0 = \frac{\Gamma_{10}^L + \Gamma_{10}^R}{\Gamma_{10}^L + \Gamma_{10}^R + \Gamma_{01}^L + \Gamma_{01}^R} \tag{3.51}$$

The current is defined positive for electrons hopping from 'right' to 'left' through the device:

$$I = (-e)(P_0\Gamma_{10}^L - P_1\Gamma_{01}^L) \tag{3.52}$$

Inserting probabilities, the current becomes:

$$I = e\frac{\Gamma_{10}^R\Gamma_{01}^L - \Gamma_{01}^R\Gamma_{10}^L}{\Gamma_{10}^R + \Gamma_{10}^L + \Gamma_{01}^R + \Gamma_{01}^L} \tag{3.53}$$

The bias voltage is the difference between the left/ right chemical potentials, $eV \equiv \mu_R - \mu_L$. We apply the bias voltage symmetrically: $\mu_R = \frac{eV}{2}$ and $\mu_L = -\frac{eV}{2}$. Replacing the chemical potentials with bias voltage in the rates yields an expression for I that depends on the two experimentally controllable voltages V and V_g.

Given some choice of the parameters g, α, δ, $\Gamma^{\eta\sigma}$, and T, the current I can be computed from (3.53) as a function of V and V_g. We define a unit Γ for the tunneling rates:

$$\Gamma = \frac{2\Gamma^L\Gamma^R}{\Gamma^L + \Gamma^R} \tag{3.54}$$

where $\Gamma^\eta = \sum_\sigma \Gamma^{\eta\sigma}$.

The IV-curves are expected to be staircases as increasing the voltage allows more matrix elements to contribute to the rates, with smearing of the steps as a result of nonzero temperature only. The differential conductance $\frac{\partial I(V_g,V)}{\partial V}$ is calculated numerically. Plots of $\frac{\partial I}{\partial V}$ at some fixed V_g are series of peaks, corresponding to thermally broadened delta functions at energies corresponding to the transitions that contribute to the rates, the area under each peak proportional to a product of two overlaps. The area under the conductance peak is the height of the corresponding step on the IV curve. We shall represent IV curves at various V_g as diamond plots, with a vertical line in the density plot corresponding to one IV-curve.

The linear conductance is defined as $\frac{\partial I}{\partial V}\Big|_{V\to 0}$.

The ground states of the 'empty' and 'filled' dimer are aligned through V_g. At $V = 0$, the dimer can switch freely between the 'empty' and 'filled' ground states when $eV_g = eV_c \equiv E_{0_0} - E_{0_1}$ because the system energy is the same in the two situations. In the standard picture [10], this gives rise to small bias, nonzero differential conductance, with current running via the molecular ground states. In-tunneling (out-tunneling) on the molecule decreases (increases) when V_g increases, and so the gate voltage controls the average number of electrons on the dimer as follows: a V_g less than V_c squeezes electrons onto the dimer from the Fermi seas with the consequence that $\langle N\rangle > N_0$ where N_0 is $\langle N\rangle$ in the $V_g = V_c$ situation. Similarly, if $V_g > V_c$ then $\langle N\rangle < N_0$. If the $\Gamma^{\eta\sigma}$ are equal, then $N_0 = \frac{1}{2}$.

This said, the above is only exactly correct for us when $\delta = 0$. In our double dot, we have a complication nonexisting in the single dot case, because the two localized site orbitals may detuned. Tunneling onto or out from the dimer happens through localized site orbitals which are not in general energetically aligned with the 'empty' ground state at $V_g = V_c$, and so at zero bias, $\partial I/\partial V = 0$. Addition of an energy $\delta\omega$ to the 'empty' energies brings the lower energy site, a, into resonance with the 'empty' ground state. This allows zero bias conductance at $V_g = E_{0_0} - E_{0_1} + \delta\omega/e$. The effect of this is a translation of the center of the diamond plots to $V_g = E_{0_0} - E_{0_1} + \delta\omega/e$. See fig.s (3.4) and (3.6) for IV curves of this.

3.5.1 Sequential transport in two simple models

The 'full' model, eq. (3.19), is not exactly solvable. Therefore, in order to eventually understand transport in the 'full' model we first describe sequential transport in the limit models, $\lambda \to 0$ and $t \to 0$.

t=0

When $t = 0$, the 'filled' dimer is an uncoupled double dot. The electron is localized to one of the sites a or b, and the oscillations are about the corresponding displaced minimum, $-l$ or l, respectively. The system eigenstates are products of localized electronic states and bosonic eigenstates of the form $|\sigma\rangle \otimes |n\rangle$, and in the case

where 2δ is an integer, the spectrum is degenerate in σ. For any δ, the 'filled' system reduces to an independent boson model as in section 1.8, except that now the electron may have entered the system on either site, and in general the onsite energies may be different. If they are not, ie. $\delta = 0$, transport must reduce essentially to the C_{60} case described in section 1.8, the only difference being a factor of 2 between in-tunnelings and out-tunnelings that come about because an electron can enter the dimer on two sites, but leave only from the one site that is occupies. Current in the large V limit thus changes from $e\frac{\Gamma^L\Gamma^R}{\Gamma^L+\Gamma^R}$ for the single dot to, eg., $e\frac{\Gamma^L\Gamma^R}{\Gamma^L+2\Gamma^R}$ for the uncoupled double dot.

If $\delta > 0$, the conductance peaks are no longer at the same energies for the two dots. Consider, for example, the a dot when an electron is inserted at time 0. At zero temperature the single dot electron Green's function at later times is

$$G_a(t) = -i\theta(t)\langle 0|c_a(t)c_a^\dagger(0)|0\rangle \tag{3.55}$$

After Fourier transforming, the spectral function in frequency space becomes [53, 67]

$$A_a(p) = -2\mathrm{Im}G_a(p) = \sum_{j=0}^{\infty} e^{-g}\frac{g^j}{j!}\,\delta(p - \delta\omega + g\omega - j\omega) \tag{3.56}$$

The single dot conductance at $V_g = V_c$ is determined by the spectral function. The current is

$$I_a(V) = \frac{\Gamma^{La}\Gamma^{Ra}}{\Gamma^{La}+\Gamma^{Ra}}\int_{p=0}^{V} \mathrm{d}p\; A_a(\frac{p}{2}) \tag{3.57}$$

The spectral function is a series of delta functions, with arguments that contain an electronic selfenergy term $g\omega$. The g factor is a measure of the geometrical difference between the final and initial states in a tunneling process, and from the Poisson factors, we see that increasing g serves to broaden the spectral function and to increase the energy for which it peaks. The existence of multiple peaks in the spectral function and therefore in the differential conductance is a ground state property of the system, caused by the electron-vibron interaction.

When g becomes large, the stepstructure of the single-dot IV characteristic is smeared out in the sense that the number of steps that contribute becomes large and the individual stepheights correspondingly small. Also, the small-bias current is inhibited, which follows from the shape of the Poissonian at large g, as the maximum of the distribution moves toward high energies at increasing g. This makes sense, because when g becomes large, the binding energy of the 'tilted' dimer, which we shall see is $g\omega$, similarly increases. The bias voltage must make up for this approximate difference in energy between 'empty' and 'filled' states for current to run.

Thus, the single-dot IV takes on a classical look in the limit. The linear conductance of a single dot is proportional to e^{-g}.

The spectral function for the b dot differs from the a dot spectral function by a sign change on δ. In the double dot, the differential conductance is essentially due

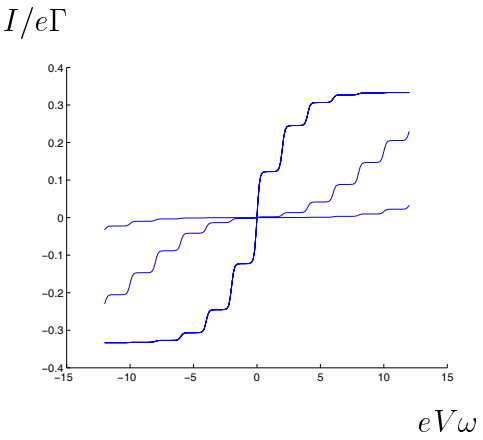

Figure 3.3: IV curves at $V_g = V_c$, $\Gamma^L = \Gamma^R$, $t = 0$, $\delta = 0$, for $g = 1, 5, 10$. Large g inhibits the linear conductance.

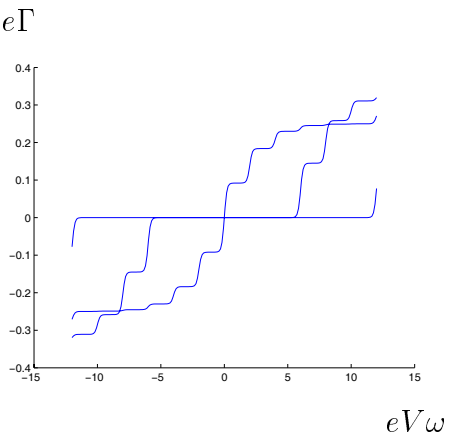

Figure 3.4: IV curves at $\Gamma^L = \Gamma^R$,$t = 0$, $g = 1$, $\delta = 3$, for $eV_g = eV_c, eV_c \pm \delta\omega$. The one with a step in $V = 0$ is for $eV_g = eV_c + \delta\omega$.

to an overlap of the two single-dot spectral functions, shifted with respect to each other by the electron level asymmetry.

λ=0

When there is no electron-vibron interaction, the system eigenstates are, trivially, the product states $|\mu\rangle \otimes |n\rangle$ with $\mu \in \{+, -\}$ denoting the electronic eigenstates from section 3.4, and n indexing the boson states. The eigenenergies are $E_{\mu,n} = (n + \frac{1}{2})\omega + \text{sign}(\mu)t\sqrt{1 + K^2}$, $K = \frac{\delta\omega}{t}$.

Sequential transport in a symmetrical device ($\Gamma^L = \Gamma^R \equiv \Gamma$) with $V_g = V_c + \delta\omega$ is very simple. For $t > 0$ and any δ, differential conductance has three peaks: one for the linear conductance, corresponding to current running via the electronic ground state, and two in $\pm 4t\sqrt{1 + K^2}$ where the electronic excited state comes into resonance. The energy $\pm 4t\sqrt{1 + K^2}$ is twice the electronic band width, with the factor of 2 following from the definition of V. There are no vibronic sidebands (at low T) because in- and out-tunnelings both are from the oscillator ground state in the absence of coupling. The effect of nonzero temperature is to smear the steps.

The current in the large V limit, call it I_{max}, is the current on the highest step ($eV >$ twice the electronic bandwidth). From the rate equations, it is easy to show:

$$\frac{I_{max}}{e} = \Gamma \frac{1 \cdot \frac{1}{2}}{1 + \frac{1}{2}} = \frac{1}{3}\Gamma \tag{3.58}$$

The in-tunneling rates are twice the out-tunneling rates, because an electron can tunnel in in twice the number of ways that it can tunnel out.

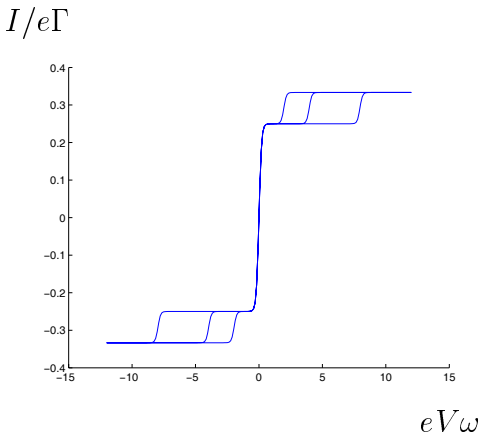

Figure 3.5: IV curves at $V_g = V_c$, $\Gamma^L = \Gamma^R$, $\lambda = 0$, $\delta = 0$, for $t = 0.5, 1, 2$.

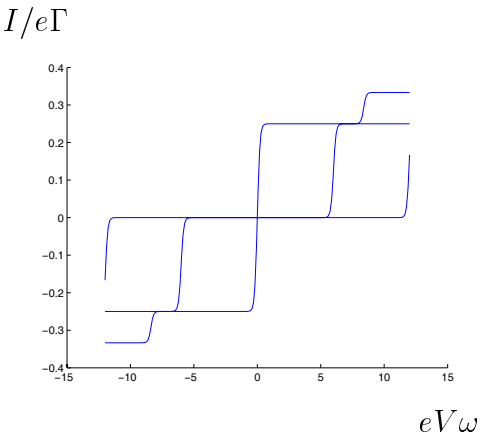

Figure 3.6: IV curves at $\Gamma^L = \Gamma^R$, $\lambda = 0$, $\delta = 3$, $t = 2$, for $eV_g = eV_c, eV_c \pm \delta\omega$. The one with a step in $V = 0$ is for $eV_g = eV_c + \delta\omega$.

The current along the first step is the intermediate value

$$\frac{I}{e} = \Gamma \frac{\frac{1}{2} \cdot \frac{1}{2}}{\frac{1}{2} + \frac{1}{2}} = \frac{1}{4}\Gamma \tag{3.59}$$

because in- and out-tunneling takes place via just one state, the electronic ground state.

Chapter 4

The 'filled' subspace

To understand the current in our model for a dimer device, we need detailed understanding of the eigenstates of H. The mechanism of electron transport described in the introduction is sequential tunneling, but we shall see that in a parameter regime where the eigenstates of H are polaronic, that may not be the relevant means of transport to consider. In this section, we therefore examine the eigenstates of H in different parameter regimes.

4.1 Spectrum and symmetries

The dimer Hamiltonian,

$$H/\omega = a^\dagger a + \frac{1}{2} + \sqrt{g}(n_a - n_b)(a^\dagger + a) - \frac{2g}{\alpha}(c_a^\dagger c_b + c_b^\dagger c_a) + \delta\ (n_a - n_b) \qquad (4.1)$$

transforms identically under the substitution:

$$c_a\ (c_a^\dagger) \leftrightarrow c_b\ (c_b^\dagger) \qquad a\ (a^\dagger) \rightarrow -a\ (-a^\dagger) \qquad \delta \rightarrow -\delta \qquad (4.2)$$

The sign change on the boson operators amounts to a sign change on x. In the special case $\delta = 0$ the system transforms identically when

$$c_a\ (c_a^\dagger) \leftrightarrow c_b\ (c_b^\dagger) \qquad x \rightarrow -x \qquad (4.3)$$

In the following, we consider the subspace of the 'filled' dimer model with n_a+n_b=1. Obviously, the system is degenerate in the electronic degree of freedom if $\alpha = \infty$, $\delta = 0$. Assuming that this is not the case, degeneracy occurs 'accidentally' at $g = 0$ if the electronic eigenenergies $\pm E_e = \pm\sqrt{t^2 + \delta^2\omega^2}$ are an integer times ω, meaning $\sqrt{\frac{4g^2}{\alpha^2} + \delta^2}$ is an integer. We show in section 4.2 that in this case, turning on the interaction lifts the degeneracies.

Considering this from the point of view of some fixed, small value of g, if the ratio E_e/ω is varied, then intuitively, levels ought to cross, because when $E_e \ll \omega$,

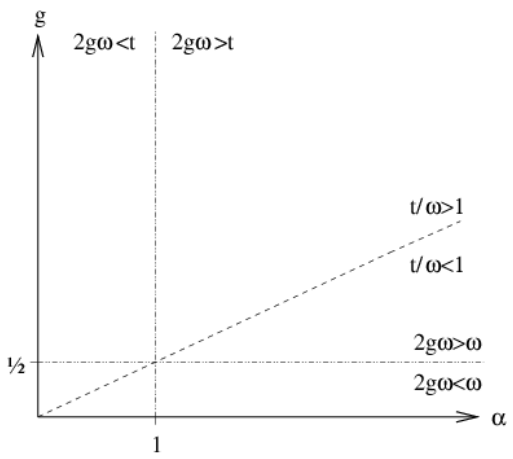

Figure 4.1: We relate the dimensionless parameter space (α, g) to (t, λ, ω). The limits $t/\omega \gg 1$ and $t/\omega \ll 1$ are referred to as 'adiabatic' and 'antiadiabatic', respectively (section 4.6). A fixed ratio t/ω corresponds to a straight line through the origin of the (α, g) plane. The crossovers in $g = \frac{1}{2}$ and $\alpha = 1$ are explained in the text.

the lower, unperturbed levels are alternating between the electronic states, while for $E_e \gg \omega$, the lower, unperturbed levels correspond to the lower energy electronic state. The crossover between the two cases, therefore, would involve level crossings if there were no interaction term. Due to the interaction, however, levels repel near the points of degeneracy and split up. Levels that become near-degenerate in this way are said to 'anticross'.

Similar to this, varying g reveals avoided level crossings in the spectrum. When g becomes large, if $\delta = 0$, levels eventually run together, with the electron hopping now the perturbation to the energy. In the unphysical limit $g \to \infty$, all levels become doubly degenerate. For nonzero δ, the level spacings approach not 0, but alternatingly ($\delta \pmod{\frac{1}{2}}$) and ($\frac{1}{2} - \delta \pmod{\frac{1}{2}}$) in unit of ω, as can be seen from the Hamiltonian with the hopping term neglected.

Our numerics confirm that for finite, nonzero values of g and α, the spectrum is nondegenerate. However, the energy differences in points of anticrossing can become arbitrarily small; see fig. (4.2) for some anticrossing levels. Also, in some parameter regimes, the lower levels run together, becoming near-degenerate in a manner to be further understood. See fig. (4.3).

Now, return to the symmetries above. First, we consider the case $\delta = 0$, with the symmetry (4.3). In any eigenstate, electronic density must be equal on the two parts of the dimer, because if in some eigenstate it were not, then there would exist a mirrorinverted state with the same energy, leading to a twofold degeneracy of the state. Therefore, from nondegeneracy of the eigenstates, $\langle n_\sigma \rangle = \frac{1}{2}$ in any

state. In terms of our numerically 'exact' eigenstates, this means $\nu_{\sigma n} = \pm\nu_{\bar{\sigma} n}$ for all n. Similarly, (4.3) leads to $\langle x \rangle = 0$, or in our numerics, $\nu_{\sigma n}\nu_{\sigma n+1} = -\nu_{\bar{\sigma} n}\nu_{\bar{\sigma} n+1}$. In this case, at large enough t, the eigenstates are approximate bonding and antibonding states. For an electron without coupling to vibrations, such states come about because the electronic, localized 'tightbinding' orbitals are nonorthogonal and therefore hybridize into symmetrical and antisymmetrical combinations. On the other hand, when the interaction is dominant and electron hopping is a perturbation, the lower electronic states are approximate symmetrical and antisymmetrical combinations of the localized states that minimize the interaction energy term. In this case, it is relevant to consider the states $\Psi_\pm \equiv \frac{1}{\sqrt{2}}(\Psi_0 \pm \Psi_1)$, where Ψ_j is the j'th eigenstate of the system. The difference in energy between Ψ_0 and Ψ_1 approaches 0 in the limit of vanishing electron hopping, and in the same limit, $\Psi_\pm$ become localized to opposite sites. Then, $\Psi_\pm$ are approximate eigenstates, within an error on the energy of $(E_1 - E_0)$, which is approximately twice the hopping energy. In the limit described, $\Psi_\pm$ become localized to opposite sites; outside the limit, the extend to which $\Psi_\pm$ are localized will turn out to be relevant for the transport properties of the system.

Nonzero δ breaks the symmetry (4.3), making states with $\langle n_\sigma \rangle \neq \frac{1}{2}$, $\langle x \rangle \neq 0$, possible. In the degenerate limit $\alpha \to \infty$, nonzero δ removes the degeneracy by lowering the symmetry of the system.

4.2 Perturbation theory from the weak interaction limit

We consider the Hamiltonian, eq. (4.1), when the electron-vibron coupling is a perturbation. The unperturbed Hamiltonian is diagonal in the basis $|\mu n\rangle$ where $\mu \in \{+, -\}$ denotes the electronic states and n the bosonic states. The unperturbed eigenenergies are

$$E^{(0)}_{\mu n} = n\omega - \mathrm{sign}(\mu) t\sqrt{1 + K^2} \tag{4.4}$$

where $\mathrm{sign}(\mu) = \pm 1$ correspond to the states $v^{(\pm)}$, see section 3.4. The perturbation is

$$H' = \omega\sqrt{g}(n_a - n_b)(a^\dagger + a) = \omega\sqrt{g}\hat{\sigma}_z(a^\dagger + a) \tag{4.5}$$

For undegenerate perturbation theory, we must assume no degeneracies,

$$\forall n : n\omega \neq \pm t\sqrt{1 + K^2} \tag{4.6}$$

There are no first order corrections to the energy, because H' has no diagonal part in the boson number. We expand to second order in $\sqrt{g}$,

$$E^{(2)}_{\mu n} = \sum_{[\mu' n'] \neq [\mu n]} \frac{|\langle \mu n | \sqrt{g}\omega\hat{\sigma}_z(a^\dagger + a)|\mu' n'\rangle|^2}{E^{(0)}_{\mu n} - E^{(0)}_{\mu' n'}} \tag{4.7}$$

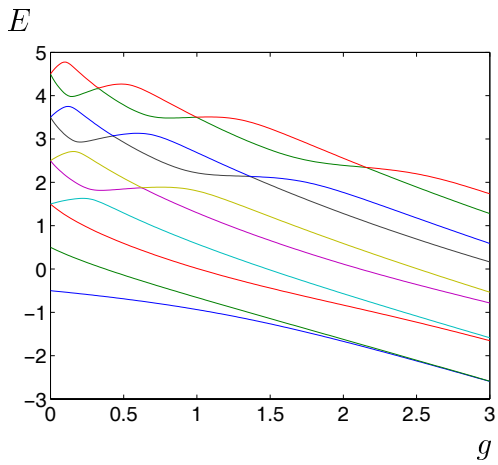

Figure 4.2: Exact energy spectrum, lower 10 levels plotted, at $t = 1$, $\delta = 0$. Function of g (note: $\alpha = 2g$ here). The degeneracies are lifted by the interaction. For increasing g, the spectrum contains anticrossing levels. In the limit $g \to \infty$, levels become pairwise degenerate.

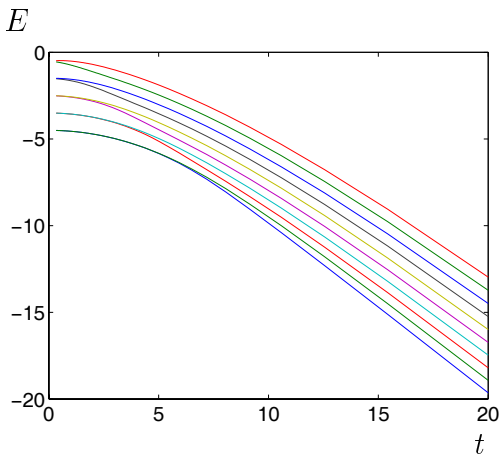

Figure 4.3: Exact energy spectrum, lower 10 levels plotted, at $g = 5$, $\delta = 0$. Function of $t/\omega = 2g/\alpha$. In the limit $t \to 0$, levels become pairwise degenerate; however, the lower levels seem to run together for finite t, becoming near-degenerate in some manner. In section 4.6, we interpret this as a polaron effect.

The calculation is straightforward, but space consuming; it is included in the appendix. The result is

$$E^{(2)}_{\mu n} = \frac{-g\omega}{1+K^2}\Big[K^2 + \omega\Big(\frac{n}{\mathrm{sign}(\mu)2t\sqrt{1+K^2}-\omega} + \frac{n+1}{\mathrm{sign}(\mu)2t\sqrt{1+K^2}+\omega}\Big)\Big] \quad (4.8)$$

The first order corrections to the eigenstates involve the unperturbed states with ± 1 phonons (appendix). The expression for the energy corrections is of course singular in the points of parameter space where the energy spectrum becomes degenerate. In the degeneracy points, all levels become doubly degenerate. We show here that λ lifts the degeneracy.

For two unperturbed states $|\mu n\rangle$ and $|\mu' n'\rangle$, degeneracy occurs if

$$(n-n')\omega = (\mathrm{sign}(\mu) - \mathrm{sign}(\mu'))\; t\sqrt{1+K^2} \quad (4.9)$$

If the states are degenerate and different from each other, we must have $\mu \neq \mu'$ and $n \neq n'$. The perturbation only connects states with $n = n' \pm 1$. If $n > n'$, then $\mu = +$, $\mu' = -$. In the 2D subspace spanned by the degenerate states $|+, n\rangle$, $|-, n-1\rangle$, we calculate the matrix elements of the perturbation. The diagonal terms:

$$\langle +, n|H'|+, n\rangle = 0 \qquad \langle -, n-1|H'|-, n-1\rangle = 0 \quad (4.10)$$

because the boson part of H' has no diagonal part. A crossterm:

$$\langle +, n|H'|-, n-1\rangle = \omega\sqrt{g}\;\langle +|\hat{\sigma}_z|-\rangle\;\langle n|(a^\dagger + a)|n-1\rangle = \omega\sqrt{g}\sqrt{n}\;\langle +|\hat{\sigma}_z|-\rangle \quad (4.11)$$

The electronic part is calculated from the eigenvectors in section 3.4:

$\langle +|\hat{\sigma}_z|-\rangle =$

$$\frac{1}{\sqrt{1+K_+^2}}\frac{1}{\sqrt{1+K_-^2}}\begin{pmatrix} K_+ \\ 1 \end{pmatrix}^T \begin{pmatrix} 1 & 0 \\ 0 & -1 \end{pmatrix}\begin{pmatrix} K_- \\ 1 \end{pmatrix} = \frac{K_+K_- - 1}{\sqrt{1+K_+^2}\sqrt{1+K_-^2}} \quad (4.12)$$

Using

$$K_+K_- = K^2 - (1+K^2) = -1 \quad (4.13)$$

and the definitions of K_+, K_-,

$$\langle +|\hat{\sigma}_z|-\rangle = \frac{-2}{\sqrt{1+[K_+^2+K_-^2]+(K_+K_-)^2}} = \frac{-2}{\sqrt{1+2[K^2+(1+K^2)]+1}} = \frac{-1}{\sqrt{1+K^2}} \quad (4.14)$$

The result is

$$\langle +, n|H'|-, n-1\rangle = -\frac{\omega\sqrt{g}\sqrt{n}}{\sqrt{1+K^2}} \quad (4.15)$$

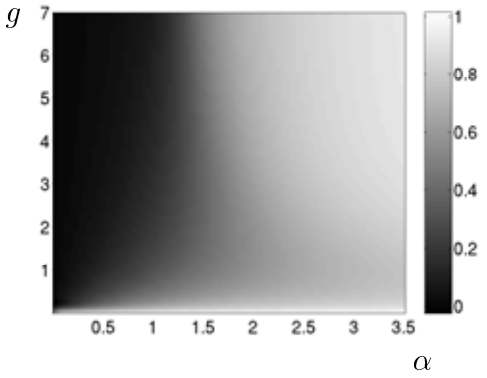

Figure 4.4: Ground state correlation function $C_{\hat{\sigma}_z,x}$ at $\delta = 0$.

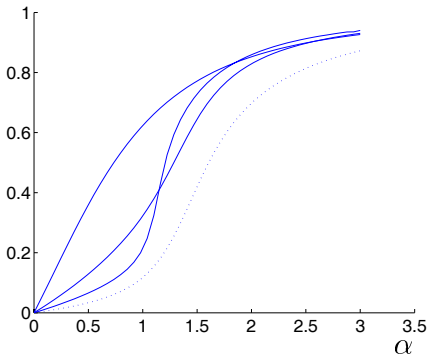

Figure 4.5: Ground state correlation function $C_{\hat{\sigma}_z,x}$ at $\delta = 0$ for $g = 0.5, 5, 20$. Dots: localization of Ψ_+ at $g = 5$.

Similarly,

$$\langle -, n-1|H'|+, n\rangle = -\frac{\omega\sqrt{g}\sqrt{n}}{\sqrt{1+K^2}} \tag{4.16}$$

The 2×2 matrix defined by eq.s (4.10), (4.15), (4.16) is easily diagonalized. The eigenenergies are

$$\pm\frac{\omega\sqrt{g}\sqrt{n}}{\sqrt{1+K^2}} \tag{4.17}$$

and the eigenvectors in the 2D subspace are the symmetric and antisymmetric combinations,

$$\frac{1}{\sqrt{2}}(|-, n-1\rangle \pm |+, n\rangle) \tag{4.18}$$

The energy split-up, to first order in $\sqrt{g}$, is

$$\frac{2\omega\sqrt{g}\sqrt{n}}{\sqrt{1+\delta^2\omega^2/t^2}} \tag{4.19}$$

The interaction prevents level crossings, but when $\sqrt{g}$ is small, or when $\delta\omega/t$ is large, levels do 'anticross', becoming near-degenerate. The lifting of degeneracy corresponds to lowering of the symmetry of the Hamiltonian, because when $\lambda = 0$, H transforms identically when $x \to -x$. In the presence of nonzero electron-vibron coupling, this symmetry is replaced by eq. (4.2).

4.3 System dynamics and correlation

Correlation between the degrees of freedom will turn out to be highly significant for transport in the dimer. Intuitively, the electronic and bosonic degrees of freedom

are expected to become correlated when electron-vibron coupling is strong, and the frequencies of the electronic hopping and of the dimer oscillations are expected to be renormalized in some manner by the interaction; we denote the effective frequencies ω_{eff} and t_{eff}. The interaction term in the Hamiltonian corresponds to a displacement of the oscillator equilibrium position, depending on the electronic 'coordinate' $\hat{\sigma}_z$, and in the symmetrical system ($\delta = 0$) the two configurations

$$(\hat{\sigma}_z, x) = (1, -l),\ (-1, l) \tag{4.20}$$

both minimize the interaction energy. Therefore, when the interaction is turned on, the symmetrical system ground state should become a state where the dimer oscillations are no longer harmonic about one welldefined point $x = 0$. Instead, the oscillatory movement of the dimer should acquire some anharmonicity, induced by the interaction. If λ is turned up even further, the displacement energy eventually becomes much larger than the electron tunneling energy. In this limit, the oscillations should become harmonic again, but now about the displaced equilibria, and only during the time intervals between the hopping events.

A way to think of this, is that the dimer movement has two components: oscillations about an instantaneous equilibrium position, and oscillations between the two equilibrium positions. The two species of movement take place on different time scales, $2\pi/\omega_{eff}$ and $2\pi/t_{eff}$, respectively, and on different length scales, l_0 and l. When there is a separation of time scales and of length scales, the system dynamics can be visualized as described in the following. When there is no such separation, dimer motion is some sort of 'hybrid' motion, where the frequency ω_{eff} could be significantly different from the 'bare' frequency ω.

The relation between the length scales is determined by $g = l^2/2l_0^2$. The quantum length l_0 is the uncertainty on the oscillator position, and l is the displacement length of the 'tilted' dimer. When $g < \frac{1}{2}$, the 'tilting' is overtaken by quantum fluctuations. The effects that we are interested in come about as a result of a transition to a 'tilted' state, which cannot occur for $g < \frac{1}{2}$. We therefore assume $g > \frac{1}{2}$ in the following qualitative discussion of the ground state. This condition is equivalent to requiring that the classical displacement energy $2g\omega$ is larger than the energy ω of the fluctuations.

Asuming now that $\delta\omega \ll t_{eff}$ (whatever t_{eff} may be), we hypothesize two distinctly different situations for the system ground state:

One limit is characterized by strong electron hopping, with the hopping frequency too fast for the (much heavier) dimer to follow the motion of the electron. In this case, the dimer does not have the time to react to the instantaneous position of the electron, but only to the average electron distribution. The electronic density is close to $\frac{1}{2}$ on each site, so the dimer performs only small oscillations about $x = 0$. The coordinates of the electron and the bosons are uncorrelated in the state, because they change on different time scales. Note that if δ, contrary to our assumption is large, $\delta\omega \gg t_{eff}$, then hopping is inhibited, and the system becomes

highly correlated in an essentially trivial manner: the electron becomes localized to the lower energy site, and the dimer 'tilts' accordingly. The constraint on the electronic position turns the system into effectively a single dot.

The other situation is weak electron hopping, with the electron largely localized between jumps, and the dimer similarly 'tilted' during these time intervals. Since the 'tilting' follows the electron, the coordinate operators describing the electron ($\hat{\sigma}_z$) and the oscillator (x) are highly correlated. The existence of a retardation effect, in the form of a nonzero time interval between the electron hops and the dimer displacement 'jumps' with it, is the origin of correlation being less than maximum. When the interaction is increased, the time scale on which interaction takes place becomes short, and we expect correlation to approach a maximum.

Correlation between $\hat{\sigma}_z$ and x signals a polaronic state, specifically a 'small' polaron because it is defined on a discrete lattice (the two-site molecule) with the electron localized on a length scale of Å. The corresponding ground state is resolved on the possibly very 'slow' time scale of the hopping frequency of the collective system of the electron + geometrical deformation. This slowing down of the resolution of the 'filled' states in a polaronic regime must be considered when we describe transport in a device.

The picture described in the above does not take quantum fluctuations in x into account. As long as $g \gg \frac{1}{2}$, fluctuations of l_0 in x should not drastically affect the picture of 'fixed' displacements between tunnelings. Also note that, had we allowed $\delta\omega$ larger than the effective electron hopping, we would be in the situation described above where the electron is near-localized to the lower energy site. Now, however, the localization effect is slightly less trivial than before, because t_{eff} may be very small due to the polaronic state.

4.3.1 A correlation measure

Now, to formalize the concept of correlation in our system. Consider the expectation value $\langle n_\sigma x\rangle$, measuring correlation between the occupation of site σ and the oscillator displacement. If $\langle n_\sigma x\rangle \neq 0$, the n_σ and x are dependent variables. If $\delta = 0$, eq. (4.3) leads to $\langle n_a x\rangle_{\delta=0} = -\langle n_b x\rangle_{\delta=0}$. If $\delta \neq 0$, eq. (4.2) leads to $\langle n_a x\rangle_\delta = -\langle n_b x\rangle_{-\delta}$. When $\langle n_\sigma x\rangle_\delta$ is maximum, then there is a polaron localized to the site σ. In this case, $\langle n_{\bar{\sigma}} x\rangle_\delta = 0$.

When $\delta \neq 0$, for the 'filled' dimer, eq. (4.2) leads to

$$\langle \hat{\sigma}_z\rangle_\delta = \langle n_a - n_b\rangle_\delta = \langle n_b - n_a\rangle_{-\delta} = \langle -\hat{\sigma}_z\rangle_{-\delta} \tag{4.21}$$

and

$$\langle x\rangle_\delta = \langle -x\rangle_{-\delta} \tag{4.22}$$

which is sensible, because the sign of δ determines which electronic site occupation number, and which direction of dimer 'tilting' is stabilized by the asymmetry.

Finally, eq. (4.2) implies

$$\langle (n_b - n_a)x\rangle_\delta = \langle (n_a - n_b)(-x)\rangle_{-\delta} = \langle (n_b - n_a)x\rangle_{-\delta} \tag{4.23}$$

Therefore, $\langle -\hat{\sigma}_z x\rangle_\delta$ is a measure of correlation that does not depend on the sign of δ. This is convenient, because we assumed $\delta \geq 0$ without loss of generality.

The measure we actually use is normalized by dividing by the displacement l,

$$C_{\hat{\sigma}_z,x} \equiv \frac{1}{l}\langle -\hat{\sigma}_z x\rangle_\delta \tag{4.24}$$

a number between 0 and 1 for the ground and lower few excited states [69]. It measures correlation between dimer 'tilting' and charge difference on the sites.

The ground state correlation function is calculated 'exactly' and plotted in fig. (4.4) for $\delta = 0$. The behaviour confirms our understanding of the limits, as $C_{\hat{\sigma}_z,x} \to 0$ when $\alpha \to 0$, and $C_{\hat{\sigma}_z,x} \to 1$ when $\alpha \to \infty$, at least for $g > \frac{1}{2}$. The crossover between the domains is strikingly sharp: for $g = 10$, correlation sets in at $\alpha = 1$, and $C_{\hat{\sigma}_z,x} \approx 0.75$ at $\alpha = 1.5$, and $C_{\hat{\sigma}_z,x} \approx 0.95$ at $\alpha = 3$. Our numerics suggest that this may be the asymptotic behaviour for $g \to \infty$, with the crossover in α less abrupt only for g smaller than, say, 5. While we had supposed that a combination of strong interaction with weak tunneling should create a correlated state, the sudden transition into a polaronic domain comes as a surprise. In section 4.6 we analyze this transition within a semiclassical framework and show that the transition involves polaronic selftrapping.

4.4 More on correlation, and entanglement

We use the results of chapter 2 and consider entanglement in the symmetric situation with $\rho_{aa} = \frac{1}{2}$. Here, entanglement is determined entirely by ρ_{ab}, with $S_L = 1 - 4\rho_{ab}^2$ and $\rho_{ab} = \sum_n \nu_{an}\nu_{bn}$. In contrast, $C_{\hat{\sigma}_z,x}$ is a sum over terms of the form $\nu_{\sigma n}\nu_{\sigma n+1}$. Trivially, if only one boson state contributes to the eigenstate, S_L=0 and $C_{\hat{\sigma}_z,x}$=0. From the dependencies on the coefficients, it seems like both functions could be maximized in a limit where the number of boson states that contribute significantly to the system eigenstate becomes large. We therefore examine the boson distributions here.

Fig. (4.6) shows, in the special case $t = 0$ ($\alpha = \infty$), the probabilities that the ground state is to be found in the boson states on site a, ie. the sum of the probabilities is $\frac{1}{2}$. The plot is a verification of something we already know from our discussion of the single dot spectral function at $T = 0$, that the boson distribution (apart from a prefactor of $\frac{1}{2}$) is a Poissonian in g in the limit considered. A Poissonian has mean value and variance both equal to the parameter, g. Therefore, the spectral weight of the bosons is 'smeared out' over approximately g states.

Of course, our interest is not in the special case where $t = 0$. Leaving the 'double dot limit', the ground state boson distribution at a large value of g ($g = 15$), is

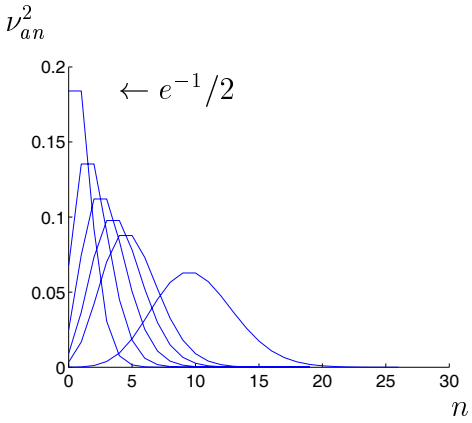

Figure 4.6: In the limit $\alpha \to \infty$, the boson distributions on the sites become Poissionian distributions in the parameter g, except for a prefactor. Here, the weights of the boson states on the site a are plotted for the ground state at $\delta = 0$, for g =1,2,3,4,5,10. The prefactor on the Poisson distribution is $\frac{1}{2}$, as the probability is equally distributed on the sites. If $\delta \neq 0$, the distributions in the $\alpha \to \infty$ limit still become Poissonians in g, but with unequal weight factors, because the electron is not on the sites with equal probability.

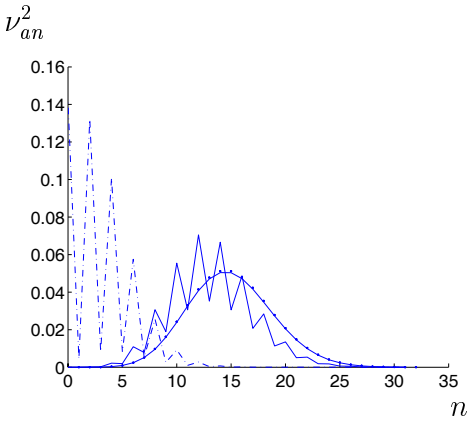

Figure 4.7: The boson weights, at $g = 15$, $\delta = 0$, $\alpha = 1.2$, 3, ∞. At small α, the weight is primarily in the boson ground state. At $\alpha = 1$, the distribution quickly broadens, approaching the Poissonian distribution which is the large α limit. The 'slash-dot' line is for $\alpha = 1.2$, the other 'zig-zag' line is for $\alpha = 3$. Dots indicate the theoretical Poissonian distribution (times 1/2), and the line connecting the dots is the exact'boson distribution in the limit. At $\alpha \approx 4$ or larger, the distribution 'zig-zags' about the limit Poissonian.

shown in fig. (4.7) for different α, indicating how the bosons develop when α is varied. At small α just the boson ground state and few lower excited states contribute, but from $\alpha = 1$, the distribution changes rapidly toward the large α limit of a Poissonian. At α larger than 3 or 4, the probabilities oscillate about the limit distribution. The larger g is, the more dramatic is this crossover in α.

It seems that correlation and entanglement should be associated with the limit of large g when α is somewhat larger than 1. This fits with our 'exact' calculations for correlation. Entanglement entropy in the ground state is plotted at $\delta = 0$ in fig. (4.8). We see the same behaviour as in fig. (4.5) for the correlation function, with a crossover in $\alpha = 1$ to an entangled domain. The crossover becomes sharp with increasing g. Three different measures of entanglement are plotted for comparision at $g = 5$ in fig. (4.9). Again, the measures show the same limit cases and a crossover that depends on g as described.

In [51] the claim of Levine and Muthukumar was that the transition to an entangled regime becomes sharp when $t/\omega \to \infty$, with $\mathrm{d}S_N/\mathrm{d}\alpha$ developing a discontinuity in $\alpha = 1$ in the limit. This fits with our findings, because when $\alpha \approx 1$ is held fixed, $t/\omega \to \infty$ if and only if $g \to \infty$. The discontinuity we cannot confirm, because increasing g requires diagonalization of increasingly large Hamiltonians. Levine and Muthukumar's interpretation of the limit was that when $t \gg \omega$, the nuclei give rise to an effectively static potential as far as the electron is concerned. For α not too close to 1, this fits with our own picture of the dynamics in the two regimes.

Now, if an asymmetry $\delta > 0$ is present and sufficiently large to effectively localize the electron to site b, and destroy all phase coherence in the process, then $\rho_{aa} \to 0$ and $\rho_{ab} \to 0$. This means that $S_L \to 0$, and entanglement is destroyed. However, in the same limit, $C_{\hat{\sigma}_z,x} \to 1$, because the dimer 'tilts' according to the electronic localization. The electronic state becomes a pure state, with the destruction of entanglement a result of the electronic Hilbert space becoming effectively one dimensional.

Fig.s (4.10), (4.11) show nonzero δ causing correlation in the ground state for $\alpha < 1$. If the coupling to vibrations did not affect the electron, then localization to site b would be determined by the ratio $\delta\omega/t$, as in section 3.4, and the correlation measure would follow the same behaviour. With g fixed, a fixed ratio $\delta\omega/t = \delta\alpha/2g$ corresponds to points on a hyperbola in the plot (4.10). The 'exact' crossover between the two domains does not actually occur around such a hyperbola, except at $\alpha < 0.2$, approximatively. This confirms that the electron hopping frequency is renormalized by the coupling to vibrations.

Fig.s (4.12), (4.13) show the effect of nonzero δ on the ground state entanglement entropy. The surprise is that in the entangled domain, an extremely small value of δ is sufficient to completely destroy the entanglement. The interpretation of this is that in the entangled regime, the ground state effective tunneling t_{eff} is very small. The destruction of entanglement happens when $\delta\omega$ becomes large

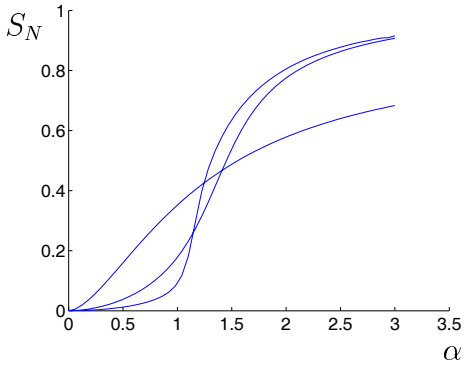

Figure 4.8: Entanglement entropy at $\delta = 0$ and $g = \frac{1}{2}, 5, 20$. The unphysically large value $g = 20$ is included to indicate the limit case, where $\mathrm{d}S_N/\mathrm{d}\alpha$ may develop a discontinuity in $\alpha = 1$. The $g = \frac{1}{2}$ line is the gradually increasing one.

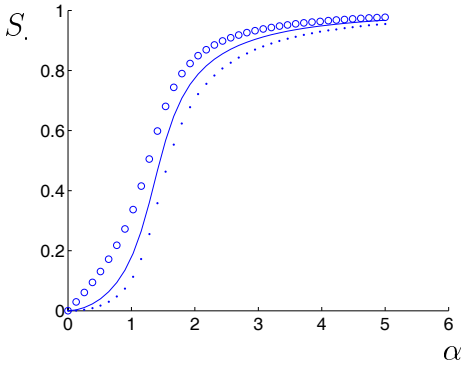

Figure 4.9: Entanglement measured in three ways at $g = 5$, $\delta = 0$: the entanglement entropy S_N (lines), the linear entropy of the qubit S_L (dots), and negativity $S_\div$ (circles).

compared to t_{eff}, localizing the state. On the plot (4.13) we see that the smaller δ is, the larger does S_N become before the sharp destruction of entanglement sets in. Also, the maxima of S_N are translated by approximately a constant when δ is decreased by a factor of 10, indicating an exponential dependence of t_{eff} on α for $\alpha > 1$. When δ becomes smaller than some value, there is no longer a sharp decrease in S_N, just a slow, gradual decrease. This is what one trivially would expect, because $t/\delta\omega \propto \alpha^{-1}/\delta\omega$ approaches 0 when α becomes large, localizing the electron.

4.5 'Tilted' states

We consider a canonical transformation that corresponds to 'tilting' of the dimer, relevant for perturbation theory in the strong electron-vibron coupling regime. The transformation is

$$\tilde{H} = e^{\zeta} H e^{-\zeta} \tag{4.25}$$

where

$$\zeta \equiv \sqrt{g}(n_a - n_b)(a^\dagger - a) = -ipl(n_a - n_b) \tag{4.26}$$

with the momentum operator

$$p = \frac{i}{\sqrt{2}l_0}(a^\dagger - a) \tag{4.27}$$

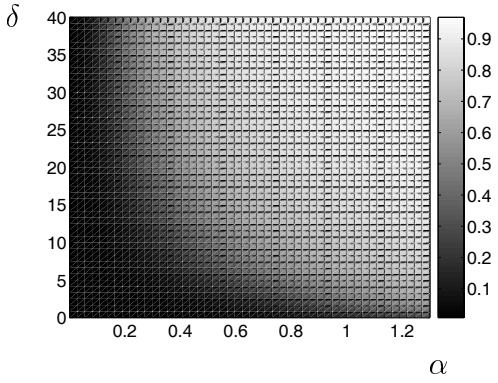

Figure 4.10: Correlation function at $g = 5$.

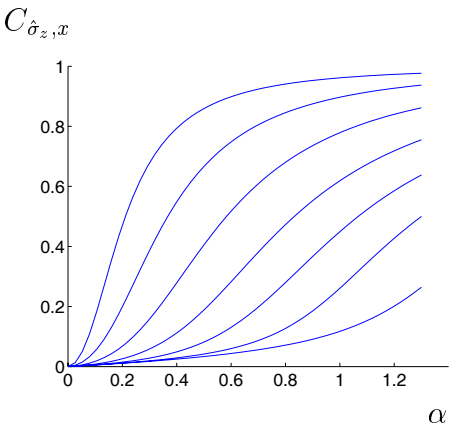

Figure 4.11: Correlation function at $g = 5$ for (from the bottom) $\delta = 0, 1, 2.5, 5, 10, 20, 40$.

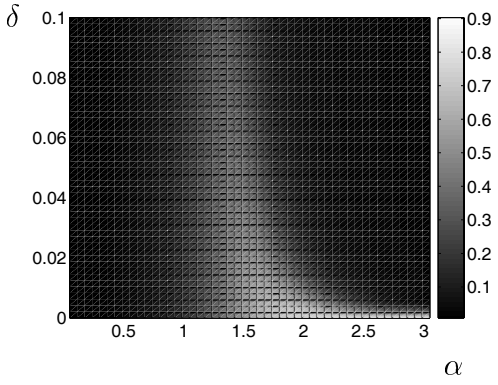

Figure 4.12: Entanglement entropy at $g = 5$.

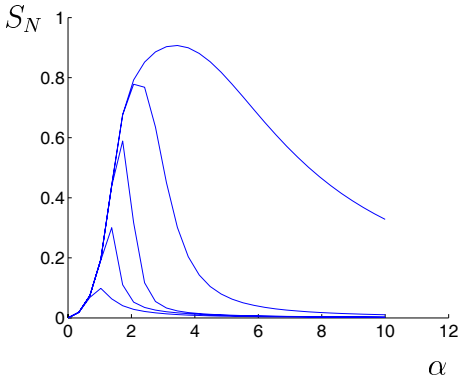

Figure 4.13: Entanglement entropy at $g = 5$ for $\delta = 1, 0.1, 0.01, 0.001, 0.0001$, from the bottom. For small enough δ, the entanglement transition sems to occur, but as α is increased, entanglement dies out again. The position and heigh of the peak of S_N both seem to follow a logarithmic behaviour. The decrease after a peak is sharp for δ sufficiently large (ie., $\delta > 0.001$).

Unitarity of the transformation:

$$(e^{\zeta})^{\dagger} = e^{(\zeta^{\dagger})} = e^{-\zeta} = (e^{\zeta})^{-1} \tag{4.28}$$

In the appendix, we transform the operators. For the boson operators, we get

$$\tilde{a} = a - \sqrt{g}(n_a - n_b) \qquad \tilde{a}^{\dagger} = a^{\dagger} - \sqrt{g}(n_a - n_b) \tag{4.29}$$

$$\tilde{N}_a = a^{\dagger}a - \sqrt{g}(n_a - n_b)(a^{\dagger} + a) + gN \tag{4.30}$$

$$\tilde{x} = x - l(n_a - n_b) \tag{4.31}$$

The transformation translates of the oscillator by $-l(n_a - n_b)$ and shifts the vibron number operator. The $\tilde{x}$ operator is the operator for displacement relative to the instantaneous equilibrium position, determined by the charge difference at that time.

For the electron operators, defining

$$A = e^{-\sqrt{g}(a^{\dagger} - a)} \qquad A^{\dagger} = e^{\sqrt{g}(a^{\dagger} - a)} \tag{4.32}$$

we get

$$\tilde{c}_a = c_a A \qquad \tilde{c}_a^{\dagger} = c_a^{\dagger} A^{\dagger} \qquad \tilde{c}_b = c_b A^{\dagger} \qquad \tilde{c}_b^{\dagger} = c_b^{\dagger} A \tag{4.33}$$

$$\tilde{n}_{\sigma} = n_{\sigma} \tag{4.34}$$

Inserting the transformed operators in the Hamiltonian yields the transformed Hamiltonian $\tilde{H}$:

$$\frac{\tilde{H}}{\omega} = a^{\dagger}a + \frac{1}{2} - gN - \frac{2g}{\alpha}\left(c_a^{\dagger}c_b e^{2\sqrt{g}(a^{\dagger} - a)} + c_b^{\dagger}c_a e^{-2\sqrt{g}(a^{\dagger} - a)}\right) + \delta\ (n_a - n_b) \tag{4.35}$$

The linear interaction terms have disappeared, and the electron-phonon interaction enters through exponential factors in the hopping terms instead. The operator $c_a^{\dagger}c_b e^{2\sqrt{g}(a^{\dagger} - a)}$ transfers the electron from the localized state b to a while shifting the oscillator from displacement $x = l$ to $x = -l$. Electronic tunneling is followed instantaneously by a change in dimer 'tilting', which effectively gives rise to a 'polaronic' hopping of electron and dimer displacement.

The electron onsite energy has been shifted by the addition of a term $-g\omega N = \frac{E_{disp}}{2}N$. The term can be understood as a 'polaronic' binding energy, because it is an energy that is gained when an electron is inserted into the system and the dimer 'tilts' correspondingly to lower the energy of the system.

The change of basis shifts the boson number operator by as much as g bosons. Eq. (4.30) with $N = 1$ can be written

$$\langle \tilde{N}_a \rangle = \langle N_a \rangle + g(1 - 2C_{\hat{\sigma}_z, x}) \tag{4.36}$$

In the correlated domain, $\langle \tilde{N}_a \rangle = \langle N_a \rangle - g$, and in the uncorrelated domain, $\langle \tilde{N}_a \rangle = \langle N_a \rangle + g$. When the dimer ground state is 'tilted', the displacement stores the

energy of the corresponding number of bosons. Numerical calculations (not shown) confirm that in the ground state, $\langle N_a \rangle \to g$ in the correlated parameter domain, while $\langle \tilde{N}_a \rangle \to g$ in the uncorrelated parameter domain. The ground state, when $C_{\hat{\sigma}_z,x} \to 1$, becomes a state in which the oscillator is shifted according to the localization of the electron.

Uncertainties, defined for a quantum variable A as $S_{(A)} \equiv \sqrt{\langle A^2 \rangle - \langle A \rangle^2}$, have been calculated for x, $\tilde{x}$, and p in the 'exact' ground state throughout parameter space. We find that when $\delta = 0$, $\langle x^2 \rangle \approx l_0^2$, $\langle p^2 \rangle \approx \frac{1}{l_0^2}$ in the weak coupling domain corresponding to Gaussian, minimal uncertainty fluctuations, as $S_{(x)} S_{(p)} \approx 1$. In the correlated domain, $\langle x^2 \rangle$ becomes large due to the existence of two minima separated in space. However, $S_{(\tilde{x})} \approx l_0^2$, $S_{(p)} \approx \frac{1}{l_0^2}$, and the oscillations become Gaussian about the displaced equilibria when $C_{\hat{\sigma}_z,x} \to 1$. The deviation from this picture is for α just above 1. Here, $S_{(p)}/l_0^2$ becomes smaller than 1, as small as 0.65. The corresponding lowering of the kinetic energy in the state indicates some sort of 'sluggish' oscillation of the dimer between two well-separated equilibria.

4.5.1 Perturbation theory from the polaronic limit

The 'tilted' states describe localized polarons. The Hamiltonian in the 'tilted' basis is used as the starting point for perturbation theory in t; the interesting case is $\delta\omega \ll t$. Restricting ourselves to the case $\delta = 0$, the transformed Hamiltonian becomes:

$$\tilde{H} = \tilde{H}_0 + \tilde{H}' \tag{4.37}$$

$$\tilde{H}_0 = \omega a^\dagger a - g\omega N \tag{4.38}$$

$$\tilde{H}' = -t(c_a^\dagger c_b e^{2\sqrt{g}(a^\dagger - a)} + c_b^\dagger c_a e^{-2\sqrt{g}(a^\dagger - a)}) \tag{4.39}$$

The unperturbed problem is degenerate in the electronic degree of freedom. The unperturbed basis states $\{|\sigma\tilde{n}\rangle\}$ are localized, the index $\tilde{n}$ specifying the vibrational state with respect to the 'tilted' number operator $\tilde{N}_a$. The matrix elements of H' can be approximated, using the overlap of the oscillator ground states, at separation $2l$:

$$\langle 0_a | 0_b \rangle = e^{-l^2/l_0^2} = e^{-2g} \tag{4.40}$$

where $|0_\sigma\rangle$ denotes the ground state of the ocillator at site σ. We approximate the matrix elements,

$$\langle \sigma\tilde{n} | \tilde{H}' | \sigma'\tilde{n}' \rangle \approx \langle 0_a | 0_b \rangle \langle \sigma n | \tilde{H}' | \sigma' n' \rangle \tag{4.41}$$

which are straightforward to calculate, because the boson operators in $\tilde{H}'$ are defined with respect to the states $|n\rangle$. We expect the approximation is valid for small n, ie. at low temperatures, and sufficiently 'deep' within the correlated parameter regime. The overlap between the displaced oscillator ground states is exponentially damped in g. Thus, the 'polaronic' tunneling is inhibited, which happens because the electron can only tunnel by dragging the dimer displacement with it.

The energy corrections to first order in t are diagonal in the bosonic degree of freedom, and lift the degeneracy of the spectrum. By degenerate perturbation theory, the first order energy corrections are the eigenenergies of the 2D matrices of H'_n, where H'_n is H' restricted to the subspace of the two degenerate states labeled by boson number n. For all n, we must calculate the matrix elements of a 2×2 matrix,

$$\langle \sigma n|H'_n|\sigma' n\rangle = \langle \sigma n| - t(c_a^\dagger c_b e^{2\sqrt{g}(a^\dagger - a)} + c_b^\dagger c_a e^{-2\sqrt{g}(a^\dagger - a)})|\sigma' n\rangle \tag{4.42}$$

We have included this straightforward, but lengthy calculation in the appendix. The result is

$$\langle \sigma n|H'_n|\sigma' n\rangle = -t\delta_{\sigma,\bar{\sigma'}} \sum_{j=0}^{n} (-1)^j \frac{n!}{(j!)^2(n-j)!} (2\sqrt{g})^{2j} \tag{4.43}$$

The eigenvectors of H'_n are $|\tau n\rangle$, $\tau \in \{+,-\}$:

$$|\pm, n\rangle = \frac{1}{\sqrt{2}}(|an\rangle \pm |bn\rangle) \tag{4.44}$$

The eigenenergies are $\pm e^{-2g}\langle \sigma n|H'_n|\sigma' n\rangle$. The energy spectrum to first order in t:

$$\omega n - g\omega N \mp t e^{-2g} \sum_{j=0}^{n} (-1)^j \frac{n!}{(j!)^2(n-j)!} (2\sqrt{g})^{2j} \tag{4.45}$$

'Exact' calculations confirm this spectrum in the large α limit.

The second order energy corrections $E^{(2)}_{\tau n}$ to the states $|\tau n\rangle$ depend on the n-off-diagonal matrix elements. By degenerate perturbation theory, each $E^{(2)}_{\tau n}$ is a sum where the degenerate subspace is avoided:

$$E^{(2)}_{\tau n} = \sum_{[\tau' n'] \neq [\tau n], [\bar{\tau} n]} \frac{|\langle \tau' n'|H'|\tau n\rangle|^2}{E^{(0)}_{\tau n} - E^{(0)}_{\tau' n'}} = \sum_{\tau', n' \neq n} \frac{|\langle \tau' n'|H'|\tau n\rangle|^2}{(n-n')\omega} \tag{4.46}$$

This depends only on matrix elements nondiagonal in n. The off-diagonal matrix elements are calculated in the appendix; we list a few special cases of the nondiagonal boson overlaps below, but we don't really need them.

Our interest is in the first order energy splittings, because when an exact energy difference becomes small at moderate α, that signals the entrance into a polaronic regime for that pair of states. For a polaronic pair of states, the energy splitting to first order in t is approximately the polaronic tunneling. We therefore consider the matrix elements which are diagonal in n (just the boson part):

$$\langle \tilde{0}|e^{-2\sqrt{g}(a^\dagger - a)}|\tilde{0}\rangle = e^{-2g} \tag{4.47}$$

$$\langle \tilde{1}|e^{-2\sqrt{g}(a^\dagger - a)}|\tilde{1}\rangle = (1-4g)\, e^{-2g} \tag{4.48}$$

$$\langle \tilde{2}|e^{-2\sqrt{g}(a^\dagger - a)}|\tilde{2}\rangle = 2\sqrt{2g}(2g-1)\, e^{-2g} \tag{4.49}$$

Matrix elements similar to these are also calculated in [29] for a different physical system. They are all exponentially damped in g, with a polynomial behaviour in $\sqrt{g}$. When $\tilde{n} > 0$, tunneling is vastly increased from the ground state value: at $g = 5$, the overlaps in unit of e^{-2g} are 1 for $\tilde{n} = 0$, 19 for $\tilde{n} = 1$, 181 for $\tilde{n} = 2$, and our numerics confirm that the overlaps remains much larger than 1 for increasing $\tilde{n}$. This suggests that increased tunneling for higher boson numbers leads to weakening of the polaronic nature of the excited states.

Just for fun, here are a few off-diagonal boson matrix elements:

$$\langle\tilde{n}|e^{-2\sqrt{g}(a^\dagger - a)}|\tilde{0}\rangle = \frac{(-1)^n}{\sqrt{n!}}(2\sqrt{g})^n\ e^{-2g} \tag{4.50}$$

$$\langle\tilde{2}|e^{-2\sqrt{g}(a^\dagger - a)}|\tilde{1}\rangle = 2\sqrt{2g}(2g-1)\ e^{-2g} \tag{4.51}$$

4.6 Semiclassical limit

To understand the crossover between the polaronic and nonpolaronic domains - specifically, it's sharpness in $\alpha = 1$ - we consider a semiclassical approximation to the Hamiltonian, where x is treated as a classical variable. We rewrite the Hamiltonian in terms of a dimensionless coordinate $X \equiv \frac{x}{l_0} = x\sqrt{m\omega}$ and the Pauli matrices in the basis of the c_σ operators:

$$H = \Big(T(X) + \omega\frac{X^2}{2}\Big)\hat{1} + (\omega\sqrt{2g}X + \delta\omega)\ \hat{\sigma}_z - \omega\frac{2g}{\alpha}\ \hat{\sigma}_x \tag{4.52}$$

where $T(X)$ is the kinetic energy of the dimer. The semiclassical system is an effective two-state quantum system, characterized by Born-Oppenheimer surfaces. Setting $T(X) = 0$, the semiclassical approximation to the ground state is determined from the minimum or minima of the lower electronic state. We write the remaining Hamiltonian compactly as

$$\omega\frac{X^2}{2}\hat{1} + \omega\frac{2g}{\alpha}\ H_e \qquad , \qquad H_e = \begin{pmatrix} -\kappa & -1 \\ -1 & \kappa \end{pmatrix} \tag{4.53}$$

where

$$\kappa \equiv -(\sqrt{2g}X + \delta)\frac{\alpha}{2g} \tag{4.54}$$

The electron part we diagonalized in section 3.4 for a different variable. Introducing

$$\kappa_+ = \kappa + \sqrt{1+\kappa^2} \qquad \kappa_- = \kappa - \sqrt{1+\kappa^2} \tag{4.55}$$

and using

$$\kappa^2 = \frac{\alpha^2}{4g^2}(2gX^2 + \delta^2 + 2\sqrt{2g}\delta X) \tag{4.56}$$

it follows from section 3.4 that the eigenenergies are

$$E_\pm(X) = \pm\omega\frac{2g}{\alpha}\sqrt{1+\kappa^2} = \pm\omega\sqrt{\frac{4g^2}{\alpha^2} + 2gX^2 + \delta^2 + 2\sqrt{2g}\delta X} \tag{4.57}$$

and the eigenvectors are

$$w^{(+)} = \frac{1}{\sqrt{1+\kappa_+^2}} \begin{pmatrix} \kappa_+ \\ 1 \end{pmatrix} \qquad w^{(-)} = \frac{1}{\sqrt{1+\kappa_-^2}} \begin{pmatrix} \kappa_- \\ 1 \end{pmatrix} \tag{4.58}$$

The electron is a two-state system moving in the spatial potential that corresponds to the electronic eigenstate. The electronic eigenstates in turn are determined by the coordinate X, and therefore, X is a collective coordinate determining both the electronic state and the classical displacement of the oscillator. For an electron moving on the lower energy surface, the classical coordinate X completely specifies the semiclassical state. The energy surfaces are Born-Oppenheimer surfaces:

$$U_\pm(X)/\omega = \frac{1}{2}X^2 \pm \sqrt{\frac{4g^2}{\alpha^2} + 2gX^2 + \delta^2 + 2\sqrt{2g}\delta X} \tag{4.59}$$

We note that the energy surfaces do not cross for nonzero t (finite α): the term in the square root in eq. (4.59) is larger than 0, because the polynomium in X, $(2gX^2 + \delta^2 + 2\sqrt{2g}\delta X)$ is never negative (the discriminant is 0 and the coefficient of X^2 is positive). The electronic states thus remain undegenerate for all dimer displacements, in accordance with the von Neumann and Wigner noncrossing rule [43]. In the case $t = 0$, the surfaces can and do cross in one point, which is discussed in a section below.

Within the semiclassical approximation, the energy surfaces are uncoupled; this approximation is unrealistic if the surfaces are close to each other. In this case, the quantum mechanical nature of $T(X)$ leads to a coupling between the surfaces, and the semiclassical approach needs to be modified. Fluctuations in x can bridge the energy gap between the surfaces if they are closer in energy than ω. We assume here that this is not a problem; the minimum distance between the surfaces is $2t$, and the surfaces can therefore be assumed uncoupled if $t/\omega \gg 1$. For the parameter values of our interest, this condition is fulfilled, justifying our assumption that an electron occupies the lower potential and remains there during it's motion.

In Holstein polaron literature, the limit $t/\omega \to \infty$ is sometimes referred to as the 'adiabatic limit', and here we see why: in the adiabatic limit, the perturbation to the electronic movement vanishes, and the electronic state develops reversibly in a potential.

4.6.1 Born-Oppenheimer surfaces in a symmetrical system

We calculate the potential minima for the symmetrical system ($\delta = 0$) in order to derive some properties of the ground state and the excited states in the semiclassical limit.

For $\delta = 0$, the Born-Oppenheimer surfaces are

$$\frac{U_{\pm}(X)}{\omega} = \frac{1}{2}X^2 \pm \sqrt{2gX^2 + \frac{4g^2}{\alpha^2}} \tag{4.60}$$

which are symmetrical about $X = 0$.

The first derivatives with respect to X:

$$\frac{1}{\omega}\frac{\partial U_{\pm}(X)}{\partial X} = X \pm \frac{2gX}{\sqrt{2gX^2 + \frac{4g^2}{\alpha^2}}} \tag{4.61}$$

The extrema of the electronic ground state potential are the solutions to $\frac{\partial U_-}{\partial X} = 0$:

$$X - \frac{2gX}{\sqrt{2gX^2 + \frac{4g^2}{\alpha^2}}} = 0 \quad \Rightarrow \quad X = 0 \;\; \text{or} \;\; 1 = \frac{2g}{\sqrt{2gX^2 + \frac{4g^2}{\alpha^2}}} \quad \Rightarrow$$

$$X = 0 \;\; \text{or} \;\; 2gX^2 + \frac{4g^2}{\alpha^2} = \pm(2g)^2 \quad \Rightarrow \quad X = 0 \;\; \text{or} \;\; X^2 = 2g\;((\pm 1) - \frac{1}{\alpha^2}) \tag{4.62}$$

The (-1) case has no solutions, so we arrive at the solutions

$$X = 0, \quad \pm X_0 \tag{4.63}$$

where

$$X_0 \equiv \sqrt{2g}\,\sqrt{1 - \frac{1}{\alpha^2}} \tag{4.64}$$

The solutions $\pm X_0$ are valid only when $\alpha > 1$.

A minimum X_s of U_- satisfies $\frac{\partial^2 U_-}{\partial X^2}(X_s) > 0$. The second derivatives of $U_{\pm}$:

$$\frac{1}{\omega}\frac{\partial^2 U_{\pm}(X)}{\partial X^2} = 1 \pm \left(\frac{2g}{\left(2gX^2 + \frac{4g^2}{\alpha^2}\right)^{1/2}} - \frac{(2gX)^2}{\left(2gX^2 + \frac{4g^2}{\alpha^2}\right)^{3/2}} \right) \tag{4.65}$$

Inserting the minima,

$$\tfrac{1}{\omega}\tfrac{\partial^2 U_-}{\partial X^2}(0) = 1 - \tfrac{2g}{2g/\alpha} = 1 - \alpha \tag{4.66}$$

$$\tfrac{1}{\omega}\tfrac{\partial^2 U_-}{\partial X^2}(\pm X_0) =$$

$$1 - \left(\frac{2g}{\left(2g(\sqrt{2g}\,\sqrt{1-\frac{1}{\alpha^2}})^2 + \frac{4g^2}{\alpha^2}\right)^{1/2}} - \frac{\left(2g\sqrt{2g}\,\sqrt{1-\frac{1}{\alpha^2}}\right)^2}{\left(2g(\sqrt{2g}\,\sqrt{1-\frac{1}{\alpha^2}})^2 + \frac{4g^2}{\alpha^2}\right)^{3/2}} \right) =$$

$$1 - \left(\frac{1}{\left((1-\frac{1}{\alpha^2}) + \frac{1}{\alpha^2}\right)^{1/2}} - \frac{1-\frac{1}{\alpha^2}}{\left((1-\frac{1}{\alpha^2}) + \frac{1}{\alpha^2}\right)^{3/2}} \right) = 1 - \tfrac{1}{\alpha^2} \tag{4.67}$$

The electronic ground state bifurcates in $\alpha = 1$, as U_- has one minimum in $X = 0$ for $\alpha < 1$, while for $\alpha > 1$, this extremum becomes unstable. The 'new'

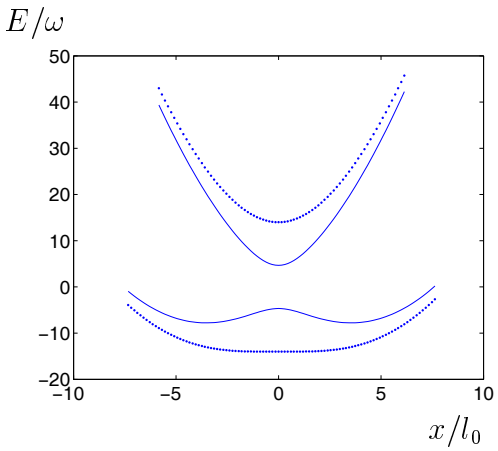

Figure 4.14: The semiclassical potentials $U_\pm$ at $g = 7$, $\delta = 0$, for $\alpha = 1$ (dots) and $\alpha = 3$ (lines). For $\alpha > 1$, the lower potential has two wells.

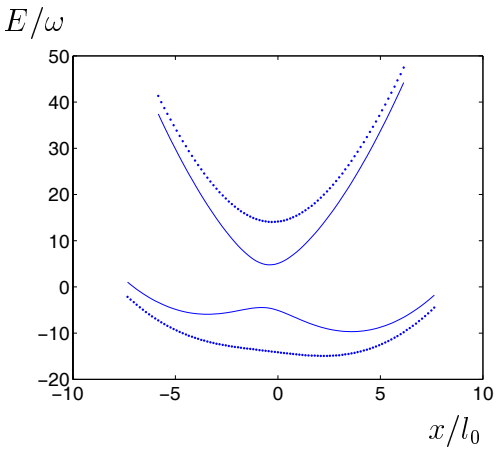

Figure 4.15: The semiclassical potentials $U_\pm$ at $g = 7$, $\delta = 2$, for $\alpha = 1$ (dots) and $\alpha = 3$ (lines). The asymmetry skews the potentials, and in the bifurcated case lifts the degeneracy of the well states.

minima in $\pm X_0$ are stable, however. The minima $\pm X_0$ move from 0 in $\alpha = 1$ towards $\pm\sqrt{2g}$ when α is increased above 1.

The electronic excited state is in it's 'ground state' with respect to X when U_+ is minimal. From eq. (4.60), we see that U_+ is a monotonously increasing function of X^2, so the minimum is in $X = 0$ for all parameter values.

Summarizing, the potential minima and the corresponding energies are:

$$\begin{array}{lllllll} U_- : & X = 0 & \text{when } \alpha < 1 & U_-(0) & = & -\frac{2g}{\alpha}\,\omega & = -t \\ & X = \pm X_0 & \text{when } \alpha > 1 & U_-(\pm X_0) & = & -g(1+\frac{1}{\alpha^2})\,\omega & \\ U_+ : & X = 0 & & U_+(0) & = & \frac{2g}{\alpha}\,\omega & = t \end{array} \tag{4.68}$$

For both of the parameter regimes $\alpha > 1$ and $\alpha < 1$, the potentials $U_\pm$ are plotted in fig. (4.14). When $\alpha > 1$, the height of the barrier between the wells is $E_b \equiv g\omega(1 + \alpha^{-2} - 2\alpha^{-1})$, and $E_b \approx g\omega$ when $\alpha \gg 1$. Bound states are possible at energies less than $-\frac{2g}{\alpha}$.

We now calculate the eigenvectors at the minima. As already noted, in $X = 0$, the eigenvectors reduce to the ones found in section (3.4), which at $\delta = 0$ are just the bonding and antibonding electron states. $U_-(0)$ corresponds to the bonding state, and $U_+(0)$ corresponds to the antibonding state.

In $X = +X_0$, $\kappa(X = X_0) = -\sqrt{\alpha^2 - 1}$ and $\kappa(X = X_0)^2 = \alpha^2 - 1$. Therefore, from eq. (4.55), $\kappa_\pm = -\sqrt{\alpha^2 - 1} \pm \alpha$, and the electron eigenvectors are

$$\frac{1}{\sqrt{1+\kappa_+^2}}\begin{pmatrix} \alpha - \sqrt{\alpha^2-1} \\ 1 \end{pmatrix} \qquad \frac{1}{\sqrt{1+\kappa_-^2}}\begin{pmatrix} -\alpha - \sqrt{\alpha^2-1} \\ 1 \end{pmatrix} \tag{4.69}$$

which reduce to bonding/ antibonding states at $\alpha = 1$. When α becomes large, the eigenvectors approach the localized states

$$\begin{pmatrix} 0 \\ 1 \end{pmatrix} \qquad \begin{pmatrix} 1 \\ 0 \end{pmatrix} \tag{4.70}$$

The expression for x_0 explains the behaviour of $C_{\hat{\sigma}_z,x}$ observed for the 'exact' ground state when $\delta = 0$. For g not too small, when α is turned up from 1, $C_{\hat{\sigma}_z,x} \to 1$ in the same manner as $X_0 \to \sqrt{2g}$. At $\alpha \approx 4$, $X_0 \approx \sqrt{2g}$, and the 'exact' boson distribution in fig. (4.7) becomes oscillatory about the Poissonian limit case.

4.6.2 Semiclassical eigenstates

The semiclassical ground state depends on the energy landscape, which is either a near-harmonic, single-well potential, or a double-well potential with a barrier separating the wells. The single-well, semiclassical ground state is the product of the electronic bonding state and the undisplaced dimer,

$$\frac{1}{\sqrt{2}}(\phi(x - x_0) + \phi(x + x_0)) \otimes |x = 0\rangle \qquad (\alpha < 1) \tag{4.71}$$

where $\phi(x)$ denote the electronic wave function localized to x =0. The expectation values $\langle x \rangle = 0$ and $\langle \hat{\sigma}_z \rangle = 0$. The degrees of freedom are uncorrelated, and the state is unentangled.

The semiclassical, double-well ground state is degenerate (at $\delta = 0$). In reality, the degeneracy is lifted by quantum mechanical tunneling between the wells, which is a small perturbation to the energy. The tunneling is polaronic, because it involves electron hopping and a 'jump' between different deformations of the 'lattice'. The hopping energy t_p is calculated in an approximate scheme in the next section. When the degeneracy is lifted, the two eigenstates become the symmetrical and antisymmetrical combinations of the well states,

$$\frac{1}{\sqrt{2}}(\phi(x - x_0) \otimes |x = x_0\rangle \pm \phi(x + x_0) \otimes |x = -x_0\rangle) \qquad (\alpha > 1) \tag{4.72}$$

and the eigenenergies to first order in the perturbation become $U_-(X_0) \pm t_p$.

The corresponding ground state electron density operator is

$$\frac{1}{2}(|a\rangle\langle a| + |b\rangle\langle b|) \tag{4.73}$$

where we have used orthogonality of the classical states $|x\rangle$ in taking the 'trace' over x in eq. (4.72), and changed notation. Different $|x\rangle$ are orthogonal within the semiclassical approximation but not quantum mechanically, of course.

The expectation values $\langle x \rangle$ and $\langle \hat{\sigma}_z \rangle$ are 0. However, the electron is localized, which follows from the fact that the electron density operator and the operator for measuring electronic position, $\hat{\sigma}_z \cong |a\rangle\langle a| - |b\rangle\langle b|$, commute:

$$\begin{aligned}[\rho_e, \hat{\sigma}_z] = & \left(\tfrac{1}{2}(|a\rangle\langle a| + |b\rangle\langle b|)(|a\rangle\langle a| - |b\rangle\langle b|)\right) - \left((|a\rangle\langle a| - |b\rangle\langle b|)\tfrac{1}{2}(|a\rangle\langle a| + |b\rangle\langle b|)\right) \\ & = |a\rangle\langle a| - |b\rangle\langle b| - \left(|a\rangle\langle a| - |b\rangle\langle b|\right) = 0 \end{aligned} \tag{4.74}$$

using orthogonality of $|a\rangle$ and $|b\rangle$. Hence, measurement of electron position does not disturb the state, which is therefore one of the localized states. The state is also maximally entangled.

In the single-well system, the excited states are delocalized and can be represented as in fig. (4.16). In the double-well system, if the barrier between the wells is sufficiently high, the first few excited states can be pictured as localized excitations in the wells that hybridize, similar to the semiclassically degenerate ground state. In fig. (4.17) we show the potential in a system where the ground and first excited states are polaronic, but the next two eigenstates are not, because one of the states lie above the well barrier. Below the barrier, pairs of semiclassically degenerate states hybridize, becoming polaronic if they lie sufficiently deep in the wells. See fig. (4.18).

The polaronic pairs in the hybridized double-wells, when the energy splitting is neglected, can be written as

$$\frac{1}{\sqrt{2}}(\phi(x - x_0) \otimes |\tilde{N}_{(b)}\rangle + \phi(x + x_0) \otimes |\tilde{N}_{(a)}\rangle) \tag{4.75}$$

where $\tilde{N}_{(\sigma)}$ denotes the vibronic number operator for a state where the electron is localized to site σ. When the energy splitting due to tunneling between the wells is nonnegligible, the polarons are less than 100 % localized. Tunneling is expected to be stronger for polarons belonging to excited vibrational states than for the vibrational ground state polarons; recall the boson overlaps in section 4.5.1. This may lead to a significant degree of delocalization of these states. However, our numerics confirm that the vibrationally excited states do eventually become polarons. The entanglement of the excited states in fig. (4.18) is plotted in fig. (4.19). At $\delta = 0$, all states become entangled in the limit $\alpha \to \infty$, but the polaron states become entangled in a manner strikingly different from the non-polaron states.

A little surprisingly, the states with energy above the top of the semiclassical barrier are not completely delocalized. See ref. [50] p.93.

4.6.3 The polaronic hopping energy

We have seen that the semiclassical bifurcation in $\alpha = 1$ indicates polaron formation when g is not too small. We can calculate the polaronic hopping energy semiclassically as the overlap between two harmonic oscillators in $\pm x_0$. This is

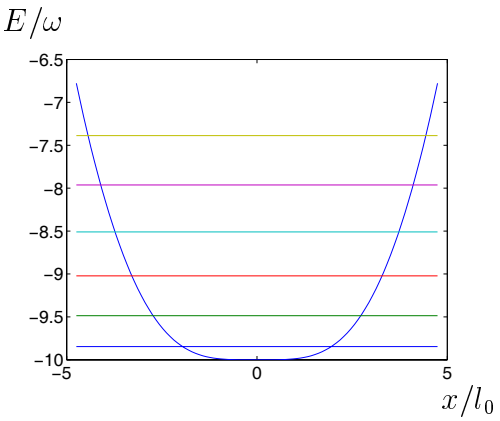

Figure 4.16: The Born-Oppenheimer surface U_- at g=5, α=1, $\delta = 0$. The exact eigenenergies are -9.8460, -9.4860, -9.0218, -8.5100, -7.9623, -7.3872.

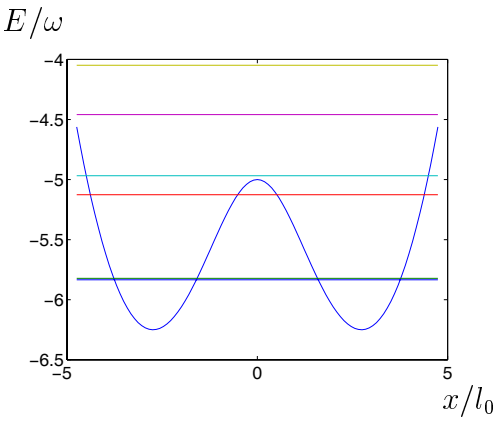

Figure 4.17: The Born-Oppenheimer surface U_- at g=5, α=2, $\delta = 0$. The exact eigenenergies are -5.8345, -5.8217, -5.1259 , -4.9681, -4.4590, -4.0480. The lower two states are nearly degenerate, and the symmetric/ antisymmetric combinations are localized to their respective sites with probabilities 0.91.

done by approximating U_- to a harmonic potential near the minima by a Taylor-expansion to second order in $(x \mp x_0)$. This yields an effective spring constant, an effective mass and hence an effective quantum oscillator length, which defines the harmonic oscillator wave functions in $\pm x_0$. The overlap of the harmonic oscillator ground states defines an effective tunneling coupling t_p between the two polaron states that hybridize into the ground and first excited states of the system.

The calculation is carried out in the appendix. The result is

$$t_p/\omega = \exp(-2g\ (1 - \frac{1}{\alpha^2})^2) \tag{4.76}$$

The effective tunneling coupling between the polaron states becomes exponentially small in g, and is modified by an α-dependence. When $\alpha = 1$, $t_p = \omega$, but the harmonic approximation is not credible for α very close to 1. When $\alpha^2 \gg 1$ the expression simplifies to

$$t_p/\omega \approx \mathrm{e}^{-2g} \tag{4.77}$$

The α-dependence disappears in the limit $\alpha \to \infty$. More to the point, the α-dependence becomes insignificant at $\alpha \approx 4$.

In fig.s (4.20), (4.21), we compare t_p to the 'exact' half energy difference between the ground and first excited states. The energy splitting between the two polaron states, to first order in t_p, is just $2t_p$, semiclassically. We previously calculated $\langle \hat{\sigma}_z \rangle$ in the state Ψ_+ at $g = 5$, the bonding combination of the exact ground and first

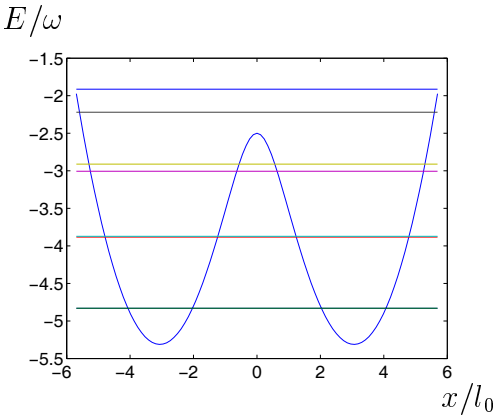

Figure 4.18: The Born-Oppenheimer surface U_- at g=5, α=4, $\delta = 0$. The exact eigenenergies are -4.8307, -4.8301, -3.8838, -3.8718, -3.0055, -2.9115, -2.2203, -1.9131. The two lower pairs of states are nearly degenerate, and the symmetric/ antisymmetric combinations are localized with probabilities 0.98 and 0.97

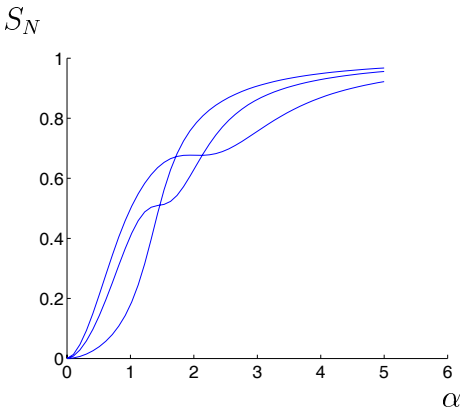

Figure 4.19: Entanglement entropies for the ground, second excited, and fourth excited states, at $g = 5$, $\delta = 0$. In the first and third excited states, S_N is nearly identical to S_N in the ground and second excited states. For the states above the first excited state, the curves have a step. For the selftrapped polaron states, the increase in S_N after this step is sharp; for nonpolaronic states, the further increase is slow.

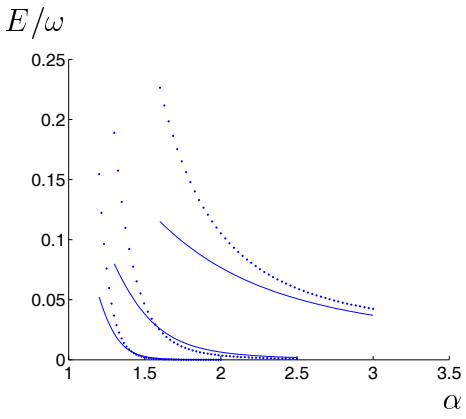

Figure 4.20: Dots: the semiclassical expression for t_p. Lines: the exact, half energy difference $(E_1 - E_0)/2$ for the lowest pair of states. Plotted for $g = 2, 5, 10$, $\delta = 0$. The larger g is, the faster does $(E_1 - E_0)/2$ converge toward t_p.

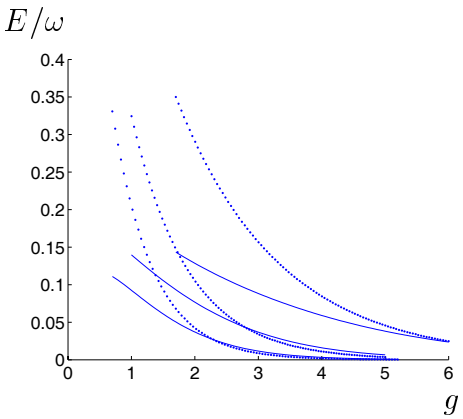

Figure 4.21: Dots: the semiclassical expression for t_p. Lines: the exact, half energy difference $(E_1 - E_0)/2$ for the lowest pair of states. Plotted for α=1.5,2,3, $\delta = 0$. The larger α is, the faster does $(E_1 - E_0)/2$ converge toward t_p.

excited states, fig. (4.5). The localization of Ψ_+ is the localization of the polaronic states, and less than 1 because $t_p > 0$.

4.6.4 Born-Oppenheimer surfaces in an asymmetrical system

We briefly consider the effect of an asymmetry δ on the Born-Oppenheimer surfaces. Representative potentials are plotted in fig. (4.15). Qualitatively, the effect of an asymmetry in the $\alpha < 1$ domain is to skew the potentials and shift the minimum of U_- toward X_0. When $\alpha > 1$, one well becomes higher in energy than the other. For any δ, a bifurcation in $\alpha = 1$ remains. It is easy to show that the two potentials have the same extrema.

In the case $\alpha = \infty$, the Born-Oppenheimer surfaces (for the uncoupled double dot) become

$$U_\pm/\omega = \pm\delta + \frac{1}{2}X(X \pm 2\sqrt{2g}) \tag{4.78}$$

which are two intersecting parabola, with extrema in $\pm\sqrt{2g}$ and $-\delta/\sqrt{2g}$. The energies in the wells are

$$U_+(-\sqrt{2g}) = (\delta - g)\ \omega \qquad\qquad U_-(+\sqrt{2g}) = (-\delta - g)\ \omega \tag{4.79}$$

and at the top of the barrier, the point of intersection between the parabola,

$$U_\pm(\frac{-\delta}{\sqrt{2g}}) = \frac{\delta^2}{4g}\ \omega \tag{4.80}$$

In this point, the energy of the dimer displacement exactly balances the 'displacement energy' of the electron, as the electron is with unequal probability on the two sites, which correspond to different onsite energies.

We note that the parabola are similar to Marcus parabola [45]. At $\delta = 2g\omega$, the intersection of the parabola occurs in the minimum of the 'upper' parabola, which therefore becomes an unstable configuration of the system.

Comparing the $\alpha = \infty$ results to the analysis for the symmetrical system, we expect that the minima of U_- for $\delta > 0$ approach $\pm\sqrt{2g}$ for α increasing above 1. For α decreasing below 1, one would expect that the single minimum approaches $\frac{-\delta}{\sqrt{2g}}$. The crossover in $\alpha = 1$ should be continuous, with the global minimum evolving from $\frac{-\delta}{\sqrt{2g}}$ to $\sqrt{2g}$ when α is increased in an interval around 1. Numerical explorations using Mathematica indicate that this is what happens, and that the width of the crossover interval is an increasing function of δ.

For the purposes of transport with polaron states, we do not need to consider the asymmetric potentials in further detail. The important thing to consider is whether the well states hybridize into delocalized polarons, ie. if the ratio $\delta\omega/t$ is small or large.

4.7 Polaron states

4.7.1 Selftrapping and polaronic excited states

The exponential dependence of t_p indicates polaronic selftrapping. The more localized the electron becomes, the more trapped it gets, because the dimer 'tilts' accordingly, and the electron must drag the displacement along with it in order to move between the sites. This happens for eigenstates below the semiclassical barrier, as the energy spacings approach 0 in a sudden manner for some $\alpha > 1$. The exponential decrease in g seems the same for all states except for a constant translation in g. See fig.s (4.22), (4.23).

4.7.2 Localized polarons

We have claimed that in the polaronic regime, the ratio $\frac{\delta\omega}{t_{eff}}$ determines the extend to which the polaron state becomes localized to one site. The effective tunneling coupling is $t_p \approx e^{-2g}$, and the exponential dependence of t_p on g should lead to exponentially small δ localizing the system.

Numerically, we find that when δ is nonzero, the system ground state becomes localized in the correlated regime for g larger than some value, g_0. This value depends logarithmically on δ, as predicted. See fig.s (4.24), (4.25).

This also makes some sense of the plot (4.13). The parameter values correspond to a polaronic state, and the entanglement peaks which are followed by a sharp decrease in entanglement are the ones corresponding to a value of δ much larger

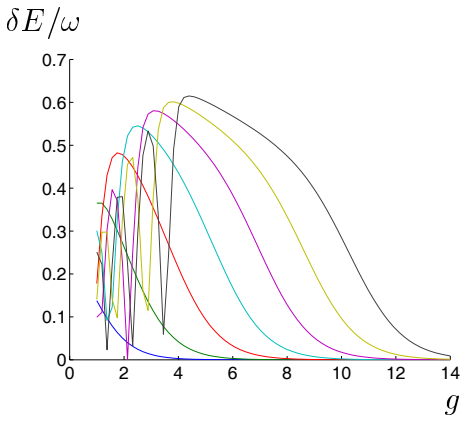

Figure 4.22: Polaronic degeneracies: at $\alpha = 4$, the 7 lower energy spacings δE between possible polaron pairs are plotted. The ones plotted all decrease in a similar manner, exponentially in g, and near-degeneracies occur in points at some constant spacing on the g axis.

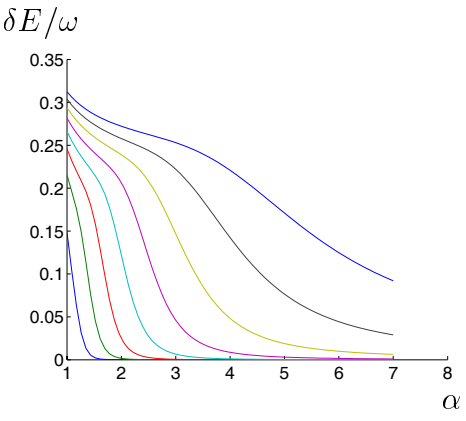

Figure 4.23: Polaronic degeneracies: at $g = 10$, the 8 lower energy spacings δE are plotted. The lower 5 or 6 energy differences approach 0 relatively sharply at some $\alpha > 1$, indicating that these states become selftrapped polarons. The higher energy differences only go to 0 gradually, indicating that no polaronic selftrapping occurs.

than $e^{-2g} \approx 5 \times 10^{-5}$. Asymmetries smaller than this are insufficient to localize the polaronic state.

Fig. (4.26) shows the α-dependence of $\langle\hat{\sigma}_z\rangle$ in the limit $\delta \gg e^{-2g}$. It looks like $\mathrm{d}\langle\hat{\sigma}_z\rangle/\mathrm{d}\alpha$ is discontinuous in $\alpha = 1$, which indeed it should become in the limit $e^{-2g}/\delta \to 0$. A small asymmetry now gives rise to a behaviour of $\langle\hat{\sigma}_z\rangle$ analogous to S_N in the large g limit when $\delta = 0$, see fig. (4.8).

4.7.3 Outlook

Now that we understand how polaron states come about in our model for a dimer, we can consider the transport properties of a dimer transistor. When a polaron state is present, the effective tunneling amplitude between the sites is strongly reduced, and our initial assumptions of small Γ and small $\boldsymbol{\gamma}$ may be violated, as $t_p \ll \Gamma, \boldsymbol{\gamma}$. In these situations, transport is no longer sequential, as the molecule can no longer be regarded as one isolated quantum system. However, it is still possible to describe transport through a rate equations approach, if t_p is small enough that the coherence of the dimer is completely destroyed. The two incoherent limits lead to different conductance properties of the molecule, as we shall see. In particular, the current through an incoherent molecule in an asymmetric device geometry may be highly nonlinear.

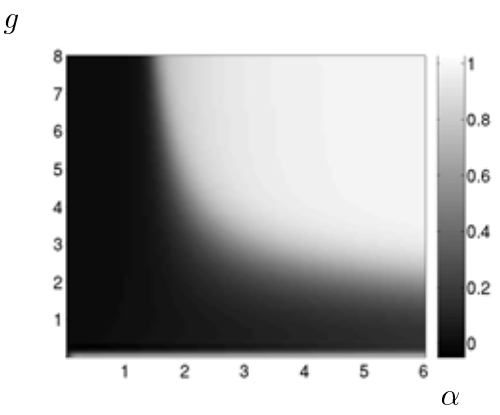

Figure 4.24: In the ground state, $\langle x \rangle / x_0$ is plotted at $\delta = 0.01$. The small value of δ is sufficient to localize the electron and 'tilt' the dimer when the effective tunneling coupling is exponentially small. This happens at approximately $\alpha > 1.5$ and at a sufficiently large g. The crossover in g follows the exponential dependence of t_p on $2g$. The crossover in α is also sharp. A plot of $\langle \hat{\sigma}_z \rangle$, not shown, is identical to this one.

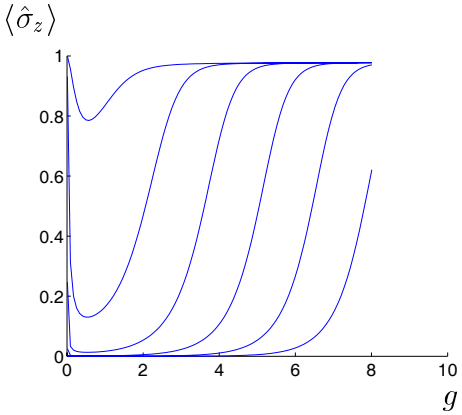

Figure 4.25: In the ground state, $\langle \hat{\sigma}_z \rangle$ is plotted at $\alpha = 5$ for δ =0.1,0.01,0.001,0.0001,0.00001,0.000001. The value g_0 of g where the electron becomes lozalized depends logarithmically on δ. The maximum that $\langle \hat{\sigma}_z \rangle$ approaches in all cases is dependent on α, approaching 1 when $\alpha \to \infty$.

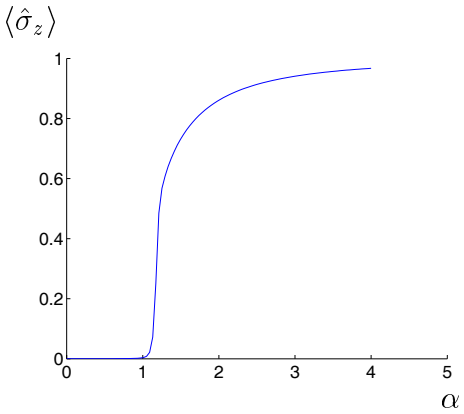

Figure 4.26: The α-dependent, δ-independent maximum that $\langle \hat{\sigma}_z \rangle$ approaches in the large g limit. Plotted for $g = 25$, $\delta = 0.01$.

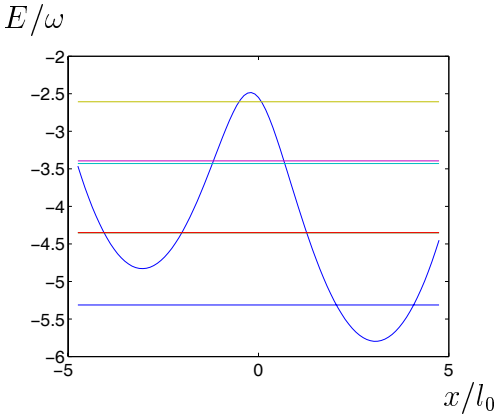

Figure 4.27: The lower Born-Oppenheimer potential surface at g=5, α=4, $\delta = 0.5$. The exact eigenenergies are -5.3125, -4.3523, -4.3494, -3.4289, -3.3934, -2.6067. The symmetric combination of the first and second excited states is localized with probability 0.98. Due to the choice of δ, the two states are close in energy, becoming degenerate in the limit $\alpha \to \infty$. This permits the electron in either state to 'spread out' over the two sites.

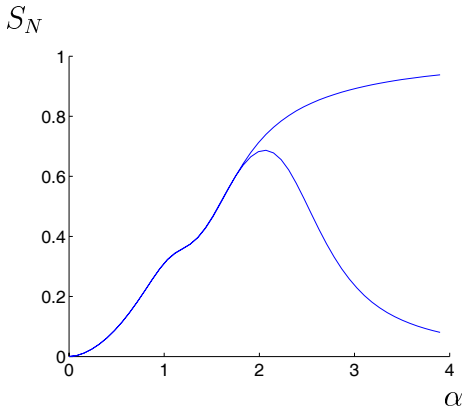

Figure 4.28: Entanglement entropy for the first excited state with parameters as in fig. (4.27) for the 'upper' curve, and with $\delta = 0.51$ for the 'lower' curve. We find that the state with δ=0.5 exactly becomes entangled in the manner of self-trapped polarons, even though the two near-degenerate well states correspond to different numbers of bosons. The opposite well states $|a,1\rangle$,$|b,0\rangle$, corresponding to different phonon numbers, nevertheless hybridize into coherent superposition states.

Chapter 5

Transport

5.1 Sequential transport

We are interested in current asymmetries that come about in devices where the dimer is placed at unequal distances to the 'left' and 'right' electrodes, and 'skewed' with respect to the gold surfaces. In terms of the tunneling rates, we focus on the situation $\Gamma^L \gg \Gamma^R$, $\Gamma^{Ra} < \Gamma^{Rb}$. This is the geometry in fig. (3.1). As a unit we use

$$\Gamma = \frac{2\Gamma^L\Gamma^R}{\Gamma^L + \Gamma^R} \tag{5.1}$$

When $\Gamma^L = \Gamma^R$, then $\Gamma = \Gamma^L = \Gamma^R$. We define an asymmetric geometry:

$$\Gamma^L = 50\Gamma^R \tag{5.2}$$

$$\Gamma^{La} + \Gamma^{Ra} = \Gamma^{Lb} + \Gamma^{Rb} \tag{5.3}$$

The 'skewed-ness' of the geometry, which we will vary, is determined by, eg., Γ^{Ra}. Given Γ^{Ra}, the other rates follow from the above equations:

$$\Gamma^{Rb} = 0.51\Gamma - \Gamma^{Ra} \qquad \Gamma^{La} = 13.005\Gamma - \Gamma^{Ra} \qquad \Gamma^{Lb} = 12.495\Gamma + \Gamma^{Ra} \tag{5.4}$$

These are the values we use whenever we calculate for an asymmetric geometry in the following. When $\Gamma^{Ra} = \Gamma^{Rb}$ the geometry is 'unskewed'.

Sequential transport in the case $\delta = 0$ does not depend on the four rates individually, but on the sums Γ^η; in this situation, the 'skewed' geometry has no effect. When the system becomes polaronic, the polaronic tunneling rates become exponentially small, and sequential transport requires exponentially small $\Gamma^{\eta\sigma}$s, $t_p \ll \Gamma$. Also, dissipation tends to localize the electron, an effect we disregard for now by assuming $t_p \gg \boldsymbol{\gamma}$. We have assumed that relaxation to a thermal distribution is 'instantaneous', $\boldsymbol{\gamma} \gg \Gamma$. Broadening of the steps on the IV is considered thermal rather than a result of dissipation or tunneling broadening, ie. $k_BT \gg \boldsymbol{\gamma}, \Gamma$. Finally, recall the condition $\boldsymbol{\gamma}/\omega \ll \pi/2g$ for dissipative broadening

to be insignificant even at $T = 0$. Putting all these conditions together, sequential transport with relaxation to thermal equilibrium distribution of states and thermal broadening of the conductance peaks corresponds to $t_p, k_BT, \omega\pi/2g \gg \boldsymbol{\gamma} \gg \Gamma$.

5.1.1 The large V limit

When the bias voltage is large, $e|V| \gg k_BT$ and the relevant energies, we can understand the current in sequential transport just from the Master equation expression, including asymmetry effects. This is a good place to start. When $V = \infty$, the Fermi functions in the expression for the current become 1 in the direction of the current and 0 in the opposite direction. In the positive current direction, with the electrons travelling from the 'right' to the 'left' electrode, the in-tunneling rates become

$$\Gamma_{10}^{R\sigma} = \Gamma^{R\sigma} \sum_{i_0} W_{i_0} (\sum_{f_1} |\langle f_1 | c_\sigma^\dagger | i_0 \rangle|^2) = \Gamma^{R\sigma} \sum_{i_0} W_{i_0} = \Gamma^{R\sigma} \tag{5.5}$$

writing W_{i_0} for the Boltzmann weights of the 'empty' initial states, and using that M (section 3.3) is an orthonormal matrix with the row sum over f_1 equal to 1. The sum over intitial states contains terms corresponding to an electron inserted on σ.

For out-tunnelings to the left, with the Boltzmann weights W_{i_1},

$$\Gamma_{01}^{L\sigma} = \Gamma^{L\sigma} \sum_{i_1} W_{i_1} (\sum_{f_0} |\langle f_0 | c_\sigma | i_1 \rangle|^2) = \Gamma^{L\sigma} \sum_{i_1} W_{i_1} \langle n_\sigma \rangle_{i_1} = \Gamma^{L\sigma} N_\sigma^{01} \tag{5.6}$$

with $\langle n_\sigma \rangle_{i_1}$ the electron density on σ for the 'filled' eigenstate i_1. Here,

$$N_a^{01} + N_b^{01} = 1 \qquad \text{If } \delta = 0: \quad N_a^{01} = N_b^{01} = \frac{1}{2} \tag{5.7}$$

The current I_{max} for large, positive V is

$$\frac{I_{max}}{e} = \frac{\Gamma_{10}^R \Gamma_{01}^L}{\Gamma_{10}^R + \Gamma_{01}^L} = \frac{\Gamma^R (\Gamma^{La} N_{01}^a + \Gamma^{Lb} N_{01}^b)}{\Gamma^R + (\Gamma^{La} N_{01}^a + \Gamma^{Lb} N_{01}^b)} \tag{5.8}$$

Let $\delta = 0$. Then, we recover the well-known expression

$$\frac{I_{max}}{e} = \frac{\Gamma^R \Gamma^L}{2\Gamma^R + \Gamma^L} \tag{5.9}$$

which is independent on the σ index.

The factor of 2 between in-tunnelings and out-tunnelings comes about because an electron can tunnel onto the dimer in two ways, via two localized site orbitals, while an electron on the dimer only occupies the two sites with a total probability of 1.

Now, if the direction of the large bias voltage is changed, the current becomes the minimum current I_{min}, which is $(-I_{max})$ with L, R interchanged. Therefore,

$$|\frac{I_{max}}{I_{min}}| = \frac{\Gamma^R + 2\Gamma^L}{2\Gamma^R + \Gamma^L} \in [\frac{1}{2}, 2] \tag{5.10}$$

equal to 1 when $\Gamma^L = \Gamma^R$. In general, the current in an asymmetrical device with $\delta = 0$ is suppressed in one direction of the current with as much as a factor of 2.

For $\delta > 0$, the electron density is not generally symmetrically distributed on the sites. The current may still be invariant under the substitution $\sigma \to \hat{\sigma}$, however, which is the case if the geometry is unskewed, with $\Gamma^{\eta a} = \Gamma^{\eta b}$ for both η. The unskewed situation therefore gives rise to no asymmetry effects beyond a factor of 2 at most. Any degree of localization of the electronic state brought on by δ does not give rise to rectification, here.

Therefore, we move on to a device geometry with four different $\Gamma^{\eta\sigma}$, and a level detuning δ. We find that the ratio $\frac{k_B T}{\delta\omega}$ is important, contrary to the usual case where the large V limit is temperature-independent. This happens because of δ-induced localization effects, which are dependent on T. Two limit cases:

In one limit case, one of two conditions is fulfilled: either the lower 'filled' eigenstates are delocalized, or $\frac{k_B T}{\delta\omega} \gg 1$. The latter means that the Boltzmann distribution of eigenstates makes irrellevant any degree of localization brought on by δ. The large $|V|$ limit is as described above.

In the opposite limit, the relevant, lower eigenstates are localized, implying $\frac{k_B T}{\delta\omega} \ll 1$. The thermal distribution of states is with a high probability localized to site b. We take eq. (5.8) as the starting point, assuming that the 'filled' dimer thermal state (call it $|T_1\rangle$) is completely localized, with $\langle n_a \rangle = 0$, $\langle n_b \rangle = 1$. It follows that out-tunnelings occur only from site b, because the overlap matrix elements $\langle a\ n|T_1\rangle = 0$ for all n. In-tunnelings, however, may occur from either site. Actually, this may seem peculiar, because it means an electron entering on site a relaxes to a state on site b in a limit where the states are effectively uncoupled by a large energy difference between the localized site orbitals. This is a result of our assumption that the system relaxes 'instantaneously' to a thermal distribution.

Setting $N_a^{01} = 0$,$N_b^{01} = 1$, eq. (5.8) becomes:

$$\frac{I_{max}}{e} = \frac{\Gamma^R \Gamma^{Lb}}{\Gamma^R + \Gamma^{Lb}} \tag{5.11}$$

The expression contains no left/ right asymmetry factor of 2 as in eq. (5.9). Instead, it resembles the current through a single dot.

In the opposite bias voltage direction, one acquires an expression similar to this, except that L and R are interchanged. The ratio between the limits expresses the asymmetry in the current:

$$|\frac{I_{max}}{I_{min}}| = \frac{\Gamma^R \Gamma^{Lb}}{\Gamma^R + \Gamma^{Lb}} \frac{\Gamma^L + \Gamma^{Rb}}{\Gamma^L \Gamma^{Rb}} = \frac{\Gamma^{Lb}(1 + \frac{\Gamma^{Rb}}{\Gamma^L})}{\Gamma^{Rb}(1 + \frac{\Gamma^{Lb}}{\Gamma^R})} \tag{5.12}$$

For $\Gamma^{Lb} = \Gamma^{Rb}$ this is 1, a symmetrical current. Since electronic localization is to site b, the ratio between the 'left' and 'right' tunneling couplings to this site determines the current asymmetry. From the expression, we see that if one of the rates $\Gamma^{\eta b}$ is close to 0, or one of the two is much larger than the other one, $|\frac{I_{max}}{I_{min}}|$

becomes close to 0 or ∞, a highly asymmetrical current. The inhibited direction is the one where a small out-tunneling rate serves as a 'bottleneck' for the current.

In an 'unskewed' system, substituting $\Gamma^{\eta\sigma} \to \Gamma^{\eta}/2$ in eq. (5.12), the expression in eq. (5.10) is recovered. This confirms our earlier claim that localization effects require the system to be 'skewed' in order to affect the current.

5.1.2 Linear current

Another limit that can be broken down in a simple fashion is the limit of small bias voltages. At temperatures sufficiently low that the ground and first excited states of both charge states are clearly resolved, the linear conductance depends only on the ground states of the 'empty' and 'filled' dimer, as well as device geometry. We define the 'linear current' ΔI_L as the full height of the step on the IV characteristic corresponding to current running via the ground states. We assume $k_B T \ll \omega, E_{1_1} - E_{0_1}$. From the rate equations, we see that the current along the first step for positive bias voltage has the value

$$\frac{\Delta I_L/2}{e} = \frac{(Q_a\Gamma^{Ra} + Q_b\Gamma^{Rb})(Q_a\Gamma^{La} + Q_b\Gamma^{Lb})}{Q_a\Gamma^{Ra} + Q_b\Gamma^{Rb} + Q_a\Gamma^{La} + Q_b\Gamma^{Lb}} \tag{5.13}$$

where $Q_\sigma \equiv |\langle 0_0|c_\sigma|0_1\rangle|^2$. The linear current transforms identically when $L \leftrightarrow R$ regardless of device geometry, and is therefore symmetrical in V. The linear current becomes 0 if the electron is localized to one site σ and just one of the corresponding rates $\Gamma^{\eta\sigma} = 0$.

If $\delta = 0$, the absolute values of the matrix elements for a and b are equal, and the small-bias current is

$$\frac{\Delta I_L/2}{e} = Q_a \frac{\Gamma^L\Gamma^R}{\Gamma^L + \Gamma^R} = \frac{Q_a}{2}\Gamma \tag{5.14}$$

For any δ, if the geometry is 'unskewed', when the substitution $\Gamma^{\eta\sigma} \to \Gamma^{\eta}/2$ is performed in eq. (5.13), we get

$$\frac{\Delta I_L/2}{e} = (Q_a + Q_b)\frac{\Gamma}{2} \tag{5.15}$$

We now consider the dependence of the linear current on the model parameters, ie. through the overlaps Q_a, Q_b. In the parameter regime where the 'filled' ground state corresponds to selftrapped polarons, the linear current is strongly reduced, because the overlap between the polaronic state and the 'empty' ground state is exponentially small in g.

Expanding the 'filled' ground state,

$$|0_1\rangle = \sum_{\sigma n} \nu_{\sigma n}|\sigma n\rangle = \sum_{\sigma} |\sigma\rangle \otimes \Big(\sum_{n} \nu_{\sigma n}|n\rangle\Big) \tag{5.16}$$

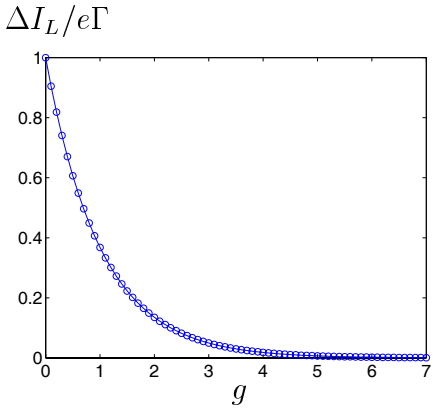

Figure 5.1: The linear current in the double dot limit (t=0), with δ=0. With circles, we have plotted e^{-g}, the linear current for a Poissonian spectral function.

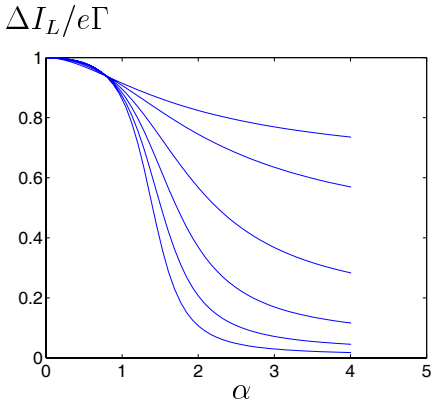

Figure 5.2: Linear current at $\delta = 0$, $\Gamma^L = \Gamma^R = \Gamma$, for $g = \frac{1}{2}$, 1, 2, 3, 4, 5, from the top.

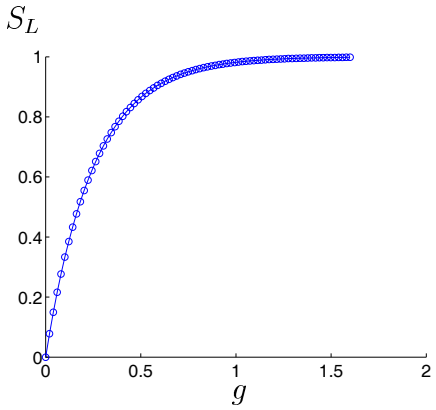

Figure 5.3: Linear entropy S_L in the double dot limit (t=0), with $\delta = 0$. With circles, we have plotted $1 - e^{-4g}$ for comparision. This establishes a connection between linear current and linear entropy in the double dot limit: $S_L = 1 - (\Delta I_L/e\Gamma)^4$ in a symmetric device. Outside the limit, linear current may measure entanglement if $\delta = 0$.

the overlap with the 'empty' ground state with an electron inserted on, say, site a, is

$$\langle a0|0_1\rangle = \langle a0| \sum_\sigma |\sigma\rangle \otimes \Big(\sum_n \nu_{\sigma n}|n\rangle\Big) = \nu_{a0} \tag{5.17}$$

The linear current is therefore determined by ν_{a0}^2 and ν_{b0}^2. We considered these probabilities in section 4.4. In the selftrapped polaron regime, they become exponentially small and the sum $\nu_{a0}^2 + \nu_{b0}^2$ approximately equal to e^{-g}.

The physics in this is that the ground state overlap becomes small when the two ground states, 'empty' and 'filled', correspond to different configurations of the dimer. From our work in previous sections, a 'filled' ground state 'tilted' configuration contains correlation between the electronic and bosonic degrees of freedom. It follows that the linear current measures correlation. As previously explained, either α sufficiently large, or sufficiently large δ will push the system into a correlated regime, and in either case, the linear current approaches a minimum, $(Q_a + Q_b)e\Gamma/2 = \exp(-g)e\Gamma/2$ (in the case of an 'unskewed' geometry). When $g \approx 6$, the linear current becomes vanishingly small. See fig. (5.1).

In the uncorrelated regime, the linear current becomes maximum: at $\delta = 0$, $\Delta I_L \to e\Gamma$ when $\alpha \to 0$ or $g \to 0$.

We plot the linear current in fig. (5.2). In fig. (5.3), we make a comparision to linear entropy.

5.1.3 Diamond plots in the nonpolaronic regime

In fig.s (5.5), (5.6), we present diamond plots for sequential transport for $\delta = 0$, $g = 1$, $k_BT = 0.1\omega$, and $\alpha = 4$ in a symmetrical and an asymmetrical geometry, for comparision with the C_{60} monomer diamond plots in [28], see section (1.8). The new features for the dimer are that the sidebands are more complicated, and that the diamond plots have lower symmetry. If α is too small, the sidebands become weak compared to the linear conductance; we therefore plot for a quite large value of α and a value of g that does not correspond to selftrapped polarons.

For the diamond plots presented here, when $V_g = V_c$, $eV_c/\omega = E_{0_0} - E_{0_1}$, the linear conductance is strong, corresponding to current running via the ground states of the 'empty' and 'filled' dimer. This is the peak in (V_g, V)=(V_c,0). Defining $\Delta E_{m,n} \equiv E_{m_1} - E_{n_0}$, for nonzero bias voltages, current runs for points in the (V_g, V) plane where $\pm\frac{eV}{2} \approx eV_g - \Delta E_{m,n} \pm k_BT$. The diamond plots exhibit Coulomb blockade and sidebands, corresponding to transitions involving excited states of the 'empty' and 'filled' molecule. At the points where the sidebands meet the Coulomb blockade area, the excitation energies may be read off at the V axis.

For C_{60}, the 'empty' and 'filled' eigenstates were both harmonic oscillator states, although the 'filled' states were displaced by the electron-vibron coupling. For the dimer, the 'empty' eigenstates are harmonic oscillator states, but the 'filled' eigenstates are the more complicated, spin-boson-like eigenstates of H. For the reasons given in section 1.8, this breaks the symmetry which exists in the monomer

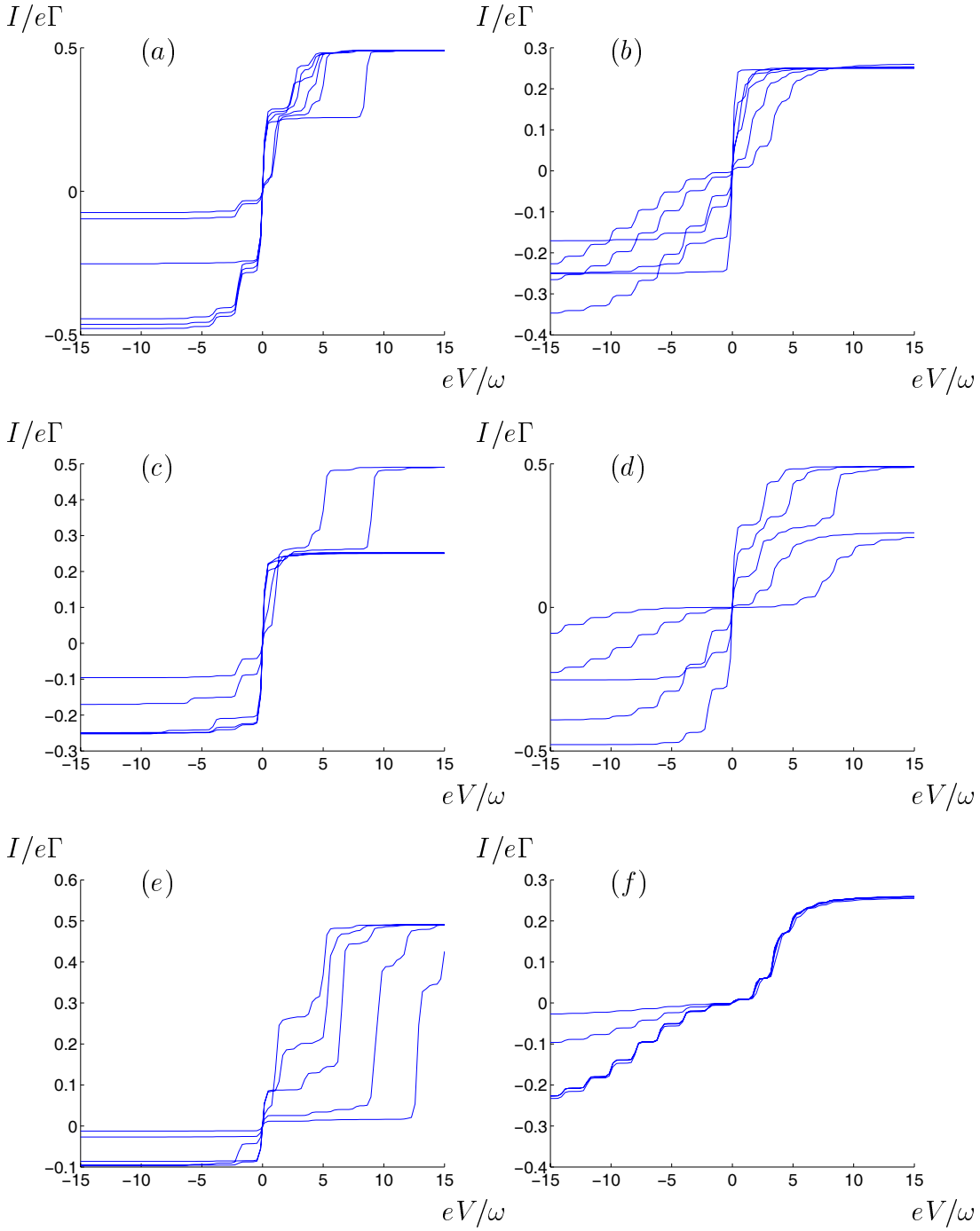

Figure 5.4: IV characteristics in sequential transport for the asymmetrical device geometry, plotted for $V_g = E_{0_0} - E_{0_1} + \delta\omega/e$, $\Gamma^{Ra} = 0$, $k_BT = 0.05\omega$. Other parameter values are: (a): $\delta = 0$, $g = 0.5$, $\alpha = 0.5, 1, 1.25, 1.5, 2, 3$. (b): $\delta = 0$, $g = 5$, $\alpha = 0.5, 1, 1.25, 1.5, 2, 3$. (c): $\delta = 0$, $\alpha = 1$, $g = 0.5, 1, 2, 5, 10$. (d): $\delta = 0$, $\alpha = 3$, $g = 0.5, 1, 2, 5, 10$. (e): $g = 0.5$, $\alpha = 1$, $\delta = 0, 0.5, 1, 2, 3$. (f): $g = 5$, $\alpha = 3$, $\delta = 0.001, 0.01, 0.02, 0.04, 0.1$.

diamond plot around the $V_g = V_c$ axis for the symmetrical device geometry.

The plot with $\Gamma^R = \Gamma^L$ is symmetrical about the $V = 0$ axis but not about the $V_g = V_c$ line, which is a result of the different overlaps between the two sets of eigenstates. The difference it makes to the conductance if an adjustment of V_g is positive or negative with respect to V_c can be seen as a result of the dissimilarity between making the number of electrons $\langle N \rangle$ on the dimer smaller or larger, respectively, with respect to the equilibrium value N_0, which is determined by the rates; $N_0 = \frac{1}{2}$ when $\Gamma^L = \Gamma^R$, $\delta = 0$. When V_g is turned down from V_c, we have $\langle N \rangle > N_0$ and the dimer is filled most of the time, and the excitation spectrum of the filled dimer dominate the IV curves, in the sense that the strong sidebands correspond to the energy differences $\Delta E_{n,0}$.

Similarly, when V_g is turned up from V_c, the excitations of the empty dimer dominate the current with strong sidebands corresponding to the energy differences $\Delta E_{0,n}$.

When the system is not symmetric, the symmetry around $V = 0$ is removed as the sidebands become weaker in one direction than in the other, as described in section 1.8. For $V < 0$ the lines we see correspond to transitions involving excited states of the 'empty' molecule, equally spaced harmonic oscillator states. For $V > 0$ we see lines corresponding to transitions involving excited states of the 'filled' molecule. This is all for 'right' tunnelings suppressed. This makes sense, because when $\Gamma^L \gg \Gamma^R$ and $V < 0$ the molecule will be 'empty' most of the time, and when $V > 0$ the molecule will be 'filled' most of the time.

5.1.4 Diamond plots in the polaronic regime when $\delta = 0$

When $\delta = 0$, the parameters α, g determine if and to what extend the ground state and the lower excited states are polaronic. Just as the linear current is inhibited by a polaronic state, so is the current through the 'filled' excited states inhibited when these states are polaronic. In the polaronic parameter regime, this results in an apparent gap in the diamond plots, separating the 'upper' and 'lower' diamonds. At $V_g = V_c$ there exists an interval in bias voltage around $V = 0$ where the current is very nearly blocked, because the differential conductance is exponentially small. See fig. (5.7).

We stress that in this parameter regime, the effective tunneling coupling between the polaronic states is exponentially small, and so sequential transport requires that the rates $\Gamma^{\eta\sigma}$ are exponentially small, too. Also, $\boldsymbol{\gamma}$ must be exponentially small, because dissipation localizes the electron when $\boldsymbol{\gamma} \gg t_p$. These assumptions may become unrealistic quite fast as we move into the polaronic parameter regime.

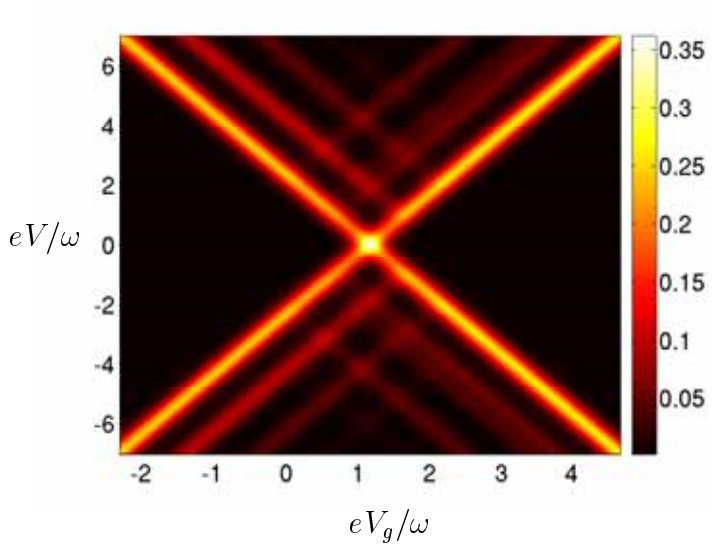

Figure 5.5: Sequential transport, with $g = 1$, $\alpha = 4$, $\delta = 0$, $k_BT = 0.1\omega$. The device geometry is symmetrical with all $\Gamma^{\eta\sigma} = \frac{1}{2}\Gamma$.

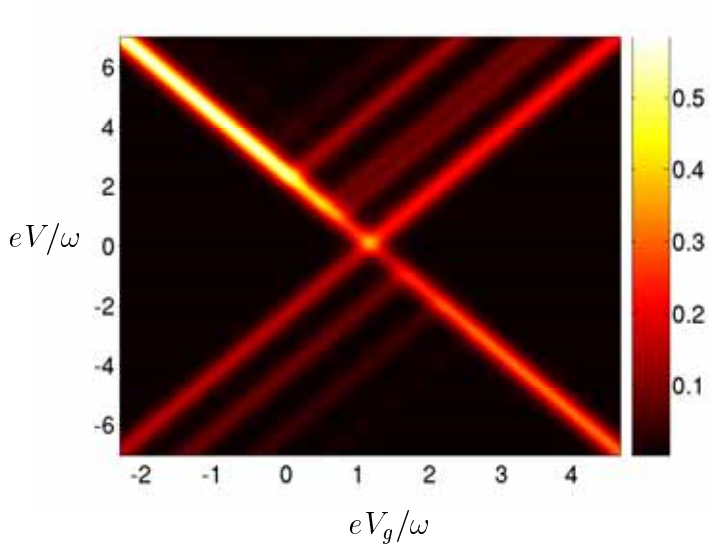

Figure 5.6: Sequential transport in our asymmetrical device geometry, with $\Gamma^{Ra} = \Gamma^{Rb}$, $g = 1$, $\alpha = 4$, $\delta = 0$, $k_BT = 0.1\omega$.

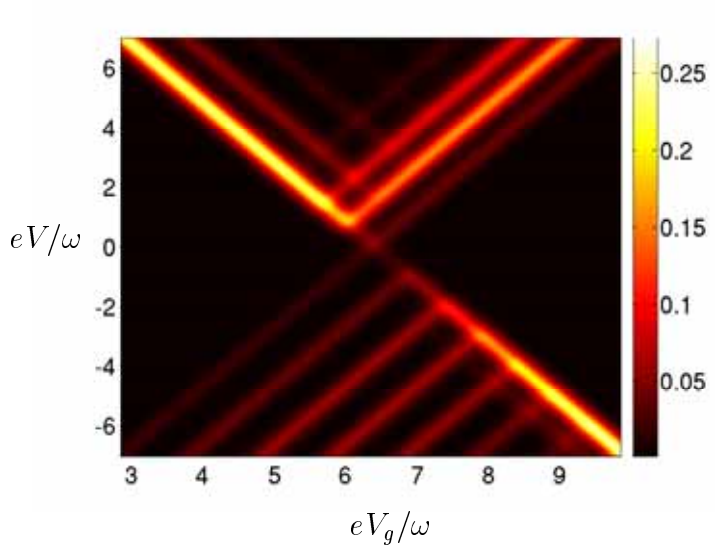

Figure 5.7: Sequential transport, with $g = 5$, $\alpha = 2$, $\delta = 0$, $k_BT = 0.1\omega$. The device geometry is asymmetrical and 'skewed', with $\Gamma^{Ra} = 0$.

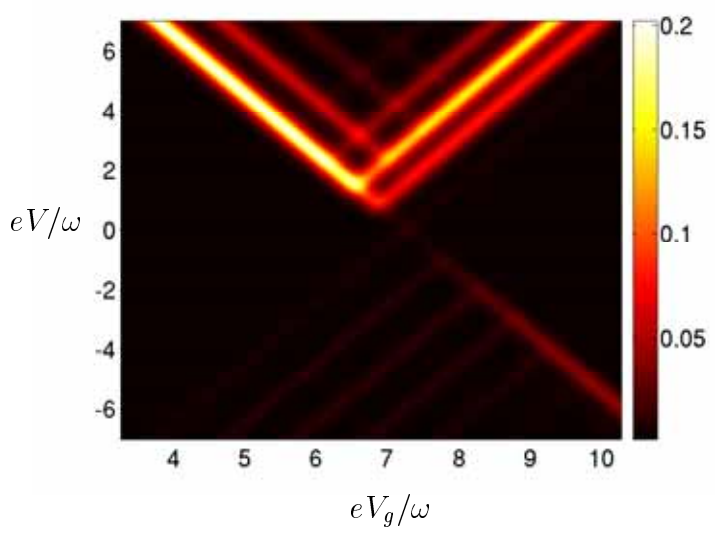

Figure 5.8: Sequential transport, with $g = 5$, $\alpha = 2$, $\delta = 0.5$, $k_BT = 0.1\omega$. Device geometry is asymmetrical and 'skewed', with $\Gamma^{Ra} = 0$.

5.1.5 Diamond plots in the polaronic regime with $\delta > 0$

For $\delta \neq 0$, the competition between $\delta\omega$ and k_BT is important in the correlated regimes, and so is the 'skewed' geometry. As before, we must have $\Gamma, \boldsymbol{\gamma} \ll t_p$.

As t_p becomes exponentially small, the ratio $\frac{\delta\omega}{t_p}$ becomes exponentially large, and the low-energy 'filled' eigenstates becomes highly site-localized states. If furthermore $\frac{k_BT}{\delta\omega} \ll 1$, the states localized to site b remain much more probable than the others. In an asymmetrical device geometry, this leads to a highly asymmetrical current due to the condition $\boldsymbol{\gamma} \gg \Gamma^{\eta\sigma}$, as previously explained. Fig. (5.4 (f)) shows how rectification sets in when δ is varied at a fixed temperature. Fig. (5.8) shows a diamond plot with some rectification effect, but here $\delta = \frac{1}{2}$ exactly, a somewhat artificial situation to consider, because here the high energy localized site orbital is close to resonance with the low energy site with one phonon added. This is the situation depicted in fig.s (4.27) and (4.28). Rectification here is a result of $\alpha < \infty$, because if α is increased, the difference in energy between the two near-degenerate states approach 0, and we are in the delocalized situation again with no rectification effect.

The situations described above lead to rectification, but not to NDC. Rectification comes about because the Franck-Condon overlap factors connecting the different dimer configurations become small, but there is no 'blocking' effect of the sort described in our 'toy model', where the occupation of a localized, effective single-dot state could block the current through another, effective single-dot state. In the current model for the current, however, the 'filled' states remain coherent states of the entire molecule, in spite of being highly localized. The states that become available when bias voltage is turned up in the inhibited direction all contribute to the current by a positive differential conductance. For this reason, the physics described here cannot lead to NDC.

For $\alpha < 1$ and large δ, small T, near-rectification is possible, because the 'filled' ground state becomes a 'tilted' configuration. See fig. (5.4 (e)).

In a real system, at very large V, the bias voltage should act as a temperature in 'smearing' the electron states, an effect that our model does not take into account. This could restore the current in the large (-V) limit. Then, the rectification described in the above would be a phenomenon associated with moderate bias voltages, only.

5.2 Transport in an incoherent double dot

In the previous section, the polaronic effects we considered required exponentially small $\boldsymbol{\gamma}$ and $\Gamma^{\eta\sigma}$s. Here, we still assume $\boldsymbol{\gamma} \gg \Gamma$, but now, the limit that we consider is $t_p, \Gamma^{\eta\sigma} \ll \boldsymbol{\gamma}$, which becomes more realistic in the polaronic domain and gives rise to new effects. In the limit, the strong dissipation localizes the electron, because the coupling to the dissipative environment is through the boson coordinate, x, which in turns couples to $\hat{\sigma}_z$. This destroys the phase coherence of the electron,

reducing ρ_{ab}. Hopping on the dimer therefore becomes small, hence the current can be modelled from a Master equation approach for the double dot, an approach that neglects the off-diagonal terms in the electron density matrix. A similar effect would result if $\Gamma \gg t_p$, because then a polaronic state is no longer resolved on the time scale defined by Γ. Either way, the physical picture is changed, because now the electron enters into a site-localized polaronic state and is not 'smeared out' into a delocalized polaron, ie. into a combination of the near-degenerate polaron states. The electron therefore leaves the molecule from the polaronic state that it entered into.

Of course, this polaronic state is probably not 100 % localized. Therefore, the electron can in fact leave the dimer from the site orbital opposite to the one it entered into. The probability for this is determined only by diagonal terms in the electron density matrix.

5.2.1 Completely localized polarons

A 'quick and dirty' approach to calculating diamond plots is to set the polaronic tunneling coupling t_p equal to 0 corresponding to completely localized polarons (or, in terms of IV curves, vanishing linear conductance). This is realistic for $g > 5$, $\alpha > 4$. The rate equations for the uncoupled double dot:

$$0 = \frac{dP_0}{dt} = \sum_\eta \Gamma_{01}^{\eta a} P_a + \Gamma_{01}^{\eta b} P_b - (\Gamma_{10}^{\eta a} + \Gamma_{10}^{\eta b}) P_0 \tag{5.18}$$

$$0 = \frac{dP_a}{dt} = \sum_\eta \Gamma_{10}^{\eta a} P_0 - \Gamma_{01}^{\eta a} P_a \tag{5.19}$$

$$0 = \frac{dP_b}{dt} = \sum_\eta \Gamma_{10}^{\eta b} P_0 - \Gamma_{01}^{\eta b} P_b \tag{5.20}$$

$$1 = P_0 + P_a + P_b \tag{5.21}$$

Here, P_0 is the probability for the dimer being empty, and P_i, $i = a, b$, the probabilities for the dimer being occupied with the electron localized to site i. The Master equations insure that an electron on the dimer can leave from the site that it entered, only.

Solving for the steady state probabilities, and defining the current positive for electrons hopping from 'right' to 'left' in the device,

$$\frac{I}{(-e)} = P_0(\Gamma_{10}^{La} + \Gamma_{10}^{Lb}) - (P_a \Gamma_{01}^{La} + P_b \Gamma_{01}^{Lb}) \tag{5.22}$$

we arrive at the following expression for the current:

$$\frac{I}{(-e)} = \frac{\sum_\sigma (\Gamma_{10}^{L\sigma} - \Gamma_{01}^{L\sigma} \frac{\sum_\eta \Gamma_{10}^{\eta\sigma}}{\sum_\eta \Gamma_{01}^{\eta\sigma}})}{1 + \sum_\sigma \frac{\sum_\eta \Gamma_{10}^{\eta\sigma}}{\sum_\eta \Gamma_{01}^{\eta\sigma}}} \tag{5.23}$$

For $\delta = 0$ we use the usual rates $\Gamma_{01}^{\eta\sigma}$, $\Gamma_{10}^{\eta\sigma}$ in the Master equations. The rates depend on energies which are now correct within an error of t_p, an error that we ignore. The overlap matrix elements in the rates are of course calculated for the delocalized states, whereas they should be calculated for the localized combinations $\Psi_\pm$. However, when the electronic densities on the sites are equal in the eigenstates Ψ_j (due to $\delta = 0$), and $\Psi_\pm$ are completely localized, the result for the rates is the same.

In our highly asymmetrical device geometry, this calculation leads to diamond plots with rectification and NDC. In fig. (5.12) we show the diamond plot in the special case of $\Gamma^{Ra} = 0$. The condition $\Gamma^{Ra} = 0$ prevents out-tunneling to the 'right' for an electron entering on site a from the 'left'. The condition that only one electron may occupy the dimer at one time means no current can run during the time intervals the electron is stuck on site a, but then the electron may escape the way it came in; if it cannot, the current is blocked, which happens for negative V. Some current does run at small enough bias voltage due to thermal excitation of the system, which allows an electron on site a to tunnel out 'uphill', against the bias voltage; the system is blocked only during finite periods of time, and current can run through the device via the b site the rest of the time. It follows that nonzero current at small bias voltage requires $T > 0$, and we must in fact have $k_B T > (-V)$. When $(-V)$ is increased beyond $k_B T$, thermal excitations can no longer free a trapped electron. This gives rise to NDC, because the current at large $(-V)$ is identically 0. A further requirement for all this is $V_g > 0$, because positive gate voltages stabilize the 'empty' state, while a $V_g < 0$ stabilizes the 'blocking' state.

Now, we briefly consider the case $0 < \Gamma^{Ra} < \Gamma^{Rb}$. Current runs in the inhibited direction for all $|V|$, but the rate Γ^{Ra} is the bottleneck that the current must pass through, and for large $|V|$ the current approaches a plateau value that is approximately proportional to Γ^{Ra}. NDC occurs when the plateau value is closer to 0 than the small-bias current. NDC dies out when $\Gamma^{Ra} \to \Gamma^{Rb}$. See fig. (5.9) for a plot of this and for some other illustrative plots. The dependencies of NDC on temperature and gate voltage are plotted in fig.s (5.10) and (5.11).

The above, rough treatment shows that rectification and NDC come about in our model for a dimer molecule in an extreme polaronic limit for an asymmetric device geometry. It happens as a result of a polaronic state that effectively destroys the coherence of the molecule on the time scale of either the lead tunnelings $\Gamma^{\eta\sigma}$ or the dissipation $\boldsymbol{\gamma}$. The simple calculation leads to the highly nonlinear current effects described by Pasupathy et al.

5.2.2 Near-localized polarons

In reality, t_p is nonzero, and as a result, the polaron states are not completely localized. Still in the incoherent limit, we improve our results by taking the delocalization of $\Psi_\pm$ into account. For the relevant parameter values, the lowest

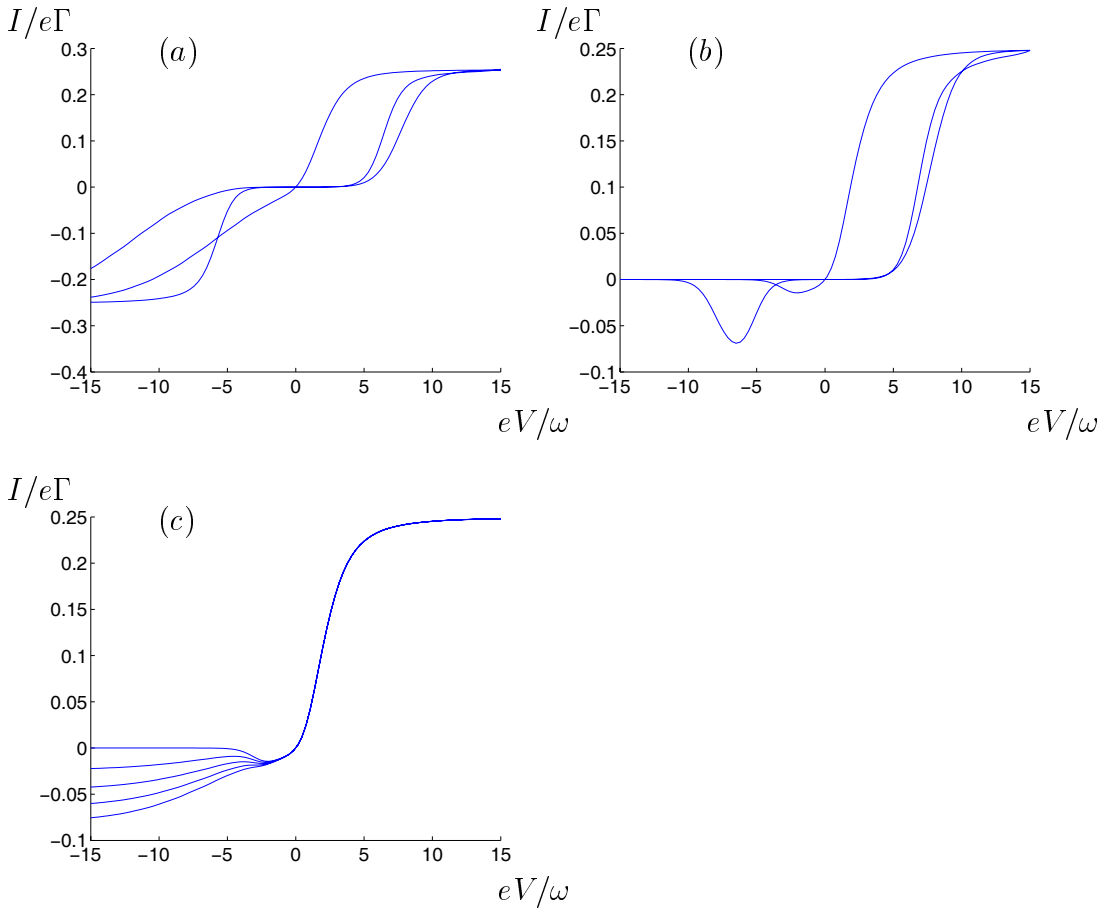

Figure 5.9: (a) and (b) present IV curves in sequential transport and for the localized polaron double dot, respectively, in the asymmetrical and 'skewed' device geometry with $\Gamma^{Ra} = 0$, at $g = 5$, $\alpha = 2$, $\delta = 0$, $k_BT = 0.3\omega$, at gate voltages $V_g = V_c, V_c \pm 3\omega/e$ In (b), the large NDC peak is for positive $(V_g - V_c)$. In (c), Γ^{Ra} is varied for the double dot, $\Gamma^{Ra}/\Gamma = 0, 0.025, 0.050, 0.075, 0.100$. We see that the plateu values the current approaches in the inhibited direction is approximately proportional to the 'bottleneck' Γ^{Ra} when $\Gamma^{Ra} \ll \Gamma^{Rb}$, and that NDC disappears when $\Gamma^{Ra} \to \Gamma^{Rb}$.

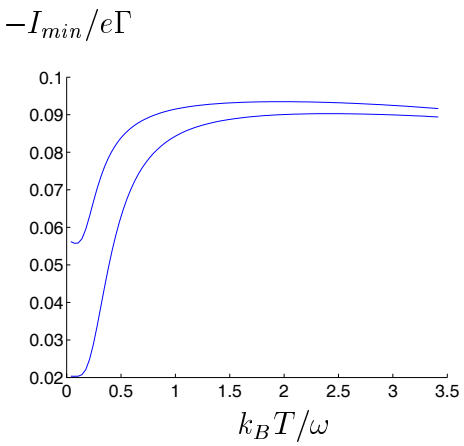

Figure 5.10: NDC measured as the minimum value of the current, I_{min}, with $g = 5$, $\delta = 0$, $eV_g = eV_c + 10\omega$, at α=2, 4, the lower curve corresponding to the larger value of α.

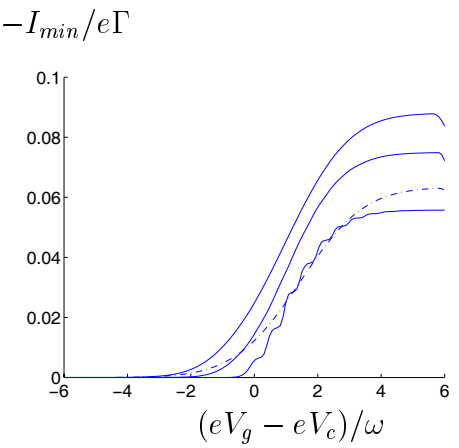

Figure 5.11: NDC measured as in fig. (5.10), with $g = 5$, $\delta = 0$. The 3 upper lines, from the bottom: $\alpha = 2$, $k_BT/\omega = 0.1, 0.3, 0.5$. 'Slash-dot' line: $T = 0.5$, $\alpha = 4$. NDC increases with temperature, decreases with increasing α.

polaron states are about 0.90-0.95 localized, so delocalization of the polaron states is an important effect. The picture is that an electron tunneling into the polaronic state on, say, site a, near-localized with some probability P_a, leaves the dimer with probability $P_a\Gamma^a$ from site a and probability (1-P_a)Γ^b from site b. On the other hand, an electron entering a nonpolaronic state is assumed completely delocalized, $P_a = P_b = \frac{1}{2}$. The current is calculated from an equation like (5.23), but with modified rates. For the calculation, we assume $\delta = 0$. In the case of small δ that are nevertheless sufficient to turn the system into a double dot, meaning $\omega \gg \delta\omega \gg t_p$, the exact polaron states are nearly completely localized, and the calculation should use not the $\Psi_\pm$ states, but the exact ones. For such δ, we know from previous sections that the effect is to effectively decouple the system. Thus, we are in the situation described in the previous section, where the polarons are completely localized. For larger δ, we could easily do a calculation along the lines of the one presented here, but we expect that no real new physics would emerge.

We reiterate that the calculation we perform, although it takes account of the degree of delocalization of the polaron states, is an incoherent one, correct in the limit $t_p/\boldsymbol{\gamma} \to 0$ when $\boldsymbol{\gamma} \gg \Gamma^{\eta\sigma}$.

Given values of the parameters g and α, let n_p denote the corresponding number of pairs of polaron states. We define new states from our 'exact' eigenstates as

$$\frac{1}{\sqrt{2}}(|\Psi_{2_j}\rangle \pm |\Psi_{2_{j-1}}) \tag{5.24}$$

and denote these states $|a_p\rangle$, $|b_p\rangle$, corresponding to the sites a and b for the localized polaron states. In an earlier section, we referred to the two lowest polaron

states as $|\Psi_\pm\rangle$. For the high energy, delocalized states, $|a_p\rangle \approx |b_p\rangle$, and when an electron tunnels into one of them, it is assumed to end up in either polaron state (ie., to fall into one of the semiclassical wells) with equal probability. This assumption is not entirely in accordance with reality, see [50] p.93, but the high-energy states only contribution to the current at high voltages, anyway, and at too high voltages our approach is not realistic to begin with. In particular, our assumption of relaxation to a thermal equilibrium distribution is only justifiable at not too large bias voltages.

The rate for tunneling into the polaron state a is

$$\Gamma_{10}^{\eta,a_p} = \sum_\sigma \frac{\Gamma^{\eta\sigma}}{Z_0} \sum_{i_0, f_1^{a_p}} |\langle f_1^{a_p}|c_\sigma^\dagger|i_0\rangle|^2 e^{-\beta E_{i_0}}\, n_F^\eta(eV_g + E_{f_1^{a_p}} - E_{i_0}) \tag{5.25}$$

The sum variable $f_1^{a_p}$ runs over the polaron states $|a_p\rangle$ and the delocalized, 'exact' 'filled' eigenstates above these states in energy. The energy $E_{f_1^{a_p}}$ does not correspond to an energy eigenstate, so we use one of the exact energies and accept an error on the energy of order t_p.

The rate for tunneling into the polaron state b is a similar expression to the one above, with a_p replaced by b_p.

The rate for tunneling out from the polaron state a is

$$\Gamma_{01}^{\eta,a_p} = \sum_\sigma \frac{\Gamma^{\eta\sigma}}{Z_1} \sum_{i_1^{a_p}, f_0} |\langle f_0|c_\sigma|i_1^{a_p}\rangle|^2 e^{-\beta E_{i_1}^{a_p}} (1 - n_F^\eta(eV_g + E_{i_1^{a_p}} - E_{f_0})) \tag{5.26}$$

and similarly for b_p. The sum variables and polaronic energies are defined as above.

The current, similar to our earlier Master equation expression for an uncoupled double dot:

$$\frac{I}{(-e)} = \frac{\sum_\tau \left(\Gamma_{10}^{L\tau}\Gamma_{01}^{R\tau} - \Gamma_{10}^{R\tau}\Gamma_{01}^{L\tau}\right)/\Gamma_{01}^\tau}{1 + \sum_\tau (\Gamma_{10}^\tau/\Gamma_{01}^\tau)} \tag{5.27}$$

where $\Gamma^\tau = \sum_{\eta=L,R} \Gamma^{\eta,\tau}$ with $\tau \in \{a_p, b_p\}$.

In fig.s (5.13) and (5.14) we calculate diamond plots for the parameter values in fig.s (4.17) and (4.18). The IV curves (fig. (5.15)) show rectification and NDC in an asymmetrical and 'skewed' device geometry, as one polaron state may block the current through the other, more strongly coupled polaron state, in one current direction. Now, however, some current runs in the inhibited direction even when $\Gamma^{Ra} = 0$. The more localized the polaron states are, the smaller is this 'residual' current.

5.3 Transport in a coherent double dot

We have seen that the time scales defined by Γ and $\boldsymbol{\gamma}$ are in competition with an internal time scale of the molecule, t_p, in determining the transport properties of

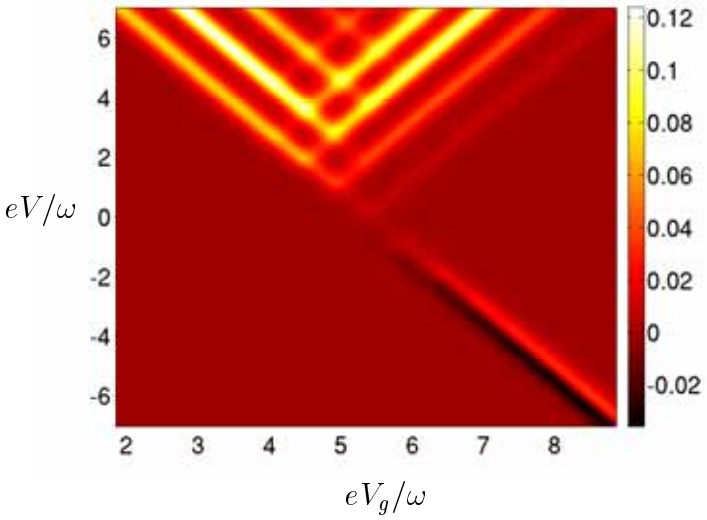

Figure 5.12: Differential conductance in the double dot with localized polaron states, with $g = 5$, $\alpha = 4$, $\delta = 0$, $k_BT = 0.1\omega$. The tunneling coupling that has been neglected is semiclassically $t_p \approx 0.001\omega$. The device geometry is asymmetrical and 'skewed', $\Gamma^{Ra} = 0$. The combination of $t_p \to 0$, $\Gamma^{Ra} = 0$, and completely localized polarons, leads to I identically 0 for large $(-V)$.

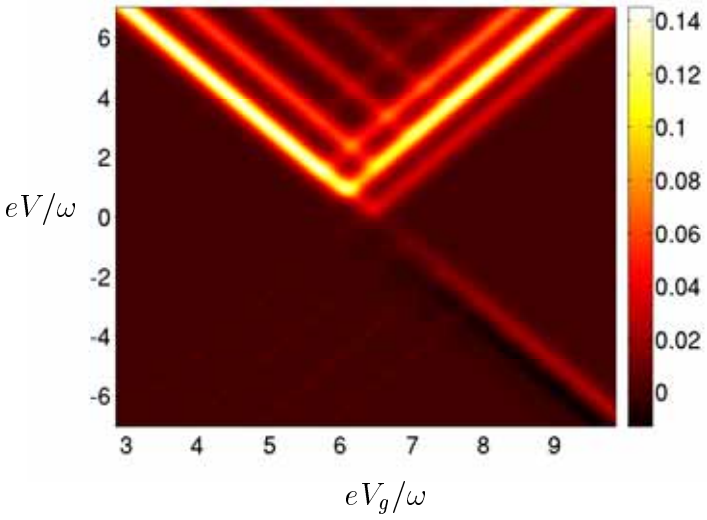

Figure 5.13: Differential conductance in the double dot with near-localized polaron states, with $g = 5$, $\alpha = 2$, $\delta = 0$, $k_BT = 0.1\omega$. The polaronic localization is 0.91, and the energy spacing between the polaron states is 0.01 ω. The device geometry is asymmetrical and 'skewed', $\Gamma^{Ra} = 0$. Not all current is blocked in the negative bias direction due to the nonperfect localization of the polaron states.

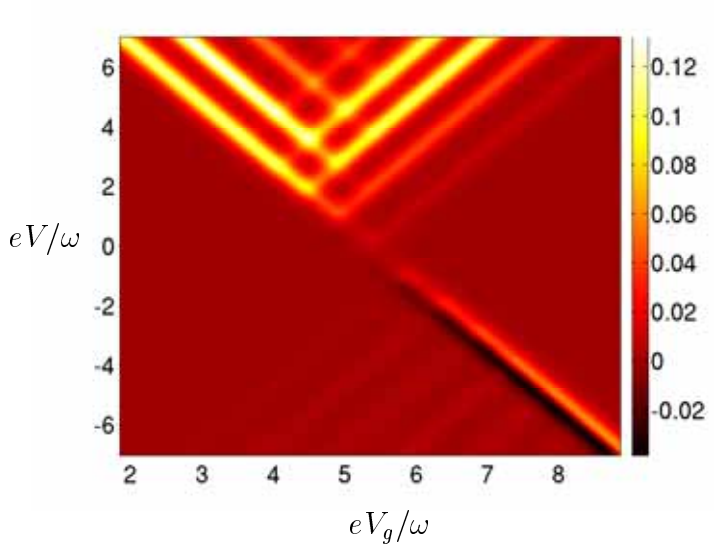

Figure 5.14: Differential conductance in the double dot with near-localized polaron states, with $g = 5$, $\alpha = 4$, $\delta = 0$, $k_BT = 0.1\omega$. The polaronic localization is 0.98, and the energy spacing between the polaron states is less than 0.001 ω. The device geometry is asymmetrical and 'skewed', $\Gamma^{Ra} = 0$. Most of the current is blocked in the negative bias direction due to strong localization of the polaron states. NDC is similarly strong.

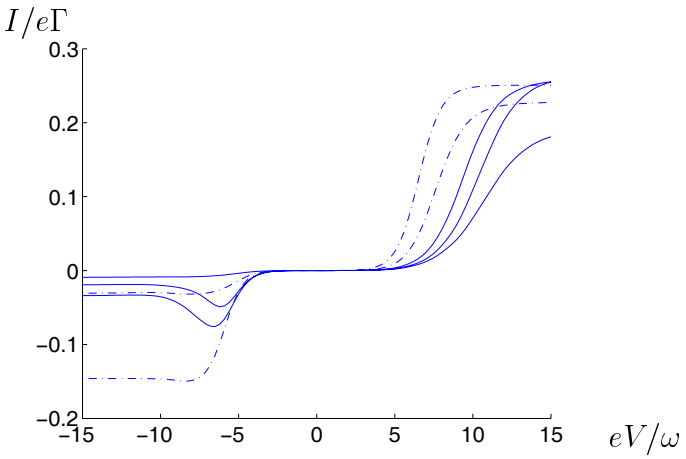

Figure 5.15: IV characteristics with incoherent transport through polaron states. The plateau value at negative V is a result of the delocalization of the polaron states. Plotted for $V_g = V_c + 3\omega/e$, $\Gamma^{Ra} = 0$, $k_BT = 0.3\omega$, $\delta = 0$, $g = 5$, $\alpha = 1$, 2 ('slash-dot' lines), 3, 4, 5 (lines). For increasing α, the polaron state becomes increasingly localized, and the plateau value approaches 0. In the same limit, the NDC effect becomes small. The $\alpha = 1$ line is nonpolaronic, but included to illustrate the limit case; it is the line that does not approach a small value, because the ground state current is through a delocalized state.

a dimer device. We have analyzed the current in the incoherent double dot case, $t_p < \Gamma^{\eta\sigma} < \boldsymbol{\gamma} < k_B T < \omega$, and in sequential transport, $\omega > k_B T > t_p > \boldsymbol{\gamma} > \Gamma^{\eta\sigma}$, both with relaxation to a thermal distribution of eigenstates. In the case $\boldsymbol{\gamma} \ll \Gamma$, the vibron distribution is not a thermal equilibrium distribution and should in general be determined. In any case, neither of the limit cases considered above is completely realistic. A general treatment should treat the entire quantum system of molecule and leads as one coherent system. Here, we analyze the crossover between the limit cases, restricting ourselves to a simplified system with just two levels in the limit of large bias voltages. The vibron states are implied in the parameter t_p but not explicitly included. Also, there is no dissipation. The limits above, therefore, are $t_p \ll \Gamma^{\eta\sigma}$ and $t_p \gg \Gamma^{\eta\sigma}$. When $t_p \approx \Gamma^{\eta\sigma}$ the electrodes induce a coupling between the near-degenerate polaron states, and electronic nondiagonal density matrix elements influence the current. The level asymmetry enters the equations as a detuning Δ between the two molecular states.

This approach will not yield any insight into NDC, which is a low bias voltage phenomenon, but it will allow us to check the rectification effects at large bias voltages.

We treat the two level problem by a Generalized Master Equation (GME) approach following the work of Gurvitz et al. [64]. In GME theory, the rate equations are replaced by a Liouvillian equation of motion for the density matrix for the molecule,

$$i\partial_t \rho = [H, \rho] \qquad (t \text{ for time}) \tag{5.28}$$

The rates of change for the diagonal elements are the Master Equations with additional terms for transitions between states of the system. The GME include rates of change for the off-diagonal matrix elements, all in all N^2 coupled equations for a N-state system.

In this approach for calculating resonant tunneling, voltage is assumed much larger than the temperature and the difference in energy between the resonant states. This means that effectively, electrons tunnel on to the double dot only from the 'right' and leave the double dot only to the 'left'. The tunneling processes are all first order in the rates $\Gamma^{\eta\sigma}$, and the approach therefore requires that these rates are nonvanishing: if one of them were much smaller than all other energies, then second order tunnelings not included in the treatment would become important.

It is furthermore assumed that the density of states in the electrodes is continuous.

For a double dot with one level in each dot, the GME, following the general solution of [64], has been written down in [65] in the case where each dot couple to one electrode only. Here, we do the same thing, except that we allow in- and out-tunnelings to take place on both of the parts of the double dot. This gives us four coupled equations for the double dot density matrix elements:

$$\partial_t \rho_{aa} = \Gamma^{Ra}\rho_0 - \Gamma^{La}\rho_{aa} + it_p(\rho_{ba} - \rho_{ab}) \tag{5.29}$$

$$\partial_t \rho_{bb} = \Gamma^{Rb}\rho_0 - \Gamma^{Lb}\rho_{bb} - it_p(\rho_{ba} - \rho_{ab}) \tag{5.30}$$

$$\partial_t \rho_{ab} = (-\frac{1}{2}(\Gamma^{La} + \Gamma^{Lb}) + i\Delta)\rho_{ab} + it_p(\rho_{bb} - \rho_{aa}) \tag{5.31}$$

$$\partial_t \rho_{ba} = (-\frac{1}{2}(\Gamma^{La} + \Gamma^{Lb}) - i\Delta)\rho_{ba} - it_p(\rho_{bb} - \rho_{aa}) \tag{5.32}$$

Here, a, b are the double dot states, and $\rho_0 \equiv 1 - \rho_{aa} - \rho_{bb}$ is the probability that the double dot is unoccupied. The $\Gamma^{\eta\sigma}$ are the rates for tunneling between the electrodes and the site orbitals, Δ is the level asymmetry, and t_p is the rate for coherent tunneling on the double dot, which we think of as a renormalized tunneling rate due to a phonon environment. Therefore, t_p may be comparable to the $\Gamma^{\eta\sigma}$ or smaller.

The diagonal terms were explained above. The off-diagonal terms contains the out-tunneling rates weighted by $\frac{1}{2}$, because a delocalized state is with equal probability on the two sites. The tunneling between the delocalized states depends on the difference in occupation probability of the sites.

The equations above rewritten as a matrix equation:

$$\frac{\partial \bar{\rho}}{\partial t} = M\bar{\rho} + \bar{C} \tag{5.33}$$

where

$$\bar{\rho} = \begin{pmatrix} \rho_{aa} \\ \rho_{bb} \\ \rho_{ab} \\ \rho_{ba} \end{pmatrix} \qquad \frac{\partial \bar{\rho}}{\partial t} = \begin{pmatrix} \partial_t \rho_{aa} \\ \partial_t \rho_{bb} \\ \partial_t \rho_{ab} \\ \partial_t \rho_{ba} \end{pmatrix} \tag{5.34}$$

and

$$M = \begin{pmatrix} -\Gamma^{Ra} - \Gamma^{La} & -\Gamma^{Ra} & -it_p & it_p \\ -\Gamma^{Rb} & -\Gamma^{Rb} - \Gamma^{Lb} & it_p & -it_p \\ -it_p & it_p & -\frac{1}{2}(\Gamma^{La} + \Gamma^{Lb}) + i\Delta & 0 \\ it_p & -it_p & 0 & -\frac{1}{2}(\Gamma^{La} + \Gamma^{Lb}) - i\Delta \end{pmatrix} \tag{5.35}$$

and

$$\bar{C} = \begin{pmatrix} \Gamma^{Ra} \\ \Gamma^{Rb} \\ 0 \\ 0 \end{pmatrix} \tag{5.36}$$

The stationary solution $\bar{\rho}_{st}$ is the solution $\bar{\rho}$ to (5.33) when $\frac{\partial \bar{\rho}}{\partial t} = 0$:

$$\bar{\rho}_{st} = -M^{-1}\bar{C} \tag{5.37}$$

We invert M using Mathematica and solve for $\bar{\rho}_{st}$. The solution for the diagonal density matrix elements:

$$\rho_{aa} = \frac{4t_p^2\Gamma^R\Gamma^L + \Gamma^{Ra}\Gamma^{Lb}(4\Delta^2 + {\Gamma^L}^2)}{4t_p^2\Gamma^L(2\Gamma^R + \Gamma^L) + \left(\Gamma^{Rb}\Gamma^{La} + (\Gamma^{Ra} + \Gamma^{La})\Gamma^{Lb}\right)(4\Delta^2 + {\Gamma^L}^2)} \tag{5.38}$$

$$\rho_{bb} = \frac{4t_p^2\Gamma^R\Gamma^L + \Gamma^{Rb}\Gamma^{La}(4\Delta^2 + {\Gamma^L}^2)}{4t_p^2\Gamma^L(2\Gamma^R + \Gamma^L) + \left(\Gamma^{Rb}\Gamma^{La} + (\Gamma^{Ra} + \Gamma^{La})\Gamma^{Lb}\right)(4\Delta^2 + {\Gamma^L}^2)} \tag{5.39}$$

The current depends only on the diagonal elements of the density matrix:

$$\frac{I}{(-e)} = \rho_{aa}\Gamma^{La} + \rho_{bb}\Gamma^{Lb} \tag{5.40}$$

This is

$$\frac{I}{(-e)} = \frac{\Gamma^R(4t_p^2{\Gamma^L}^2 + \Gamma^{La}\Gamma^{Lb}(4\Delta^2 + {\Gamma^L}^2))}{4t_p^2\Gamma^L(2\Gamma^R + \Gamma^L) + \left(\Gamma^{Rb}\Gamma^{La} + (\Gamma^{Ra} + \Gamma^{La})\Gamma^{Lb}\right)(4\Delta^2 + {\Gamma^L}^2)} \tag{5.41}$$

We define

$$\chi_\eta \equiv \frac{4t_p^2}{4\Delta^2 + {\Gamma^\eta}^2} \tag{5.42}$$

All dependence of I on t_p and Δ is contained in χ_L:

$$\frac{I}{(-e)} = \Gamma^R\Gamma^L\frac{\chi_L\Gamma^L + \Gamma^{La}\Gamma^{Lb}/\Gamma^L}{(\Gamma^L + 2\Gamma^R)\chi_L\Gamma^L + \Gamma^{La}\Gamma^{Lb}(1 + \frac{\Gamma^{Ra}}{\Gamma^{La}} + \frac{\Gamma^{Rb}}{\Gamma^{Lb}})} \tag{5.43}$$

First we consider the case $\Delta = 0$, ie. $\chi_L = \frac{4t_p^2}{{\Gamma^L}^2}$. When χ_L is large, meaning the on-dimer tunneling is fast compared to the out-tunneling rates, the current reduces to the sequential transport result,

$$\frac{I}{(-e)} = \frac{\Gamma^R\Gamma^L}{\Gamma^L + 2\Gamma^R} \tag{5.44}$$

which is independent of t_p.

The same expression results for any χ_L if one of the out-tunneling rates $\Gamma^{L\sigma}$ is 0. This is an artifact of the model, which requires that none of the tunneling rates vanish, as explained above.

In the opposite limit, $\chi_L \to 0$, tunneling on the dimer does not have the time to occur during the short dwell time. Assuming that neither $\Gamma^{Ra} \gg \Gamma^{Rb}$ or $\Gamma^{Rb} \gg \Gamma^{Ra}$, we are once again in the situation where the electron must leave the dimer from the site that it entered. When $\chi_L = 0$ the current becomes

$$\frac{I}{-e} = \frac{\Gamma^R}{(1 + \frac{\Gamma^{Ra}}{\Gamma^{La}} + \frac{\Gamma^{Rb}}{\Gamma^{Lb}})} \tag{5.45}$$

which is in fact the large V limit of the double dot expression, eq. (5.23). The current is maximum when out-tunneling is instantaneous (infinite $\Gamma^{L\sigma}$), because the out-tunneling rates are the bottleneck that makes the current smaller than it's maximum value given by the in-tunneling rate Γ^R.

Returning to the current (5.43), the large bias current in the opposite bias voltage direction is a similar expression with L and R interchanged. With $I_\rightarrow$

denoting the current (5.43), and $I_{\leftarrow}$ the opposite direction current, we express the current asymmetry as $|I_{\leftarrow}/I_{\rightarrow}|$. In the case $\Delta = 0$, we use Mathematica to expand $I_{\leftarrow}/I_{\rightarrow}$ to second order in t_p and implement the condition $\Gamma^L \gg \Gamma^R$, $\Gamma^{Ra} < \Gamma^{Rb}$ by throwing out terms, and then arrive at

$$|\frac{I_{\leftarrow}}{I_{\rightarrow}}| = \frac{\Gamma^L \Gamma^{Ra}}{\Gamma^{La}\Gamma^R} + \frac{\Gamma^L 4t_p^2}{\Gamma^{La}\Gamma^{R\,2}} \tag{5.46}$$

When t_p is smaller than the rates, the small rate Γ^{Ra} determines the ratio between the currents, serving as a 'bottleneck' in the 'backwards' current direction and giving rise to rectification. When t_p is larger and the t_p^2 term dominant, the current ratio is determined by t_p/Γ^R, with $t_p \ll \Gamma^R$ causing rectification.

Now, we let $\Delta > 0$. This corresponds to the replacement $\frac{4t_p^2}{\Gamma^{R\,2}} \rightarrow \frac{4t_p^2}{4\Delta^2+\Gamma^{R\,2}}$ in the above equation. When t_p is already small, the asymmetry makes no difference, but for larger t_p, Δ works with Γ^R against t_p, making the system more rectifying than it otherwise would be.

Finally, consider the case where Γ^R is small but $\Delta \gg t_p$. This also turns the system into a double dot with Γ^{Ra} serving as the 'bottleneck', which makes sense, because the large detuning prevents tunneling between the sites.

All this argues for the validity of our diamond plots in the appropriate limits. It also shows that the asymmetry Δ plays a role alongside the out-tunneling rates, through the parameter χ_η, in inhibiting tunneling on the dot and increase the probability that an electron leaves from the polaronic state that it entered into.

Chapter 6

Comparision with reality

In the C_{140} experiments of Pasupathy et al., the interesting mode was at ω=11 meV, and the corresponding g-factors were between 1 and 5, assuming a Poissonian distribution for the stepheights on the IV characteristics. The mass of C_{70} is approximately 980 atomic mass units, and the distance between the electrodes was about 1 nm. Realistic values for tunneling and dissipation are $\Gamma = \mu$eV and $\boldsymbol{\gamma}=\omega$, corresponding to a Q-factor of 1. This violates the condition $\boldsymbol{\gamma}/\omega \ll \pi/2g$ for the values of g of our interest, which means there should be some dissipative broadening of the steps in the experiments. Temperatures were less than 0.2 meV $\sim 0.02\ \omega$, indicating that step-broadening was dissipative rather than thermal.

The values $\omega = 11$ meV $= 1.762 \times 10^{-21}$ J, the reduced mass of the dimer (corresponding to an intercage oscillation) $\frac{m_{C_{70}}}{2} = 490 \times 1.66 \times 10^{-27}$ kg, and $g = 5$, leads to $\lambda = 2.00 \times 10^{-9}$ J/m and $l_0 = 2.79 \times 10^{-12}$ m. Estimating λ theoretically is tricky, because it may depend strongly on the geometry of the device: the dimer has a length comparable to the distance between the electrodes, and is orientated in an unknown manner, hence an electron on the dimer could be situated essentially anywhere within the constriction. Furthermore, the distance between the electron sites may be comparable to the constriction length. The site orbitals are of an unknown geometry: they may be highly 'smeared out' on the respective 'balls', or they may be localized, perhaps to the doble bonds at separation 1.5 Å, or to the opposite ends of the dimer at separation 10-15 Å. Clearly, this is a mess, but the possibility that the distance between an electrode and a localized orbital on the dimer is small could account for the strong electron-vibron interaction and observed polaron effects. From the Hamiltonian, $\lambda' = \lambda l_0/\sqrt{2}$ is the change in energy of the system when the electron is moved a distance l in the potential of the electrodes. A simple calculation for the corresponding change in Coulomb energy between an electron and one mirror charge in the nearest electrode, when the experimental values are inserted, leads to an electron-electrode distance of 0.5 nm. This at least confirms the energy scale.

6.1 Tightbinding model for the dimer

In our model for a dimer device, the electron hopping energy t is the overlap of two hybridizing orbitals of the C_{70}s. The ground state of charge-neutral C_{140} is a closed shell configuration, which does not allow charge to move about on the molecule. The obvious candidates for the 'filled' charge state are the ions C_{140}^{-1} and C_{140}^{+1} (the positive ion corresponding to hole, rather than electron transport). The main contributions would then be expected to be from the C_{140} LUMO and HOMO, respectively. More realistically, several levels of the C_{70}s hybridize, giving rise to an effective hopping energy for the 'filled' state (whatever charge number that may correspond to). To estimate t, we calculate a spectrum for C_{140} within a tightbinding model:

We take the $2sp^2$ orbitals as fixed and calculate the spectrum of the $2p_z$ electrons, one for each C atom, each in the direction normal to the 'surface' of the 'ball' to which it is attached. For simplicity, we allow only nearest neighbour hopping and assume that the hopping energies are all the same constant t_1 on the 'balls', neglecting the different band lengths in C_{70}. On the other hand, we do take into account that the hopping across the double bonds connecting the 'balls' is probably a different energy t_2, a parameter that we vary.

The tightbinding Hamiltonian:

$$H = t_1 \sum_{\sigma} \sum_{[i,j]} (C_{i,\sigma}^{\dagger} C_{j,\sigma} + C_{j,\sigma}^{\dagger} C_{i,\sigma}) + t_2 \sum_{j=1}^{2} (C_{j,a}^{\dagger} C_{j,b} + C_{j,b}^{\dagger} C_{j,a}) \qquad (6.1)$$

The sites are labeled by (j,σ), where $\sigma \in \{a, b\}$ denotes the 'ball' and $j \in [1, 70]$ denotes the site on the 'ball'. The sites that connect the 'balls' are (1,a) to (1,b), and (2,a) to (2,b), the most symmetrical combination of the C_{70}s. The $C_{j,\sigma}$ operators are the annihilation operators for an electron on the corresponding site. The sum $\sum_{[i,j]}$ runs over all nearest neighbour pairs on a 'ball' exactly once. Each site has three nearest neighbours on the 'ball'. See fig.s (1.13), (1.14).

The Hamiltonian is diagonalized numerically. The spectrum is plotted in fig. (6.1).

We find the obvious result that the spectrum of two uncoupled C_{70}s (ie., $t_2 = 0$) is doubly degenerate, with energies identical to the energies of the C_{70} tightbinding spectrum, which we have calculated as a check. The shape of C_{70} is an elongated 'football', a feature that seems to accumulate charge near the 'equator' of the molecule, by our calculations for the charge densities on the sites (not plotted).

For t_1, the overlap of two $2p_z$ orbitals at 1.5 Å separation can of course be calculated, but we fix our energy unit by assuming that [36] is correct in the value of 1.23 eV for the C_{70} HOMO-LUMO gap. Our tightbinding calculations result in the value of 0.5293 t_1 for the C_{70} HOMO-LUMO gap (and similarly, for the C_{140} HOMO-LUMO gap when $t_2 = 0$). This yields $t_1 = 1.23$ eV / $0.5293 = 2.32$ eV. The ionization energy of C_{70} is the maximum energy in the spectrum minus the HOMO

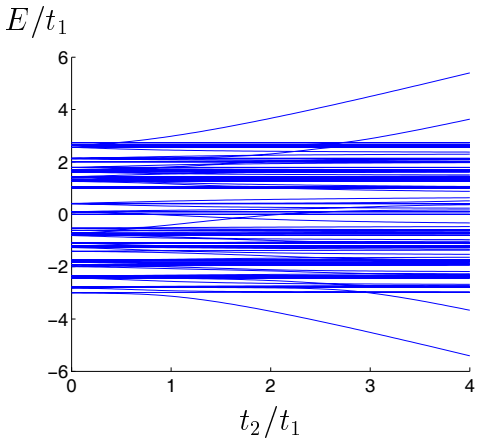

Figure 6.1: The tightbinding spectrum for the $2p_z$ orbitals of the most symmetrical C_{140} isomer.

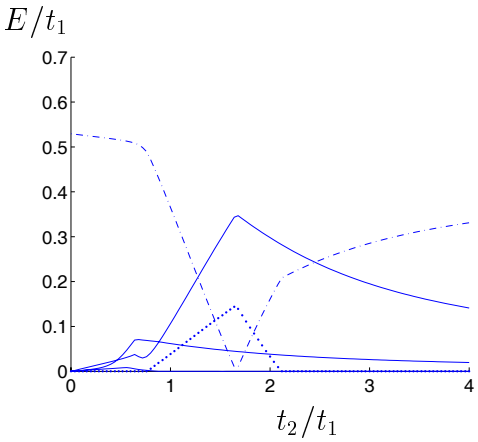

Figure 6.2: The energy splitups in the C_{140} tightbinding spectrum between the levels below the Fermi level that were degenerate at $t_2 = 0$. Also plotted: the HOMO-LUMO gab (· -) and the splitup of the LUMO (·).

level energy; we get $(2.7321 + 0.5293)\ t_1 = 7.57$ eV ~ 7.6 eV, the value given in [32]. For the LUMO energy we get 0, corresponding to a closed shell configuration.

For C_{140}, varying t_2, we find that the splitups of the LUMO, the HOMO and the degenerate levels below become as much as 0.15 t_1, 0.35 t_1, 0.08 t_1 and some smaller values, respectively; see fig. (6.2). In degenerate states, find that the electron is sometimes localized to one of the parts of the dimer. When degeneracies are lifted, this does not happen due to the symmetry of the dimer molecule. According to [36], the HOMO-LUMO gap is reduced from 1.23 eV to 0.96 eV in the dimer. In fig. (6.2), 0.96 eV $\sim 0.4131\ t_1$ for the value of the HOMO-LUMO gap, and we read off the plot that the gap reduction corresponds to $t_2/t_1 = 0.9$. At $t_2 = 0.9t_1$ the maximum values for the splitups are not quite reached, but still sufficiently large that a half-energy splitting of 50 meV or even more seems realistic as a value for t.

For polaron states to be present in our model with $g = 5$, we must have at least $\alpha \approx 2$. With $\omega = 11$ meV, this corresponds to $t = \frac{2g\omega}{\alpha} = 55$ meV. This is consistent with the C_{70} hybridization energies from the tightbinding calculation.

6.2 Final words

A paper by Karsten Flensberg and myself describing transport in a dimer with polaron states has been submitted to Physical Review B, and may be found at http://arxiv.org/abs/cond-mat/0411173. A poster, presented at ADMOL 2004, is included in the appendix.

Appendix A

Exact calculations of expectation values

We relate here the expectation values of operators to the realvalued eigenstate coefficients $\nu_{\sigma n}$.

The probability that the electron is on site σ is

$$\rho_{\sigma\sigma} = \langle n_\sigma \rangle = \langle c_\sigma^\dagger c_\sigma \rangle = \sum_n \nu_{\sigma n}^* \nu_{\sigma n} = \sum_n \nu_{\sigma n}^2 \tag{A.1}$$

because the $\nu_{\sigma n} = \nu_{\sigma n}^*$. Easy calculation yields

$$\langle \hat{\sigma}_z \rangle = 2\rho_{aa} - 1 \tag{A.2}$$

The probability that the system is in a bonding ($\tau = +$) or antibonding ($\tau = -$) state is

$$\langle n_\tau \rangle = \frac{1}{2}(1 + \mathrm{sign}(\tau) \sum_n (\nu_{an}^* \nu_{bn} + \nu_{bn}^* \nu_{an})) = \frac{1}{2} + \mathrm{sign}(\tau) \sum_n \nu_{an}\nu_{bn} \tag{A.3}$$

The electronic hybridization in the state is described by

$$\langle \hat{\sigma}_x \rangle = 2\rho_{ab} = \langle c_a^\dagger c_b + c_b^\dagger c_a \rangle = 2 \sum_n \nu_{an}\nu_{bn} = \langle n_+ \rangle - \langle n_- \rangle \tag{A.4}$$

The expectation value of the operator a in some eigenstate is

$$\begin{aligned} \langle a \rangle = \Big(\sum_{\sigma n} \nu_{\sigma n}^* \langle \sigma n | \Big) \cdot a \Big(\sum_{\sigma' n'} \nu_{\sigma' n'} |\sigma' n'\rangle \Big) \quad &= \\ \sum_{\sigma n} \Big(\nu_{\sigma n} \langle \sigma n | \Big) \Big(\nu_{\sigma n+1} \sqrt{n+1} |\sigma n\rangle \quad &= \quad \sum_{\sigma n} \sqrt{n+1} \nu_{\sigma n}\nu_{\sigma n+1} \end{aligned} \tag{A.5}$$

As the $\nu_{\sigma n}$ are all real,

$$\langle a \rangle = \langle a^\dagger \rangle \tag{A.6}$$

Hence,

$$\langle x\rangle = \frac{l_0}{\sqrt{2}}\langle(a^\dagger + a)\rangle = \frac{l_0}{\sqrt{2}}\sum_{\sigma n} 2\sqrt{n+1}\nu_{\sigma n}\nu_{\sigma n+1} \tag{A.7}$$

For the momentum operator,

$$\langle p\rangle = -\frac{i}{\sqrt{2}l_0}\langle(a^\dagger - a)\rangle = 0 \tag{A.8}$$

The expectation value of the number of bosons in an eigenstate is

$$\langle N_a\rangle \equiv \langle a^\dagger a\rangle = \sum_{\sigma n} n\ |\nu_{\sigma n}|^2 \tag{A.9}$$

Expectation values nonlinear in a, $a^\dagger$ include $\langle x^2\rangle$, $\langle p^2\rangle$, determined by:

$$\langle(a^\dagger \pm a)^2\rangle = \langle a^\dagger a^\dagger\rangle + \langle aa\rangle \pm (\langle a^\dagger a\rangle + \langle aa^\dagger\rangle) = \langle a^\dagger a^\dagger\rangle + \langle aa\rangle \pm (2\langle a^\dagger a\rangle + 1) \tag{A.10}$$

The uncertainty in x, call it Δx, expresses fluctuations:

$$\langle\Delta x\rangle^2 = \langle x^2\rangle - \langle x\rangle^2 \tag{A.11}$$

$$\langle\Delta x\rangle^2 = \frac{l_0^2}{2}\Big(\sum_{\sigma n}(2\sqrt{n+1}\sqrt{n+2}\nu_{\sigma n}\nu_{\sigma n+2} + 2n\nu_{\sigma n}^2 + 1) - (\sum_{\sigma n} 2\sqrt{n+1}\nu_{\sigma n+1}\nu_{\sigma n})^2\Big) \tag{A.12}$$

Using $\langle p\rangle = 0$,

$$\langle\Delta p\rangle^2 = \langle p^2\rangle = -\frac{1}{2l_0^2}\sum_{\sigma n}\Big(2\sqrt{n+1}\sqrt{n+2}\nu_{\sigma n}\nu_{\sigma n+2} - 2n\nu_{\sigma n}^2 - 1\Big) \tag{A.13}$$

The kinetic, vibrational energy of the molecule, E_{vibr}:

$$\langle E_{vibr}\rangle = \frac{\langle p^2\rangle}{2M} \tag{A.14}$$

The site σ correlation function:

$$\langle n_\sigma x\rangle = 2\frac{l_0}{\sqrt{2}}\sum_n \sqrt{n+1}\nu_{\sigma n}\nu_{\sigma n+1} \tag{A.15}$$

A better measure of correlation is

$$C_{\hat\sigma_z,x} \equiv \frac{1}{\sqrt{2g}l_0}\langle-\hat\sigma_z x\rangle = \frac{1}{\sqrt{2g}l_0}\langle(n_b - n_a)x\rangle =$$

$$\frac{1}{\sqrt{g}}\sum_n \sqrt{n+1}(\nu_{bn}\nu_{bn+1} - \nu_{an}\nu_{an+1}) \tag{A.16}$$

Entanglement entropy and linear entropy are calculated from the reduced density matrix for the electron:

$$S_N = -\mathrm{Tr}[\rho_e \log_2 \rho_e] \tag{A.17}$$

$$S_l = 1 - \mathrm{Tr}[\rho_e^2] \tag{A.18}$$

Appendix B

A simplistic calculation for ω

Let $\hat{e}_1$ denote a unit vector pointing in the direction of the oscillations due to the interaction with the electrodes; we assume that this direction is the same for both parts of the dimer. The motions of a, b along the direction $\hat{e}_1$ couple to the number operators of the corresponding electron sites. The intercage mode is in the direction of the dimer, call the unit vector $\hat{e}_I$. The device geometry is defined by the angle $\theta_0 \equiv \frac{\pi}{2} - v$ where v is the angle between $\hat{e}_1$ and $\hat{e}_I$. When $\theta_0 = 0$ the intercage vibration has no component in the $\hat{e}_1$ direction. When $\theta_0 = \frac{\pi}{2}$ the intercage vibration is along $\hat{e}_1$. The three oscillatory modes ω_a, ω_b, and ω_I give rise to effective frequencies for the oscillations of the sites a and b in the direction $\hat{e}_1$. Oscillations in the direction orthogonal to $\hat{e}_1$, call it $\hat{e}_2$, are of no importance because they don't couple to phonons.

The motion of the dimer along $\hat{e}_1$ is resolved into two components: the 'tilting coordinate' $x \equiv x_a - x_b$, and the 'cm coordinate' $y \equiv x_a + x_b$. In the following derivation, we use the distance between the sites as the unit of length. The force on site a is

$$\bar{F}_a = -m\omega_a^2 x_a \hat{e}_1 - \frac{m}{2}\omega_I^2 x_I \cos(\frac{\pi}{2} - \theta)\hat{e}_1 + \frac{m}{2}\omega_I^2 x_I \cos(\theta)\hat{e}_2 \tag{B.1}$$

The force on site b is

$$\bar{F}_b = -m\omega_b^2 x_b \hat{e}_1 + \frac{m}{2}\omega_I^2 x_I \cos(\frac{\pi}{2} - \theta)\hat{e}_1 - \frac{m}{2}\omega_I^2 x_I \cos(\theta)\hat{e}_2 \tag{B.2}$$

The factor $\frac{m}{2}$ is the reduced mass for the 'intercage' oscillator.

The 'tilting' force is the $\hat{e}_1$ component of $\bar{F}_b - \bar{F}_a$:

$$F_{tilt} = m\omega_a^2 x_a - m\omega_b^2 x_b + m\omega_I^2 x_I \sin(\theta) \tag{B.3}$$

using $\cos(\frac{\pi}{2} - \theta)$=$\sin(\theta)$. Here, x_a, x_b, x_I, and θ can all be expressed in terms of x, y, and θ_0.

The displacement x_I follows from the law of cosines and solving a second degree polynomium:

$$x_I = -1 + \sqrt{1 + 2x\sin(\theta_0) + x^2} \equiv -1 + s \tag{B.4}$$

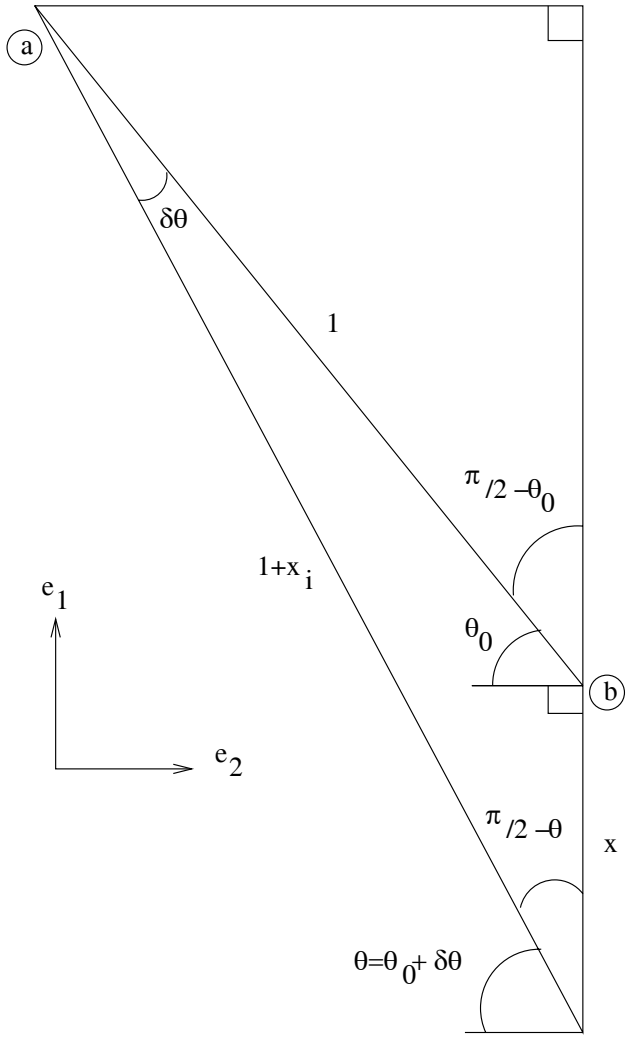

Figure B.1: Spring geometry

For the angle θ,

$$\sin(\theta) = \frac{x + \sin(\theta_0)}{1 + x_I} \tag{B.5}$$

We calculate $x_I \sin(\theta)$:

$$x_I \sin(\theta) = x_I \frac{x + \sin(\theta_0)}{1 + x_I} = (x + \sin(\theta_0)) \frac{(s-1)}{1 + (s-1)} =$$

$$(x + \sin(\theta_0)) \Big(1 - \frac{1}{\sqrt{1 + 2x\sin(\theta_0) + x^2}}\Big) \tag{B.6}$$

In our chosen units, x is no larger than about $\frac{1}{100}$ because the oscillator displacement length is some picometers and the distance between the sites is a few Ångstrøm. We now assume $\sin(\theta_0) \gg |x|$ meaning we exclude the geometry where the springs are in orthogonal directions. Then,

$$\frac{1}{\sqrt{1 + 2x\sin(\theta_0) + x^2}} \approx 1 - \frac{2x\sin(\theta_0)}{2} = 1 - x\sin(\theta_0) \tag{B.7}$$

where we have let $x^2 \to 0$ and used the series expansion of the inverse square root.

The result is

$$x_I \sin(\theta) \approx (x + \sin(\theta_0)) \frac{2x\sin(\theta_0)}{2} \approx x\sin^2(\theta_0) \tag{B.8}$$

The contribution to the 'tilting' force is a spring force,

$$m_1 \omega_I^2 \sin^2(\theta_0) x \tag{B.9}$$

The total 'tilting' force in terms of coordinates x, y, and parameter θ_0:

$$y(\frac{m_1}{2}(\omega_a^2 - \omega_b^2)) + x(\frac{m_1}{2}(\omega_b^2 + \omega_a^2 + 2\omega_I^2 \sin^2(\theta_0))) \tag{B.10}$$

Since we don't want to consider the y dependence, we assume $\omega_b = \omega_a$. Integrating with respect to x, we end up with 'tilting energy'

$$\frac{1}{2} m \omega^2 x^2 \tag{B.11}$$

where we have defined the effective frequency of the tilting mode as

$$\omega^2 \equiv \omega_a^2 + \omega_I^2 \sin^2\theta_0 \tag{B.12}$$

Similarly, calculating the $\hat{e}_1$ component of $\bar{F}_a + \bar{F}_b$, the cm motion of the molecule corresponds to an energy

$$\frac{1}{2} m \omega_a^2 y^2 \tag{B.13}$$

when $\omega_a = \omega_b$.

Appendix C

The isolated electron

C.1 Diagonalization

Defining

$$K \equiv -\frac{\delta\omega}{t} \qquad K_+ = K + \sqrt{1+K^2} \qquad K_- = K - \sqrt{1+K^2} \tag{C.1}$$

the electronic Hamiltonian in basis of the c operators can be written

$$H_e = t \begin{pmatrix} -K & -1 \\ -1 & K \end{pmatrix} \tag{C.2}$$

The characteristic polynomium (variable E):

$$(E + Kt)(E - Kt) - (-t)^2 \tag{C.3}$$

The eigenvalues are the roots $E_\pm$,

$$E_\pm = \pm t\sqrt{1+K^2} \tag{C.4}$$

The eigenvectors are denoted $v^{(\pm)} = (v_1^{(\pm)}, v_2^{(\pm)})$ corresponding to $E_\mp$ and are the solutions to

$$0 = (H_e - E_\mp \hat{1})v^{(\pm)} = \begin{pmatrix} -Kt - E_\mp & -t \\ -t & Kt - E_\mp \end{pmatrix} \begin{pmatrix} v_1^{(\pm)} \\ v_2^{(\pm)} \end{pmatrix} \tag{C.5}$$

For v^+ the 'second row' equation yields

$$v_1^+ = (K - \frac{E_-}{t})v_2^+ = (K + \sqrt{1+K^2})v_2^+ = K_+ v_2^+ \tag{C.6}$$

and v_2^+ can be chosen as $\frac{1}{\mathrm{N}_+}$ with some normalization N_+. Then, the normalization condition $(v_1^+)^2 + (v_2^+)^2 = 1$ leads to $\mathrm{N}_+ = \sqrt{1+K_+^2}$.

By a similar calculation for $v^{(-)}$, the eigenvectors are

$$v^{(+)} = \frac{1}{\sqrt{1+K_+^2}} \begin{pmatrix} K_+ \\ 1 \end{pmatrix} \qquad v^{(-)} = \frac{1}{\sqrt{1+K_-^2}} \begin{pmatrix} K_- \\ 1 \end{pmatrix} \tag{C.7}$$

C.2 Calculation of expectation values

First, localization in the electronic eigenstate $v^{(+)}$:

$$\langle \hat{\sigma}_z \rangle_+ = \frac{1}{1+K_+^2} \begin{pmatrix} K_+ \\ 1 \end{pmatrix}^T \begin{pmatrix} 1 & 0 \\ 0 & -1 \end{pmatrix} \begin{pmatrix} K_+ \\ 1 \end{pmatrix} = \frac{K_+^2 - 1}{K_+^2 + 1} \tag{C.8}$$

For K_+^2 we use

$$K_+^2 = 2K^2 + 2K\sqrt{1+K^2} + 1 \tag{C.9}$$

and get

$$\langle \hat{\sigma}_z \rangle_+ = \frac{(2K^2 + 2K\sqrt{1+K^2})}{(2K^2 + 2K\sqrt{1+K^2}) + 2} = \frac{1}{1 + (K^2 + K\sqrt{1+K^2})^{-1}} = \frac{K}{K + K_+^{-1}} \tag{C.10}$$

The denominator can be rewitten as

$$K + K_+^{-1} = \sqrt{1+K^2} \tag{C.11}$$

which follows from

$$K_+\sqrt{1+K^2} = (K + \sqrt{1+K^2})\sqrt{1+K^2} = K\sqrt{1+K^2} + (1+K^2) =$$

$$K(K + \sqrt{1+K^2}) + 1 = KK_+ + 1 = K_+(K + K_+^{-1}) \tag{C.12}$$

Eq. (C.11) is aquired by dividing both sides by K_+.

Therefore,

$$\langle \hat{\sigma}_z \rangle_+ = \frac{K}{\sqrt{1+K^2}} \tag{C.13}$$

By a calculation similar to eq.s (C.8)-(C.10), for the state $v^{(-)}$:

$$\langle \hat{\sigma}_z \rangle_- = \frac{K}{K + K_-^{-1}} \tag{C.14}$$

Note that

$$K_+^{-1} + K_-^{-1} = \frac{(K - \sqrt{1+K^2}) + (K + \sqrt{1+K^2})}{(K - \sqrt{1+K^2})(K + \sqrt{1+K^2})} = \frac{2K}{K^2 - (1+K^2)} = -2K \tag{C.15}$$

from which now follows,

$$\langle\hat{\sigma}_z\rangle_- = \frac{K}{K + (-K_+^{-1} - 2K)} = -\frac{K}{K + K_+^{-1}} = -\langle\hat{\sigma}_z\rangle_+ \tag{C.16}$$

The two eigenstates are to equal degree localized, but to opposite sites. Therefore, regardless of the state, electronic localization is described by the absolute value

$$|\langle\hat{\sigma}_z\rangle| = \frac{|K|}{\sqrt{1+K^2}} = \sin(\arctan(|K|)) \tag{C.17}$$

Our hybridization measure, $|\langle\hat{\sigma}_x\rangle|$, can be derived from (3.28) by applying the transformation to bonding/ antibonding states. Transforming H_e,

$$H_e = \delta\omega\hat{\sigma}_z - t\hat{\sigma}_x \rightarrow -\delta\omega\hat{\sigma}_x - t\hat{\sigma}_z \tag{C.18}$$

we see that the Hamiltonian is transformed by interchanging $\delta\omega$ and t and then changing the sign on t; in other words, $K \rightarrow -K^{-1}$. From (3.28), it follows that $|\langle\hat{\sigma}_x\rangle|$ is $|\langle\hat{\sigma}_z\rangle|$ with $K \rightarrow -K^{-1}$. The result is

$$|\langle\hat{\sigma}_x\rangle| = \frac{1}{\sqrt{1+K^2}} = \cos(\arctan(|K|)) \tag{C.19}$$

which holds regardless of the state. This can also be derived in a manner analogous to the calculation for $|\langle\hat{\sigma}_x\rangle|$. As before, we have a relation

$$\langle\hat{\sigma}_x\rangle_- = -\langle\hat{\sigma}_x\rangle_+ \tag{C.20}$$

Appendix D

Weak interaction perturbation theory

$$E_{\mu n}^{(0)} = n\omega - \mathrm{sign}(\mu)t\sqrt{1+K^2} \tag{D.1}$$

is perturbed by

$$\sqrt{g}\omega(n_a - n_b)(a^\dagger + a) = \sqrt{g}\omega\hat{\sigma}_z(a^\dagger + a) \tag{D.2}$$

and we assume the unperturbed spectrum is undegenerate.

There are no first order corrections to the energy, because eq. (D.2) contains no diagonal part in the bosonic degree of freedom.

The second order corrections depend on the matrix elements:

$$\langle \mu n|\sqrt{g}\omega\hat{\sigma}_z(a^\dagger + a)|\mu' n'\rangle = \sqrt{g}\omega\langle\mu|\hat{\sigma}_z|\mu'\rangle\langle n|(a^\dagger + a)|n'\rangle \tag{D.3}$$

The bosonic part of the matrix elements:

$$\langle n|(a^\dagger + a)|n'\rangle = \sqrt{n}\delta_{n-1,n'} + \sqrt{n+1}\delta_{n,n'-1} \tag{D.4}$$

The diagonal part of the electronic part has been derived in section (3.4):

$$\langle \pm|\hat{\sigma}_z|\pm\rangle = \pm\langle\hat{\sigma}_z\rangle_+ = \pm\frac{K}{\sqrt{1+K^2}} \tag{D.5}$$

For the offdiagonal part of the electronic part,

$$\langle +|\hat{\sigma}_z|-\rangle = \frac{1}{\sqrt{1+K_+^2}}\frac{1}{\sqrt{1+K_-^2}}\begin{pmatrix} K_+ \\ 1 \end{pmatrix}^T \begin{pmatrix} 1 & 0 \\ 0 & -1 \end{pmatrix}\begin{pmatrix} K_- \\ 1 \end{pmatrix} = \frac{K_+K_- - 1}{\sqrt{1+K_+^2}\sqrt{1+K_-^2}} \tag{D.6}$$

As

$$K_+K_- = K^2 - (1+K^2) = -1 \tag{D.7}$$

and because the expression (D.6) is symmetrical in +, -, we get

$$\langle \pm|\hat{\sigma}_z|\mp\rangle = \frac{-2}{\sqrt{1+[K_+^2+K_-^2]+(K_+K_-)^2}} = \frac{-2}{\sqrt{1+2[K^2+(1+K^2)]+1}} = \frac{-1}{\sqrt{1+K^2}} \tag{D.8}$$

where we used the definitions of K_+, K_-.

The electronic part of the matrix elements is therefore

$$\frac{1}{\sqrt{1+K^2}}\Big(\text{sign}(\mu)K\delta_{\mu,\mu'} - \delta_{\bar{\mu},\mu'}\Big) \tag{D.9}$$

The second order corrections to the energies:

$$E_{\mu n}^{(2)} = \sum_{[\mu' n']\neq[\mu n]} \frac{|\langle \mu n|\sqrt{g}\omega\hat{\sigma}_z(a^\dagger + a)|\mu' n'\rangle|^2}{E_{\mu n}^{(0)} - E_{\mu' n'}^{(0)}} \tag{D.10}$$

Summing over n', this becomes

$$\sum_{\mu'=\mu,\bar{\mu}} \frac{g\omega^2(\text{sign}(\mu)K\delta_{\mu,\mu'} - \delta_{\bar{\mu},\mu'})^2}{1+K^2}\cdot$$

$$\Big(\frac{n}{\omega + (\text{sign}(\mu') - \text{sign}(\mu))t\sqrt{1+K^2}} + \frac{n+1}{-\omega + (\text{sign}(\mu') - \text{sign}(\mu))t\sqrt{1+K^2}}\Big) \tag{D.11}$$

Summing over μ', and using sign($\bar{\mu}$)=-sign(μ), this becomes

$$\frac{g\omega^2}{1+K^2}\Bigg[(\text{sign}(\mu)K)^2(\frac{n}{\omega} + \frac{n+1}{-\omega}) +$$

$$(-1)^2\Big(\frac{n}{\omega - 2\text{sign}(\mu)t\sqrt{1+K^2}} + \frac{n+1}{-\omega - 2\text{sign}(\mu)t\sqrt{1+K^2}}\Big)\Bigg] \tag{D.12}$$

The final result for the second order corrections to the energies:

$$E_{\mu n}^{(2)} = \frac{-g\omega^2}{1+K^2}\Big[\frac{K^2}{\omega} + \Big(\frac{n}{\text{sign}(\mu)2t\sqrt{1+K^2} - \omega} + \frac{n+1}{\text{sign}(\mu)2t\sqrt{1+K^2} + \omega}\Big)\Big] \tag{D.13}$$

Now, we calculate the first order corrections to the nondegenerate eigenstates. Let $\Psi_{\mu n}$ denote the eigenstates, and the unperturbed states $\Psi_{\mu n}^{(0)} = |\mu n\rangle$.

$$\Psi_{\mu n}^{(1)} = \sum_{[\mu' n']\neq[\mu n]} \frac{\langle \mu' n'|\sqrt{g}\omega\hat{\sigma}_z(a^\dagger + a)|\mu n\rangle}{E_{\mu n}^{(0)} - E_{\mu' n'}^{(0)}} \Psi_{\mu' n'}^{(0)} \tag{D.14}$$

When we insert matrix elements and energies as before, and sum over n', the expression becomes:

$$\sum_{\mu'} \langle \mu'| \frac{\sqrt{g}\omega}{\sqrt{1+K^2}}(\text{sign}(\mu)K\delta_{\mu,\mu'} - \delta_{\bar{\mu},\mu'}) \cdot$$

$$\left[\frac{\sqrt{n}\ \Psi^{(0)}_{\mu' n-1}}{(\mathrm{sign}(\mu')-\mathrm{sign}(\mu))t\sqrt{1+K^2}+\omega}+\frac{\sqrt{n+1}\ \Psi^{(0)}_{\mu' n+1}}{(\mathrm{sign}(\mu')-\mathrm{sign}(\mu))t\sqrt{1+K^2}-\omega}\right]|\mu\rangle \tag{D.15}$$

Summing over μ', we arrive at

$$\Psi^{(1)}_{\mu n}=\frac{\sqrt{g}\omega}{\sqrt{1+K^2}}\Bigg[\mathrm{sign}(\mu)\frac{K}{\omega}\Big(\sqrt{n}\ \Psi^{(0)}_{\mu n-1}-\sqrt{n+1}\ \Psi^{(0)}_{\mu n+1}\Big)+$$

$$\Big(\frac{\sqrt{n}\ \Psi^{(0)}_{\bar{\mu} n-1}}{\mathrm{sign}(\mu)2t\sqrt{1+K^2}-\omega}+\frac{\sqrt{n+1}\ \Psi^{(0)}_{\bar{\mu} n+1}}{\mathrm{sign}(\mu)2t\sqrt{1+K^2}+\omega}\Big)\Bigg] \tag{D.16}$$

Appendix E

Transformation to the 'tilted' basis

We define a canonical transformation in the Hilbert space of the full Hamiltonian:

$$\tilde{H} = e^{\zeta} H e^{-\zeta} \tag{E.1}$$

Here,

$$\zeta \equiv \sqrt{g}(n_a - n_b)(a^\dagger - a) = -ipl(n_a - n_b) \tag{E.2}$$

with the momentum operator

$$p = \frac{i}{\sqrt{2}l_0}(a^\dagger - a) \tag{E.3}$$

Unitarity of the transformation:

$$(e^{\zeta})^\dagger = e^{(\zeta^\dagger)} = e^{-\zeta} = (e^{\zeta})^{-1} \tag{E.4}$$

The Hamiltonian is transformed operator-wise: for all operators O in (4.1), we use the Baker-Hausdorff formula:

$$\tilde{O} = e^{\zeta} O e^{-\zeta} = O + [\zeta, O] + \frac{1}{2!}[\zeta, [\zeta, O]] + \frac{1}{3!}[\zeta, [\zeta, [\zeta, O]]] + \cdots \tag{E.5}$$

For the transformed operator $\tilde{a}$,

$$[\zeta, a] = \sqrt{g}(n_a - n_b)[(a^\dagger - a), a] = -\sqrt{g}(n_a - n_b) \tag{E.6}$$

where we used

$$[a, a^\dagger] = 1 \tag{E.7}$$

From this follows

$$[\zeta, [\zeta, a]] = [\sqrt{g}(n_a - n_b)(a^\dagger - a), -\sqrt{g}(n_a - n_b)] = 0 \tag{E.8}$$

and therefore all higher-order commutators are 0, too. Performing a similar calculation for $a^\dagger$ results in

$$\tilde{a} = a - \sqrt{g}(n_a - n_b) \qquad \tilde{a}^\dagger = a^\dagger - \sqrt{g}(n_a - n_b) \tag{E.9}$$

For the transformed boson number operator,

$$\tilde{N}_a = \tilde{a}^\dagger \tilde{a} = a^\dagger a - \sqrt{g}(n_a - n_b)(a^\dagger + a) + g(n_a - n_b)^2 \tag{E.10}$$

and the transformed oscillator displacement operator is

$$\tilde{x} = \frac{l_0}{\sqrt{2}}(\tilde{a}^\dagger + \tilde{a}) = \frac{l_0}{\sqrt{2}}\Big((a^\dagger + a) - 2\sqrt{g}(n_a - n_b)\Big) = x - l(n_a - n_b) \tag{E.11}$$

where we have used the definitions of λ', l_0, l.

For the transformed electron operator $\tilde{c}_a$,

$$[\zeta, c_a] = \sqrt{g}(a^\dagger - a)\ [(n_a - n_b), c_a] = \sqrt{g}(a^\dagger - a)\ [n_a, c_a] = -\sqrt{g}(a^\dagger - a)c_a \tag{E.12}$$

where we used

$$[n_a, c_a] = c_a^\dagger c_a^2 - c_a c_a^\dagger c_a = -c_a \tag{E.13}$$

From this follows

$$[\zeta, [\zeta, c_a]] = [\zeta, -\sqrt{g}(a^\dagger - a)c_a] = -\sqrt{g}(a^\dagger - a)[\zeta, c_a] = (-\sqrt{g}(a^\dagger - a))^2 c_a \tag{E.14}$$

The n'th order commutator is

$$[\zeta, ..., [\zeta, [\zeta, c_a]]...] = (-\sqrt{g}(a^\dagger - a))^n c_a \tag{E.15}$$

The result for $\tilde{c}_a$ is

$$\tilde{c}_a = c_a - \sqrt{g}(a^\dagger - a)c_a + \frac{1}{2!}(\sqrt{g}(a^\dagger - a))^2 c_a - \cdots = e^{-\sqrt{g}(a^\dagger - a)} c_a \tag{E.16}$$

We define

$$A = e^{-\sqrt{g}(a^\dagger - a)} \qquad A^\dagger = e^{\sqrt{g}(a^\dagger - a)} \tag{E.17}$$

Then, similar calculations for $\tilde{c}_a^\dagger$, $\tilde{c}_b$, $\tilde{c}_b^\dagger$ yield

$$\tilde{c}_a = c_a A \qquad \tilde{c}_a^\dagger = c_a^\dagger A^\dagger \tag{E.18}$$

$$\tilde{c}_b = c_b A^\dagger \qquad \tilde{c}_b^\dagger = c_b^\dagger A \tag{E.19}$$

The electron number operators transform identically:

$$\tilde{n}_\sigma = \tilde{c}_\sigma^\dagger \tilde{c}_\sigma = c_\sigma^\dagger c_\sigma A^\dagger A = n_\sigma \tag{E.20}$$

For the electronic hopping term,

$$\tilde{c}_a^\dagger \tilde{c}_b = c_a^\dagger c_b A^{\dagger 2} \qquad \tilde{c}_b^\dagger \tilde{c}_a = c_b^\dagger c_a A^2 \tag{E.21}$$

Inserting the transformed operators in eq. (4.1) yields the transformed Hamiltonian $\tilde{H}$:

$$\begin{aligned}\frac{\tilde{H}}{\omega} = \quad & \Big(a^\dagger a + \tfrac{1}{2} - \sqrt{g}(n_a - n_b)(a^\dagger + a) + g(n_a - n_b)^2\Big) \\ & + \sqrt{g}(n_a - n_b)\Big(a^\dagger - \sqrt{g}(n_a - n_b) + a - \sqrt{g}(n_a - n_b)\Big) \\ & - \tfrac{2g}{\alpha}\ (c_a^\dagger c_b A^{\dagger 2} + c_b^\dagger c_a A^2) + \delta\ (n_a - n_b)\end{aligned} \tag{E.22}$$

This is

$$\begin{aligned}\frac{\tilde{H}}{\omega} = \quad & a^\dagger a + \tfrac{1}{2} - \tfrac{2g}{\alpha}\ (c_a^\dagger c_b A^{\dagger 2} + c_b^\dagger c_a A^2) + \delta\ (n_a - n_b) + H_p \\ \frac{H_p}{\omega} = \quad & \Big(- \sqrt{g}(n_a - n_b)(a^\dagger + a) + g(n_a - n_b)^2\Big) \\ & + \sqrt{g}(n_a - n_b)\Big(a^\dagger - \sqrt{g}(n_a - n_b) + a - \sqrt{g}(n_a - n_b)\Big)\end{aligned} \tag{E.23}$$

Rewriting H_p,

$$\begin{aligned}\frac{H_p}{\omega} &= -\sqrt{g}(n_a - n_b)(a^\dagger + a) + g(n_a - n_b)^2 + \sqrt{g}(n_a - n_b)\Big((a^\dagger + a) - 2\sqrt{g}(n_a - n_b)\Big) \\ &= -g(n_a - n_b)^2 = -g(n_a^2 + n_b^2 - 2n_a n_b) = -g(n_a + n_b)\end{aligned} \tag{E.24}$$

The result is

$$\frac{\tilde{H}}{\omega} = a^\dagger a + \frac{1}{2} - gN - \frac{2g}{\alpha}\ (c_a^\dagger c_b e^{2\sqrt{g}(a^\dagger - a)} + c_b^\dagger c_a e^{-2\sqrt{g}(a^\dagger - a)}) + \delta\ (n_a - n_b) \tag{E.25}$$

Appendix F

Polaronic hopping matrix elements

F.1 n-diagonal matrix elements

We want to calculate

$$\langle \sigma n|\tilde{H}'_n|\sigma' n\rangle = \langle \sigma n| - t(c_a^\dagger c_b e^{2\sqrt{g}(a^\dagger - a)} + c_b^\dagger c_a e^{-2\sqrt{g}(a^\dagger - a)})|\sigma' n\rangle \tag{F.1}$$

Using

$$e^{\hat{X}} = \sum_j \frac{\hat{X}^j}{j!} \tag{F.2}$$

we have, for the bosonic part of the first term in (F.1),

$$\langle n|e^{2\sqrt{g}(a^\dagger - a)}|n\rangle = \langle n|\Big(\sum_{j=0}^{\infty}\frac{1}{j!}\Big(2\sqrt{g}\Big)^j (a^\dagger)^j\Big)\Big(\sum_{k=0}^{\infty}\frac{1}{k!}\Big(2\sqrt{g}\Big)^k a^k\Big)|n\rangle \tag{F.3}$$

Due to orthogonality of the boson eigenstates, the only nonzero contributions are from terms with $k = j$, and the expression becomes

$$\langle n|\sum_{j=0}^{\infty}\frac{(-1)^j}{(j!)^2}\Big(2\sqrt{g}\Big)^{2j}(a^\dagger)^j a^j|n\rangle \tag{F.4}$$

We use

$$a^j|n\rangle = \sqrt{\frac{n!}{(n-j)!}}|n-j\rangle \tag{F.5}$$

along with the Hermitian conjugate of this expression to get

$$\langle n|(a^\dagger)^j a^j|n\rangle = \Big(\langle n-j|\sqrt{\frac{n!}{(n-j)!}}\Big)\Big(\sqrt{\frac{n!}{(n-j)!}}|n-j\rangle\Big) = \frac{n!}{(n-j)!} \tag{F.6}$$

In eq. (F.4), terms with $j > n$ are 0. The result is

$$\langle n|e^{2\sqrt{g}(a^\dagger - a)}|n\rangle = \sum_{j=0}^{n}(-1)^j \frac{n!}{(j!)^2(n-j)!}\Big(2\sqrt{g}\Big)^{2j} \tag{F.7}$$

From the calculation, it is clear that

$$\langle n|e^{-2\sqrt{g}(a^\dagger - a)}|n\rangle = \langle n|e^{2\sqrt{g}(a^\dagger - a)}|n\rangle \tag{F.8}$$

Therefore, the bosonic part can be 'taken outside' in (F.1). The electronic part is

$$\langle\sigma|(c_a^\dagger c_b + c_b^\dagger c_a)|\sigma'\rangle = \delta_{\sigma,\bar{\sigma'}} \tag{F.9}$$

The elements of the 2×2 matrix are only nonzero on the off-diagonal. The nonzero matrix elements are

$$\langle\sigma n|\tilde{H}'_n|\bar{\sigma}n\rangle = -t\sum_{j=0}^{n}(-1)^j \frac{n!}{(j!)^2(n-j)!}\Big(2\sqrt{g}\Big)^{2j} \tag{F.10}$$

F.2 Non-diagonal matrix elements

We rewrite the operators $c_a^\dagger c_b$, $c_b^\dagger c_a$ as matrices in the basis of the d operators, which create/ annihilate the bonding and antibonding states, and the offdiagonal matrix elements become

$$\langle\tau n| - \frac{t}{2}\Big(\begin{pmatrix} 1 & 1 \\ -1 & -1 \end{pmatrix} e^{2\frac{\lambda'}{\omega}(a^\dagger - a)} + \begin{pmatrix} 1 & -1 \\ 1 & -1 \end{pmatrix} e^{-2\frac{\lambda'}{\omega}(a^\dagger - a)}\Big)|\tau' n'\rangle \tag{F.11}$$

For the electronic part,

$$\begin{pmatrix} 1 \\ 0 \end{pmatrix}\begin{pmatrix} 1 & 1 \\ -1 & -1 \end{pmatrix}\begin{pmatrix} 0 \\ 1 \end{pmatrix} = \begin{pmatrix} 1 \\ 0 \end{pmatrix}\begin{pmatrix} 1 \\ -1 \end{pmatrix} = 1 \tag{F.12}$$

$$\begin{pmatrix} 0 \\ 1 \end{pmatrix}\begin{pmatrix} 1 & 1 \\ -1 & -1 \end{pmatrix}\begin{pmatrix} 1 \\ 0 \end{pmatrix} = \begin{pmatrix} 0 \\ 1 \end{pmatrix}\begin{pmatrix} 1 \\ -1 \end{pmatrix} = -1 \tag{F.13}$$

$$\begin{pmatrix} 1 \\ 0 \end{pmatrix}\begin{pmatrix} 1 & -1 \\ 1 & -1 \end{pmatrix}\begin{pmatrix} 0 \\ 1 \end{pmatrix} = \begin{pmatrix} 1 \\ 0 \end{pmatrix}\begin{pmatrix} -1 \\ -1 \end{pmatrix} = -1 \tag{F.14}$$

$$\begin{pmatrix} 0 \\ 1 \end{pmatrix}\begin{pmatrix} 1 & -1 \\ 1 & -1 \end{pmatrix}\begin{pmatrix} 1 \\ 0 \end{pmatrix} = \begin{pmatrix} 0 \\ 1 \end{pmatrix}\begin{pmatrix} 1 \\ 1 \end{pmatrix} = 1 \tag{F.15}$$

Putting it together, we see that the τ-non-diagonal electronic part is just a sign, which is opposite for the two terms:

$$\langle\tau|\begin{pmatrix} 1 & 1 \\ -1 & -1 \end{pmatrix}|\bar{\tau}\rangle = -\langle\tau|\begin{pmatrix} 1 & -1 \\ 1 & -1 \end{pmatrix}|\bar{\tau}\rangle \tag{F.16}$$

For the τ-diagonal terms,

$$\begin{pmatrix} 1 \\ 0 \end{pmatrix} \begin{pmatrix} 1 & 1 \\ -1 & -1 \end{pmatrix} \begin{pmatrix} 1 \\ 0 \end{pmatrix} = 1 \tag{F.17}$$

$$\begin{pmatrix} 1 \\ 0 \end{pmatrix} \begin{pmatrix} 1 & -1 \\ 1 & -1 \end{pmatrix} \begin{pmatrix} 1 \\ 0 \end{pmatrix} = 1 \tag{F.18}$$

$$\begin{pmatrix} 0 \\ 1 \end{pmatrix} \begin{pmatrix} 1 & 1 \\ -1 & -1 \end{pmatrix} \begin{pmatrix} 0 \\ 1 \end{pmatrix} = -1 \tag{F.19}$$

$$\begin{pmatrix} 0 \\ 1 \end{pmatrix} \begin{pmatrix} 1 & -1 \\ 1 & -1 \end{pmatrix} \begin{pmatrix} 0 \\ 1 \end{pmatrix} = -1 \tag{F.20}$$

With $\hat{O}$ denoting either of the two electron operators in the above, we have

$$\langle \tau | \hat{O} | \tau \rangle = \mathrm{sign}(\tau) \tag{F.21}$$

The two terms have the same sign.

For the bosonic part of the first term,

$$\langle n | e^{2\sqrt{g}(a^\dagger - a)} | n' \rangle = \langle n | \Big(\sum_{j=0}^{\infty} \frac{1}{j!} \Big(2\sqrt{g} \Big)^j (a^\dagger)^j \Big) \Big(\sum_{k=0}^{\infty} \frac{1}{k!} \Big(-2\sqrt{g} \Big)^k a^k \Big) | n' \rangle \tag{F.22}$$

and the only contributing terms have $n' - k = n - j$. Assuming $n \geq n'$, we substitute $\sum_{j=0}^{\infty} \sum_{k=0}^{\infty} \to \sum_{k=0}^{n'} \delta_{j,k+n-n'}$, where we use that terms with $k > n'$ are 0. For the contributing terms, $n \geq n'$ insures $j \geq k$.

$$\langle n | e^{2\sqrt{g}(a^\dagger - a)} | n' \rangle = \sum_{k=0}^{n'} (-1)^k \frac{\sqrt{n!\ n'!}}{(k+n-n')!\ k!\ (n'-k)!} \Big(2\sqrt{g} \Big)^{2k+n-n'} \tag{F.23}$$

Here, we have used eq. (F.5) twice. By substituting $2\sqrt{g} \to -2\sqrt{g}$ follows ($n \geq n'$),

$$\langle n | e^{-2\sqrt{g}(a^\dagger - a)} | n' \rangle = \langle n | e^{2\sqrt{g}(a^\dagger - a)} | n' \rangle (-1)^{n-n'} \tag{F.24}$$

Consider $\tau' = \bar{\tau}$. If $(n - n') = 0 \pmod 2$, the boson terms are equal, and eq. (F.16) leads to the terms killing each other off. If $(n - n') = 1 \pmod 2$, the boson sign difference on the terms and the electron sign difference cancels out, and the matrix element eq. (F.11) becomes

$$(\pm) - t \sum_{k=0}^{n'} (-1)^k \frac{\sqrt{n!\ n'!}}{(k+n-n')!\ k!\ (n'-k)!} \Big(2\sqrt{g} \Big)^{2k+n-n'} \tag{F.25}$$

If instead $\tau' = \tau$, the matrix element is nonzero if the boson terms have the same sign, that is, if $(n - n') = 0 \pmod 2$.

For $n \leq n'$, we substitute $k \to j - n + n'$ in eq. (F.22) and get the result eq. (F.23) time a factor $(-1)^{n'-n}$. This leads to the boson terms being equal, and the matrix elements eq. (F.11) different from 0 if and only if $\tau' = \tau$. The situation, therefore, is opposite $n \geq n'$.

Conclusion: Matrix elements are nonzero in either of two situations: $\tau' = \tau$, $(n - n') = 1 \pmod 2$, or $\tau' = \bar{\tau}$, $(n - n') = 0 \pmod 2$.

Appendix G

Polaronic tunneling, semiclassically

We expand U_- to order X^2 about the minima $\pm X_0$. From this, we will determine approximate wave functions for the polaronic states.

Taylorexpanding near $+X_0$,

$$U_-(X) = U_-(X_0) + \frac{\partial U_-(X_0)}{\partial X}(X - X_0) + \frac{1}{2}\frac{\partial^2 U_-(X_0)}{\partial X^2}(X - X_0)^2 + O[(X - X_0)^3] \tag{G.1}$$

The partial derivates have been calculated previously. By definition of X_0, the term $\frac{\partial U_-(X_0)}{\partial X}$ is 0. From eq. (4.66), $\frac{\partial^2 U_-(X_0)}{\partial X^2} = 1 - \frac{1}{\alpha^2}$. Inserting X_0 in the Taylorexpansion,

$$\frac{U_-(X)}{\omega} = -g(1 + \frac{1}{\alpha^2}) + \frac{1}{2}(1 - \frac{1}{\alpha^2})(X - \sqrt{2g}\sqrt{1 - \frac{1}{\alpha^2}})^2 + O[(X - X_0)^3] \tag{G.2}$$

As $U_-(X_0) = U_-(-X_0)$, we neglect this constant energy term in the Taylorexpansions around $\pm X_0$, translating the energy scale such that $U_-(\pm X_0) = 0$. In terms of a coordinate $\delta X \equiv X - X_0$, the effective potential to second order near $+X_0$ becomes

$$\frac{U_-^{eff}(\delta X)}{\omega} = \frac{1}{2}(1 - \frac{1}{\alpha^2})(\delta X)^2 \tag{G.3}$$

Near $-X_0$, with $\delta X \equiv X + X_0$, the effective potential is an identical expression.

The higher-order terms in X should be important for $\alpha \approx 1$, but we neglect them here. What we are left with are harmonic potentials in $\pm X_0$, defined by the same spring constant. Reinserting l_0,

$$U_-^{eff}(\delta X) = \frac{1}{2}k_{eff}(\delta x)^2 \tag{G.4}$$

where the effective spring constant is

$$k_{eff} = \omega(1 - \frac{1}{\alpha^2})/l_0^2 \tag{G.5}$$

This defines an effective mass and an effective quantum oscillator length,

$$l_{0,eff} = \sqrt{\frac{1}{k_{eff}/\omega}} = \sqrt{\frac{l_0^2}{1-\frac{1}{\alpha^2}}} = l_0(1-\frac{1}{\alpha^2})^{-1/2} \tag{G.6}$$

which approaches l_0 for $\alpha \to \infty$.

In terms of a coordinate $\xi \equiv x/l_{0,eff}$ and defining $\xi_0 \equiv x_0/l_{0,eff} = \sqrt{2g}(1-\frac{1}{\alpha^2})$, the wave functions for the harmonic oscillator ground states in $\pm x_0$ are

$$\phi_\pm(\xi) = \pi^{-1/4} {l_{0,eff}}^{-1/2} e^{-(\xi\pm\xi_0)^2/2} \tag{G.7}$$

The overlap is the effective polaronic tunneling coupling in unit of ω,

$$t_p/\omega = \int_{-\infty}^{\infty} \mathrm{d}\xi \; l_{0,eff} \; \phi_+(\xi)\phi_-(\xi) = \pi^{-1/2} {l_0}^{-1} \int_{-\infty}^{\infty} \mathrm{d}\xi \; l_{0,eff} \; e^{-\xi^2} e^{-\xi_0^2} \tag{G.8}$$

Using $\int_{-\infty}^{\infty} d\xi \; e^{-\xi^2} = \sqrt{\pi}$,

$$t_p/\omega = e^{-\xi_0^2} = \exp(-2g \; (1-\frac{1}{\alpha^2})^2) \tag{G.9}$$

Appendix H

Poster

The poster on the next page was presented at the ADMOL 2004 workshop, see: www.mpipks-dresden.mpg.de/ admol/

Transport through single molecular dimers

Gregers Alexander Kaat and Karsten Flensberg
Nano-Science Center, Niels Bohr Institute, Universitetsparken 5, 2100 Copenhagen, Denmark

Abstract

- We study transport through a molecular dimer coupled to a vibrational mode.
- The vibron couples to the charge difference between the two parts of the dimer.
- This leads to an entanglement between the bosonic and electronic degrees of freedom.
- We calculate the entanglement entropy of the double dot ground state.
- The entanglement entropy increases sharply with hybridization of the dimer.
- The increase in entanglement signals the formation of a polaron.
- The differential conductance reflects the degree of entanglement.
- We also discuss the relation to recent experiment on C_{76} dimers.

Motivation:
Experiments by Pasupathy et al., 2004.
cond-mat/0311150

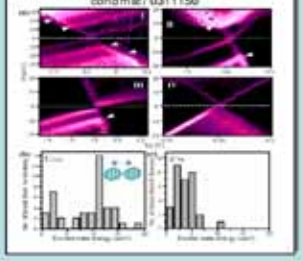

Experiments show:
- Electron-vibron coupling (intercage mode = 11 meV), some devices agree with Frank-Condon physics.
- Some devices show anomalous large electron-vibron coupling and peculiar asymmetry, not consistent with Frank-Condon theory (not show).

Model

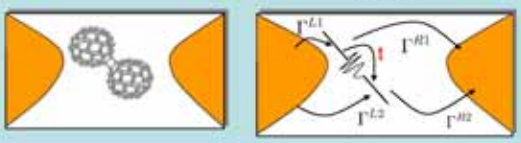

The dimer model Hamiltonian:

$$H = \frac{p^2}{2m} + \frac{1}{2}m\omega^2 x - t(c_1^\dagger c_2 + c_2^\dagger c_1) + \lambda x(n_1 - n_2)$$

or in dimensionless form:

$$H/\omega = \alpha^\dagger a + \frac{1}{2} + \sqrt{g}(a + a^\dagger)\hat{\sigma}_z - \frac{2g}{\alpha}\hat{\sigma}_x$$

where $\alpha = \frac{\lambda^2}{m\omega^2 t}$ and $g = \frac{\lambda^2}{2m\omega^3}$

THE MODEL HAMILTONIAN IS SOLVED NUMERICALLY

Entanglement

We study the entanglement of the electronic and bosonic degrees of freedom in the ground state. Our measure of the entanglement is the von Neumann entropy of the reduced density matrix: $\rho' = \mathrm{Tr}_{\rm ph}\rho$ (here $\mathrm{Tr}_{\rm ph}$ is the trace over boson states, and ρ is the full density matrix). The von Neumann entropy is:

$$S_{\rm N}(\rho') = -\mathrm{Tr}(\rho' \log_{10} \rho')$$

For sufficiently large g the entanglement of the ground state increases sharply near $\alpha = 1$. Here, $g = 50$.

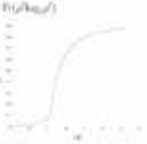

Semiclassical picture of polaron

- For $\omega \to 0$, x is a classical coordinate.
- The electronic eigenenergies become x dependent: $U_{\pm} = \frac{1}{2}m\omega^2 x^2 \pm \sqrt{\lambda^2 x^2 + t^2}$
- The ground state displays a bifurcation at $\alpha = 1$: for $\alpha < 1$ the minimum is in $x = 0$, and for $\alpha > 1$ the minima are in $x = \pm x_0$, $x_0 = t\sqrt{\alpha^2 - 1}/\lambda$.
- The ground state is the maximally entangled state: $|\eta, x\rangle = \frac{1}{\sqrt{2}}(|1, -x_0\rangle + |2, x_0\rangle)$

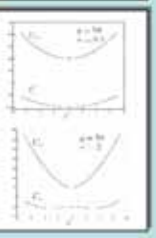

Transport: sequential tunneling

The tunneling rates are

$$\Gamma^{n\sigma}_{ij} = \frac{2\pi}{\hbar}\Gamma^{n\sigma}\sum_{i_n}\sum_{j_n}|\langle f_j|c^\dagger_\sigma|i_n\rangle|^2\frac{e^{-\beta E_{i_n}}}{Z_0}n_{\rm F}(eV_g + E_{j_n} - E_{i_n})$$

$$\Gamma^{n\sigma}_{ji} = \frac{2\pi}{\hbar}\Gamma^{n\sigma}\sum_{i_n}\sum_{j_n}|\langle f_j|c_\sigma|i_n\rangle|^2\frac{e^{-\beta E_{j_n}}}{Z_1}[1 - n_{\rm F}(eV_g - E_{j_n} + E_{i_n})]$$

where: i and f denote initial and final dimer states, "0" and "1" denote "empty" and "filled" dimer states.

Current in non-polaron state

The dimer is in a coherent state and the current is

$$I = e\frac{\Gamma^R_{10}\Gamma^L_{01} - \Gamma^R_{01}\Gamma^L_{10}}{\Gamma^R_{10} + \Gamma^L_{10} + \Gamma^R_{01} + \Gamma^L_{01}}$$

where $\Gamma^n_{01} = \sum_\sigma \Gamma^{n\sigma}_{01}$

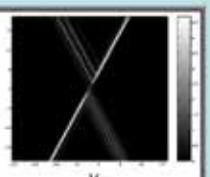

$g = 2,\ \alpha = 0.4,\ T = 0.1\omega$

Current with polaron state

If the tunneling coupling between the two polaron sites is smaller than the tunneling coupling to the leads we have an effective double dot system.

In this case we have three different states: empty and left/right polaron states.

Solve three coupled master equations.

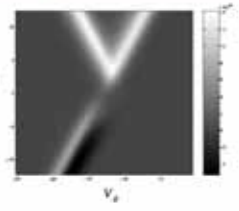

In the figure: $g = 11,\ \alpha = 2,\ \Gamma^{R1} = 0,\ T = 0.5\,\omega.$

Conclusions

- For strong electron-vibron coupling a polaron is formed.
- The coupling between the two polaron sites become exponentially small, hence a double dot is formed.
- The double dot leads to a strongly asymmetric IV characteristic.
- May have been observed in experiments on C_{140}

Bibliography

[1] Orbitals downloaded from www.cm.utexas.edu/CH310M/

[2] Arieh Aviram, Mark A. Ratner, Chem. Phys. Lett., **29**, 277 (1974)

[3] Ari Aviram, J. Am. Chem. Soc., **110**, 5687 (1988)

[4] Noel S. Hush et al., J. Am. Chem. Soc., **112**, 4192 (1990)

[5] M. A. Reed et al., Science **278**, 252 (1997)

[6] Robert M. Metzger et al., J. Am. Chem. Soc., **119**, 10455 (1997)

[7] C. Joachim, J.K. Gimzewski, Chem. Phys. Lett., **265**, 353 (1997)

[8] J. Chen et al., Science **286**, 1550 (1999)

[9] H. Park et al., Appl. Phys. Lett. **75** (2), 301 (1999)

[10] H. Park et al., Nature, **407**, 57 (2000)

[11] Henk W. Ch. Postma et al., Science **293**, 76 (2001)

[12] V. Derycke et al., Nano Lett. **1** (9), 453 (2001)

[13] Yu Huang et al., Science **294**, 1313 (2001)

[14] Adrian Bachtold et al., Science **294**, 1317 (2001)

[15] N. B. Zhitenev, H. Meng, and Z. Bao, Phys. Rev. Lett., **88** (22), 226801 (2002)

[16] Jiwoong Park, A. N. Pasupathy, et al., Nature, **417**, 722 (2002)

[17] Wenjie Liang, Matthew P. Shores, Marc Bockrath, Jeffrey R. Long, and Hongkun Park, Nature, **417**, 725 (2002)

[18] Sergey Kubatkin, Andrey Danilov, Mattias Hjort, Jerome Cornil, Jean-Luc Bredas, Nicolai Stuhr-Hansen, Per Hedegård, and Thomas Bjørnholm, Nature, **425**, 698 (2003)

[19] L. Y. Gorelik et al., Phys. Rev. Lett., **80** (20), 4526 (1998)

[20] R. I. Shekhter, Yu Galperin, L. Y. Gorelik, A. Isacsson, and M. Jonson, J. Phys.: Condens. Matter **15**, R441, *Shuttling of electrons and Cooper pairs* (2003)

[21] T. Novotny, A. Donarini, and A. P. Jauho, Phys. Rev. Lett. **90**, 256801 (2003)

[22] D. Fedorets, L. Y. Gorelik, R. I. Shekhter, and M. Jonson, Phys. Rev. Lett. **92** (16), 166801 (2004)

[23] D. Fedorets, Phys. Rev. B **68**, 033106 (2003)

[24] Kevin D. McCarthy, Nikolay Prokof'ev, and Mark T. Tuominen, Phys. Rev. B, **67**, 245415 (2003)

[25] A.P. Jauho et al., cond-mat/0411190 v1 (2004)

[26] D. Boese and H. Schoeller, Europhys. Lett., **54** (5), 668 (2001)

[27] Karsten Flensberg, Phys. Rev. B, **68**, 205323 (2003)

[28] Stephan Braig and Karsten Flensberg, Phys. Rev. B, **68**, 205324 (2003)

[29] A. Mitra, I. Aleiner, and A. J. Millis, Phys. Rev. B, **69**, 245302 (2004)

[30] A. N. Pasupathy et al., cond-mat/0311150 (2003)

[31] Private communication with J. Park

[32] Gustavo E. Scuseria, Chem. Phys. Lett., **180** (5), 451 (1991)

[33] D. R. McKenzie, C. A. Davis, D. J. H. Cockayne, D. A. Muller, and A. M. Vassallo, Nature, **355**, 622 (1992)

[34] Sang Jeong Woo, Eunja Kim, and Young Hee Lee, Phys. Rev. B, **47**, 6721 (1993)

[35] A. M. Rao, M. Menon, Kai-An Wang, P. C. Eklund, K. R. Subbaswamy, D. S. Cornett, M. A. Duncan, and I. J. Amster, Chem. Phys. Lett., **224**, 106 (1994)

[36] Madhu Menon, A. M. Rao, K. R. Subbaswamy, and P.C. Eklund, Phys. Rev. B, **51** (2), 800 (1995)

[37] Sergei Lebedkin, William E. Hull, Alexander Soldatov, Burkhard Renker, and Manfred M. Kappes, J. Phys., Chem. B, **104**, 4101 (2000)

[38] T. L. Makarova, Semiconductors, **35** (3), 243 (2001)

[39] Giorgio Orlandi and Fabrizia Negri, Photochem. Photobiol. Sci., **1**, 289 (2002)

[40] Luis Echegoyen and Lourdes E. Echegoyen, Acc. Chem. Res., **31**, (9), 593 (1998)

[41] A. S. Alexandrov et al., Phys. Rev. B, **33** (7), 4526 (1986)

[42] George C. Schatz, Mark A. Ratner, *Quantum Mechanics in Chemistry*, Prentice Hall, Inc., Englewood Cliffs (1993)

[43] B. H. Bransden and C. J. Joachan, *Physics of Atoms and Molecules*

[44] A. O. Caldera and A. J. Legget, Ann. Phys. (N.Y.), **149**, 374 (1983)

[45] Ulrich Weiss, *Quantum Dissipative Systems*, 2nd edition

[46] T. Holstein, Ann. Phys. (N.Y) **8**, 343 (1959)

[47] A. J. Leggett et al., Rev. Mod. Phys. **59**, 1 (1987)

[48] Y. Makhlin et al., Rev. Mod. Phys. **73**, 357 (2001)

[49] H. Köppel, W. Domcke, and L. S. Cederbaum, Adv. in Chem. Phys., **LVII**, 59, *Multimode Molecular Dynamics beyond the Born-Oppenheimer approximation*

[50] R. Englman, *The Jahn-Teller Effect in Molecules and Crystals*

[51] Gregory Levine and V. N. Muthukumar, Phys. Rev. B **69**, 113203 (2004)

[52] Henrik Bruus and Karsten Flensberg, *Many-Body Quantum Theory in Condensed Matter Physics*, Oxford University Press (2004)

[53] Gerald D. Mahan, *Many-Particle Physics*, 3. edition

[54] *Molecular Electronics*, edited by J. Jortner and M. Ratner, Blackwell Science Ltd. (1997)

[55] A. S. Alexandrov, V. V. Kabanov, and D. K. Ray, Phys. Rev. B, **49** (14), 9915 (1994)

[56] Jayita Chatterjee and A. N. Das, Phys. Rev. B, **61** (7), 4592 (2000)

[57] H. Löwen, Phys. Rev. B, **37** (15), 8661 (1988)

[58] V. Vedral, Rev. Mod. Phys. **74**, 197 (2002)

[59] Tzu-Chieh Wei et al., quant-ph/0208138 v1

[60] Michael Sørensen, *En introduktion til sandsynlighedsregning* (2002)

[61] Robert L. Fulton and Martin Gouterman, Journal of Chem. Phys., **35** (3), 1059 (1961)

[62] Robert L. Fulton and Martin Gouterman, Journal of Chem. Phys., **41** (8), 2280 (1964)

[63] Martin Gouterman, Journal of Chem. Phys., **42** (1), 351 (1965)

[64] S. A. Gurvitz and Ya. S. Prager, Phys. Rev. B, **53** (23), 15932 (1996)

[65] T. H. Stoof and Yu. V. Nazarov, Phys. Rev. B, **53** (3), 1050 (1996)

[66] M. Wegewijs et al., in *Introducing Molecular Electronics*, eds. G. Cuniberti et al. (Springer), to be published

[67] Solved as a problem in the course Many Particle Physics 2, spring 2003, take-home exam 1.

[68] In 'classical', nonquantum probability theory, if variables are independent, then they are uncorrelated, but the inverse implication is not generally true. The instance where the inverse implication is necessarily true is the case where the simultaneous distribution of the variables follow a Gaussian distribution [60].

[69] In the high energy states, not plotted, the function may take on negative values and values numerically larger than 1.